The Probe of Inflation and Cosmic Origins

A Space Mission Study Report
December, 2018

Principal Investigator:
Steering Committee:
Executive Committee:
Contributors:
Endorsers:

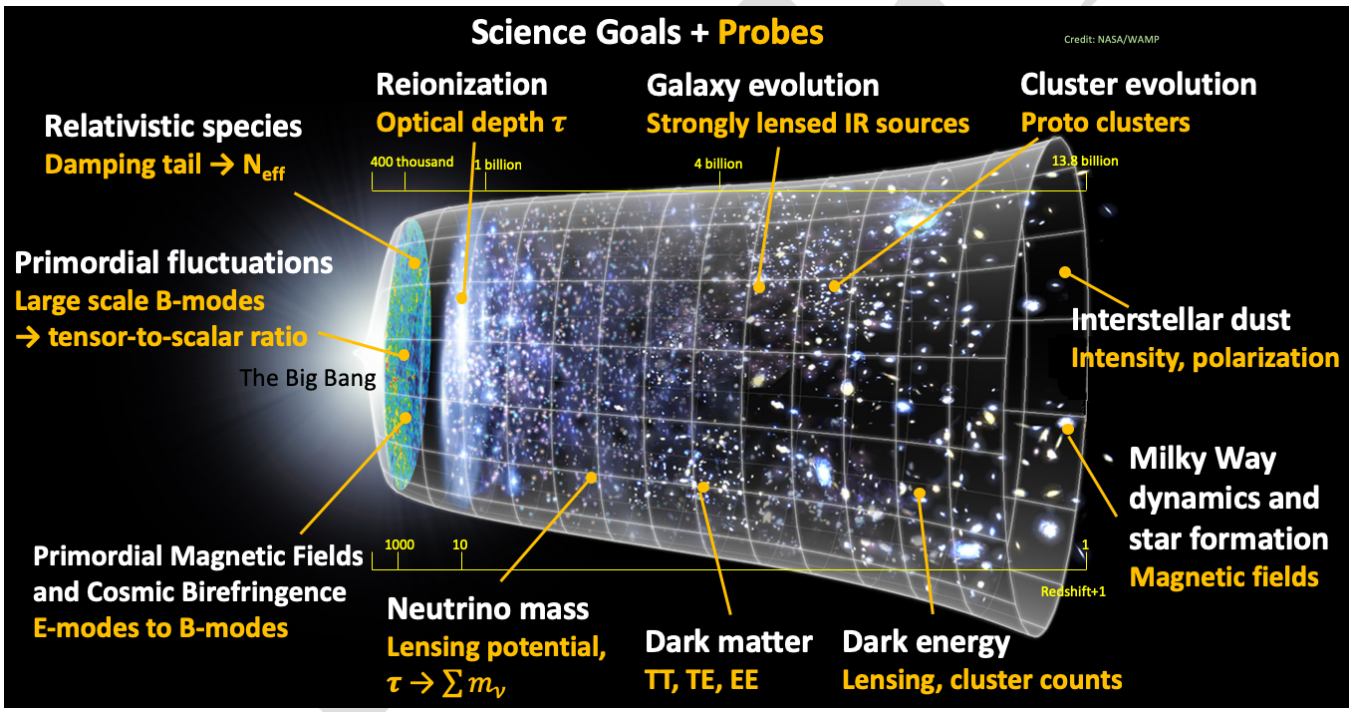

The Probe of Inflation and Cosmic Origins

A Space Mission Study Report
December, 2018

Principal Investigator: Shaul Hanany
Steering Committee: Charles Bennet, Scott Dodelson, Lyman Page
Executive Committee: May be incomplete Jamie Bock, Julian Borrill, Brendan Crill, Mark Devlin, Raphael Flauger, Shaul Hanany (PI), William Jones, Lloyd Knox, Al Kogut, Charles Lawrence (ex-officio), Jeff McMahon, Clem Pryke, Amy Trangsrud (ex-officio)

Authors

Marcelo Alvarez
Peter Ashton
Jonathan Aumont
Ranajoy Banerji
Belen Barreiro
James G. Bartlett
Soumen Basak
Nicholas Battaglia
Jamie Bock
Kimberly K. Boddy
Matteo Bonato
Julian Borrill
Francois Boulanger
Blakesley Burkhart
David Chuss
Susan E. Clark
Brendan Crill
Jacques Delabrouille
Eleonora Di Valentino
Joy Didier
Olivier Doré
Alexander van Engelen
Josquin Errard
Tom Essinger-Hileman
Stephen Feeney
Jeffrey Filippini
Laura Fissel
Raphael Flauger
Vera Gluscevic
Kris Gorski
Dan Green
Brandon Hensley
Diego Herranz
Colin Hill
Eric Hivon
Johannes Hubmayr
Brad Johnson
William Jones
Terry Jones
Lloyd Knox
Al Kogut
Marcos López-Caniego
Charles Lawrence
Alex Lazarian
Zack Li
Mathew Madhavacheril
Jean-Baptiste Melin
Mattia Negrello
Giles Novak
Roger O'Brient
Chris Paine
Tim Pearson
Levon Pogosian
Clem Pryke
Mathieu Remazeilles
Graca Rocha
Marcel Schmittfull
Douglas Scott
Ian Stephens
Brian Sutin
Maurizio Tomasi
Amy Trangsrud
Flavien Vansyngel
Qi Wen
Siyao Xu
Karl Young
Andrea Zonca
Gianfranco De Zotti

Endorsers

Zeeshan Ahmed
Jason Austermann
Darcy Barron
Karim Benabed
Federico Bianchini
Colin Bischoff
J. Richard Bond
François Bouchet
Robert Caldwell
Xingang Chen
Jens Chluba
Francis-Yan Cyr-Racine
Tijmen de Haan
Aurelien Fraisse
Silvia Galli
Ken Ganga
Tuhin Ghosh
Sunil Golwara
Jon E. Gudmundsson
Kevin M. Huffenberger
Marc Kamionkowski
Reijo Keskitalo
Rishi Khatri
Ely Kovetz
Daniel Lenz
Marilena Loverde
Carlos Martins
Silvia Masi
Joel Meyers
Lorenzo Moncelsi
Pavel Motloch
Tony Mroczkowski
Pavel Naselsky
Federico Nati
Elena Orlando
Francesco Piacentini
Giuseppe Puglisi
Benjamin Racine
Christian Reichardt
Anirban Roy
Maria Salatino
Benjamin Saliwanchik
Neelima Sehgal
Sarah Shandera
Erik Shirokoff
Anže Slosar
Aritoki Suzuki
Eric Switzer
Andrea Tartari
Grant Teply
Peter Timbie
Matthieu Tristram
Caterina Umiltà
Patricio Vielva
Benjamin Wallisch
Scott Watson
Edward J. Wollack

DRAFT

Export-Controlled Material Statement

This document has been reviewed and determined not to contain export controlled technical data.

DRAFT

Contents

1 Executive Summary **1**

2 Science **2**
2.1 Introduction . . . 2
2.2 Science Objectives . . . 6
2.2.1 Fundamental Physics . . . 6
2.2.2 Cosmic Structure Formation and Evolution . . . 12
2.2.3 Galactic Structure and Star Formation . . . 17
2.3 Legacy Surveys . . . 20
2.3.1 Early phases of galaxy evolution . . . 20
2.3.2 Early phases of cluster evolution . . . 22
2.3.3 Additional products of PICO surveys . . . 22
2.4 Complementarity with Other Surveys and with Sub-Orbital Measurements . . . 23
2.4.1 Complementarity with Astrophysical Surveys in the 2020s . . . 23
2.4.2 Complementarity with Sub-Orbital Measurements . . . 23
2.5 Signal Separation . . . 24
2.5.1 PICO Foreground Separation Methodology . . . 26
2.5.2 Results and Discussion . . . 26
2.6 Systematic Uncertainties . . . 27
2.6.1 List of Systematics . . . 28
2.6.2 Absolute polarization angle calibration . . . 29
2.6.3 Gain Stability . . . 30
2.6.4 Far-Sidelobe Pickup . . . 30
2.6.5 Key Findings . . . 30
2.7 Measurement Requirements . . . 31

3 Instrument **33**
3.1 Telescope . . . 33
3.2 Focal plane . . . 35
3.2.1 Low-frequency detectors . . . 35
3.2.2 High-frequency detectors . . . 36
3.2.3 Sensitivity . . . 36
3.3 Detector readout . . . 38
3.4 Thermal . . . 38
3.4.1 cADR Sub-K Cooling . . . 38
3.4.2 4 K Cooler . . . 39
3.4.3 Radiative cooling . . . 40
3.5 Instrument integration and test . . . 40

4 Design reference mission **40**
4.1 Concept of operations . . . 41
4.1.1 Mission design and launch . . . 41
4.1.2 Survey design . . . 42
4.2 Ground segment . . . 42
4.3 Spacecraft . . . 42
4.3.1 Attitude determination and control . . . 43

DRAFT

5 Technology maturation **44**
5.1 Current state of technologies . . . 44
5.1.1 Optical Coupling and Detectors . . . 44
5.1.2 Readout electronics status . . . 45
5.2 Development plan . . . 45
5.2.1 Detector development . . . 45
5.2.2 Readout electronics development . . . 46
5.3 Technology descopes . . . 46
5.4 Enhancing technologies . . . 47

6 Project management, heritage, risk, and cost **47**
6.1 PICO Study Participants . . . 47
6.2 Project management plan . . . 47
6.3 Heritage . . . 48
6.4 Risk assessment . . . 49
6.4.1 Pre-mission risks . . . 49
6.4.2 Development risks . . . 49
6.4.3 Operations risks . . . 49
6.5 Mission cost . . . 50

DRAFT

1 Executive Summary

The cosmic microwave background (CMB) comes to us from the furthest reaches of the observable Universe, and its photons experience all of cosmic history. Created when the Universe was a hotter, simpler place, CMB photons probe fundamental physics, provide exquisite measurements of the constituents of the cosmos, and tests of relativity. On their journey they feel the impact of the gravitational potentials formed from the assembling cosmic web of superclusters, clusters and galaxies. They interact with the ionized gas in the inter- and circum-galactic medium, gas that eventually fuels star and galaxy formation. Superposed upon the CMB is the emission from multiple extragalactic sources and from our Galaxy. All of this leaves an imprint which sensitive measurements can disentangle so that CMB studies impact essentially every aspect of cosmology and astrophysics.

Building upon a long legacy of successful measurements, the next decade holds tremendous potential for new, exciting CMB discoveries. Such discoveries, delivered by the Probe of Inflation and Cosmic Origins (PICO, Fig. 1.1), promise to be revolutionary, affecting physics, astrophysics, and cosmology. PICO is an imaging polarimeter that will scan the sky for 5 years with 21 frequency bands spread between 21 and 800 GHz; see Table 2.1. It will produce 10 independent full sky surveys of intensity and polarization with a final combined-map noise level equivalent to 3250 *Planck* missions for the baseline required specifications, though in our current best-estimate (CBE) it would perform as 6400 *Planck* missions. It will produce the first ever full sky polarization maps at frequencies above 350 GHz, and it will have diffraction limited resolution of 1' at 800 GHz.

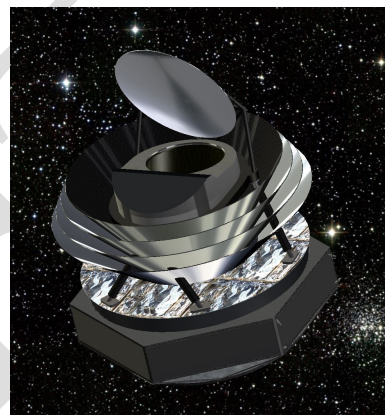

Figure 1.1: The PICO spacecraft

With these capabilities, unmatched by any other existing or proposed platform, PICO will have compelling and broad science deliverables. The mission will respond to seven science objectives (SOs), which are listed in Table 2.2. Delivering this set was the basis for selecting PICO's design and for setting instrument requirements. But PICO's science reach is far broader than the baseline set.

PICO could determine the energy scale of inflation and give a first, direct probe of quantum gravity; this is SO1 (§ 2.2.1). If the signal is not detected PICO will constrain broad classes of inflationary models, and exclude at 10σ models for which the characteristic scale in the potential is the Planck scale (SO1 and SO2). The combination of PICO with LSST can constrain features in the inflationary potential, the field content during inflation and could rule out all models of slow-roll single-field inflation, marking a watershed in studies of inflation.

The mission will have a deep impact on particle physics by measuring the expected sum of the neutrino masses in two independent ways, each with at least 4σ confidence, rising to 7σ if the sum is near 0.1 eV (SO3). this is not quite right; the cluster constraint will require follow up, so the second way is not from the mission The measurements will either detect or strongly constrain deviations from the standard model of particle physics by counting the number of light particles in the early universe at an energy range that is up to 400 times higher than available today this needs to be modified (SO4). The data will constrain dark matter candidates by pushing down *Planck* constraints on the dark matter annihilation cross section by a factor of 25, specifically at low energy scales that are not accessible to direct detection experiments. The data will probe the existence of cosmic fields that could give rise to cosmic birefringence. what about dark energy?

PICO will transform our knowledge of the structure and evolution of the universe. It will measure the redshift at which the universe reionized, impacting physical models describing when and how the first luminous objects formed (SO5). more quantitative regarding τ? It will make a map of the projected matter

DRAFT

throughout the universe with a signal-to-noise ratio exceeding 500. This will constrain the mass of dark matter halos hosting galaxies, groups, and clusters from the present day to the very first such objects. more quantitative? The map will be cross-correlated with other next-decade galaxy surveys, such as LSST, to measure the growth of large-scale structure with sub-percent precision. An extraordinary amount of information about the role of 'energetic feedback' on structure formation will come from correlating PICO's map of the thermal Sunyaev-Zel?dovich effect with galaxy and lensing maps from WFIRST and LSST. The correlation – forecast to have a signal-to-noise of 3000 with LSST weak lensing – will enable measurements in dozens of tomographic redshift bins, giving extraordinarily detailed information about the evolution of thermal energy injection over cosmic time.

Magnetic fields thread galaxies and affect their structure and evolution, but the origins of these magnetic fields is a hotly debated question. PICO will test whether galactic magnetic fields have been seeded by primordial magnetic fields of cosmic origin. It will map the entire Milky Way in polarization with unprecedented detail at many frequency bands. Such maps are not planned by any other survey, and can not be produced other than in space. From these unique maps we will strongly constrain the properties of the diffuse interstellar medium, including dust grain composition, temperature, and emissivities, and will map the Galactic magnetic field structure elucidating the relative roles of turbulence and magnetic fields in the observed low star formation efficiency (SO6 and SO7).

The cosmic infrared background (CIB) encodes information from star-formation, obscured or unobscured, across cosmic time and PICO will improve upon existing measurements of CIB clustering by an order of magnitude what is CIB clustering. By discovering 150,000 clusters, 50,000 proto-clusters (up to z=4.5), and 4500 strongly lensed galaxies (up to z=5), PICO will enable a unique view into early galaxy and cluster evolution. The window PICO provides because of its high frequency bands is entirely unique and not available to any other experiment. PICO's sub-mm maps will provide ancillary information (including polarization) for all future measurements anywhere on the sky. dark energy science removed; put back?

This scientifically ground-breaking mission is based on technologies that are being used actively today by ground- and balloon-based experiments, but over a more restricted range of frequency band. These technologies will continue to mature by a host of recently funded sub-orbital activities well before the mission's Phase-A. Section **??** now here include: single instrument, simple scan; need funding for foregrounds and systematics

All the implementation aspects are mature, benefiting from thousands of person-years of experience studying the sky at these wavelengths. These span over more than 50 years of mapping the CMB and include three enormously successful space missions. This combined experience unambiguously shows that the unlimited frequency coverage and thermally benign environment aboard a space-based platform give unparalleled capability to separate the combination of galactic and cosmological signals and to control systematic uncertainties. These qualities, which are critical ingredients for any next-decade experiment, make PICO the optimal platform for a next generation CMB experiment.

2 Science

2.1 Introduction

The Probe of Inflation and Cosmic Origins (PICO) is an imaging polarimeter designed to survey the entire sky at 21 frequency bands spread between 21 and 799 GHz. The telescope has an aperture of 1.4 meter giving diffraction limited resolution between $38'$ and $1'$. The instrument and mission requirements, which define our 'baseline' design, flow down from a set of seven key science objectives (SOs) listed in Table 2.2. The seven objectives derive from NASA's three science strategic goals: to explore how the Universe began; to discover how the Universe works; and to explore how the Universe evolved. This baseline design gives rise to a mission that will deliver an extraordinarily broad set of science targets, ranging from the physics of the early universe, to constraints on fundamental particles and fields, to cosmic structure formation, and to

DRAFT

Table 2.1: **Mission Specifications**

Bands	GHz	21	25	30	36	43	52	62	75	90	108	129	155	186	223	268	321	385	462	555	666	799
FWHM	arcmin	38.4	32.0	28.3	23.6	22.2	18.4	12.8	10.7	9.5	7.9	7.4	6.2	4.3	3.6	3.2	2.6	2.5	2.1	1.5	1.3	1.1
Polarization map depth																						
Baseline	μK_{CMB} arcmin	23.9	18.4	12.4	7.9	7.9	5.7	5.4	4.2	2.8	2.3	2.1	1.8	4.0	4.5	3.1	4.2	4.5	9.1	45.8	177.2	1047
Baseline	Jy/sr	8.3	10.9	11.8	12.9	19.5	23.8	45.4	58.3	59.3	77.3	96.0	119.1	433.1	604.2	433.4	577.8	429.1	551.1	1580	2075	2884
CBE[a]	μK_{CMB} arcmin	16.9	13.0	8.7	5.6	5.6	4.0	3.8	3.0	2.0	1.6	1.5	1.3	2.8	3.2	2.2	3.0	3.2	6.4	32.4	125.3	740.3
CBE[a]	Jy/s	5.9	7.7	8.3	9.2	13.8	16.8	32.1	41.3	41.8	53.5	69.3	83.7	301.5	436.3	303.5	411.1	303.1	387.3	1117	1467	2040

Cost: $100M Launch mass: 2147 kg
Mission length: 5 years Total power: 1526 W

Combined polarization map depth

0.87 μK_{CMB} equivalent to 3250 *Planck* Missions

0.61 μK_{CMB} equivalent to 6400 *Planck* Missions

[a] Current best estimate

Table 2.2: **Science Traceability Matrix (STM)**

Science Goals from NASA Science Plan	Science Objectives	Scientific Measurement Requirements: Model Parameters	Scientific Measurement Requirements: Physical Parameters	Scientific Measurement Requirements: Observables	Instrument (single instrument, single mode): Functional Requirements	Instrument (single instrument, single mode): Projected Performance	Mission Functional Requirements
Explore how the Universe began (Inflation)	SO1. Probe the physics of the big bang by detecting the energy scale at which inflation occurred if it is above 4×10^{15} GeV, or place an upper limit if it is below (§ 2.2.1)	Tensor-to-scalar ratio r: $\sigma(r)=1\times10^{-4}$ at $r=0$; $r<5\times10^{-4}$ at 5σ confidence level[a]	CMB polarization BB power spectrum for modes $2<\ell<300$ to cosmic-variance limit, and CMB lensing power spectrum for modes $2<\ell<1000$ to cosmic-variance limit	Linear polarization across $60<\nu<300$ GHz over entire sky; foreground separation requires $21<\nu<799$ GHz	Frequency coverage: central frequencies ν_c from 21 to 799 GHz. Frequency resolution: $\Delta\nu/\nu_c=25\%$. Sensitivity: See Table 2.1. Combined instrument noise: $<0.61\,\mu K_{CMB}\sqrt{s}$. Angular resolution [for delensing and foreground separation]: $\mathrm{FWHM}=6.2'\times(155\,\mathrm{GHz}/\nu_c)$. Effective aperture: 1.4 m. Sampling rate: $(3/\mathrm{BeamFWHM})\times(336'/\mathrm{s})$.	Frequency coverage: See Table 2.1. 21 bands with ν_c from 21 to 799 GHz. Frequency resolution: $\Delta\nu/\nu_c=25\%$. Sensitivity: See Table 2.1. Combined instrument noise: $0.43\,\mu K_{CMB}\sqrt{s}$. Angular resolution: See Table 2.1. $\mathrm{FWHM}=6.2'\times(155\,\mathrm{GHz}/\nu_c)$; $1.1'$ for $\nu_c=799$ GHz. Sampling rate: See Table 3.1. $(3/\mathrm{BeamFWHM})\times(336'/\mathrm{s})$	Sun-Earth L2 orbit with Sun-Probe-Earth $<15°$. 5 yr survey with $\geq95\%$ survey efficiency. Full sky survey: Spin instrument at 1 rpm; boresight 69° off spin axis; spin axis 26° off anti-Sun line, precessing 360° / 10hr. Pointing control: Spin axis $60'$ (3σ, radial). Spin 1 ± 0.1 rpm (3σ) Pointing stability: Drift of spin axis $<1'$/1min (3σ, radial); jitter $<20''$/20 ms (3σ, radial). Pointing knowledge (telescope boresight): $10''$ (3σ, each axis) from spacecraft attitude; $1''$ (1σ, total) final reconstructed; Return and process instrument data: 1.5 Tbits/day (after 4× compression) Thermally isolate instrument from solar radiation and from spacecraft bus
	SO2. Probe the physics of the big bang by excluding classes of potentials as the driving force of inflation (§ 2.2.1, Fig. 2.2)	Spectral index (n_s) and its derivative (n_{run}): $\sigma(n_s)<0.0015$; $\sigma(n_{run})<0.002$	CMB polarization BB power spectrum for modes $2<\ell<1000$ to cosmic-variance limit	Intensity and linear polarization across $60<\nu<220$ GHz over the entire sky			
Discover how the Universe works (neutrino mass and N_{eff})	SO3. Determine the sum of neutrino masses. (§ 2.2.1, Fig. 2.5)	Sum of neutrino masses (Σm_ν): $\Sigma m_\nu<15$ meV with DESI or Euclid[b]	CMB polarization BB power spectrum for modes $2<\ell<4000$ to cosmic-variance limit; CMB intensity maps (to give Compton Y map from which we extract clusters)				
	SO4. Tightly constrain the thermalized fundamental particle content of the early Universe (§ 2.2.1, Fig. 2.4)	Number of neutrino effective relativistic degrees of freedom (N_{eff}): $\sigma(N_{eff})<0.03$	CMB temperature and EE polarization power spectra $2<\ell<4000$ to cosmic-variance limit				
Explore how the Universe evolved (reionization)	SO5. Distinguish between models that describe the formation of the earliest stars in the Universe (§ 2.2.2, Fig. 2.6)	Optical depth to reionization (τ): $\sigma(\tau)<0.002$	CMB polarization EE power spectrum for modes $2<\ell<20$ to cosmic-variance limit	Linear polarization across $60<\nu<300$ GHz over entire sky; foreground separation enveloped by SO1			
Explore how the Universe evolved (Galactic structure and dynamics)	SO6. Constrain the temperatures and emissivities characterizing the Milky Way's interstellar diffuse dust (§ 2.2.3)	Intrinsic polarization fractions of the components of the diffuse interstellar medium to accuracy better than 3% when averaged over $10'$ pixels	Fractional polarization and intensity as a function of frequency	Intensity and linear polarization maps in 12 frequency bands between 108 and 799 GHz.	Enveloped by SO1–4, except: Angular resolution: $\leq1.1'$ (at highest frequency) Sensitivity at 799 GHz: 27.4 kJy/sr		
	SO7. Determine if magnetic fields are the dominant cause of low Galactic star-formation efficiency (§ 2.2.3)	Ratio of cloud mass to maximum mass that can be supported by magnetic field ("Mass to flux ratio" μ); ratio of turbulent energy to magnetic energy (Alfvén Mach number $\mathscr{M}_A$) on scales 0.05–100 pc	The turbulence power spectrum on scales 0.05–100 pc; magnetic field strength (B) as a function of spatial scale and density; hydrogen column density; gas velocity dispersion	Intensity and linear polarization with <1 pc resolution for thousands of molecular clouds and with <0.05 pc for the 10 nearest molecular clouds; maps of polarization with 1' resolution over the entire sky			

[a] The values predicted include delensing and foreground subtraction; see Section 2.2.1.
[b] Using the PICO τ and BB lensing power spectrum, and BAO from DESI or Euclid. The same strength constraint can be derived independently using clusters detected by PICO, if their redshift becomes available, and using σ_8 from LSST.

DRAFT

Galactic science. Science targets that are beyond the seven SOs are summarized in Table ??.

The PICO implementation, with 12,996 transition edge sensor (TES) bolometric detectors in a focal plane maintained at a temperature of 0.1 K, contains a margin of 40% in detector noise. Experience with past space missions, most recently with *Planck*, shows that pre-mission calculated detector performance is in fact achieved in space [1, 2]. We therefore include throughout this report performance estimates that are based both on the baseline design and on our current estimate for the actual performance. Those are labeled current best estimate (CBE). Table 2.1 gives the frequency bands, resolution, both baseline and CBE noise levels, as well as other key mission parameters.

The transformative science that PICO will deliver is enabled through the implementation of a single instrument that scans the sky with a 1.4 m entrance aperture, two-reflector telescope. The instrument scans the sky in a single, simple, repeated pattern for the entire duration of the 5-year mission. The entire sky is scanned every 6 months giving 10 independent full sky maps of intensity (T) and polarization (Stokes Q and U). The scan pattern is optimized for polarization measurements as each sky pixel is scanned in multiple orientations. Therefore full-sky maps of the Stokes parameters can be reconstructed from the data of each of the 12,996 polarization sensitive detectors words about 1/f?.

Some of the PICO science goals are more appropriately described in terms of E and B polarization maps rather than Q and U[1]. This is because sources of polarization signatures that are scalar in nature, such as primordial density perturbations, can only produce E-mode polarization. Sources that are tensor in nature, such as gravity waves, can produce both E- and B-mode polarization. The angular power spectra of E and B maps will be denoted as EE and BB.

This report assumes that PICO's phase A will start in 2023. The science outcomes are expected to break new ground, and to be complementary to data sets available at the end of 2020s and the beginning of the following decade. Throughout the report we are including performance comparisons to funded projects that are in implementation and for which final design specifications and projections exist in the literature. Such next generation CMB experiments are collectively denoted as Stage-III (S3).

now here

say something about Stage3

between with a polarization sensitivity that is 57 or 82 times that of the *Planck* mission for the PICO baseline and current best estimate (CBE) configurations, respectively.

Lensing of the CMB photons by structures as they traverse the Universe provides a projected map of all the matter in the Universe from the epoch of decoupling until today. The non-zero mass of neutrinos affects the clustering of matter and thus can be inferred from maps of the projected matter distribution. The quantity that can specifically be inferred is the sum of the neutrino masses. The current constraint from the combination of *Planck* and large-scale structure data is $\sum m_\nu < 0.12$ eV (95%). This is approaching the minimum summed mass allowed in the inverted neutrino hierarchy of ≈ 0.1 eV and is within a factor of two of the minimal mass allowed in the normal hierarchy of ≈ 0.06 eV. A detection thus appears imminent. However, the precision of determining the neutrino mass scale, using the CMB or *any* other cosmological probe, is limited by knowledge of τ, due to the strong degeneracy between τ and the amplitude of matter fluctuations. PICO's map of the projected matter, with signal-to-noise ratio (SNR) exceeding 500 – a result of its low noise and high angular resolution – *and* its own cosmic-variance-limited measurement of τ, will give a 4σ detection of $\sum m_\nu$ in the normal hierarchy, rising to 7σ for the inverted hierarchy; see SO3.

The CMB offers a unique window into the thermal history of the Universe, from the time of reheating through today. It is during these eras that the matter and radiation that fill the Universe were produced and evolved to form the structures observed at low redshifts. Measurements of the CMB on small angular scales are sensitive to the many components that make up the Universe including the baryons, cosmic neutrinos, dark matter, and a wide variety of particles motived by extensions of the Standard Model. The Standard Model of particle physics posits three neutrino families, but it also allows for additional light, relativistic

[1] For full sky maps the representation is equivalent.

DRAFT

particles, if they existed early enough during the evolution of the Universe. We count the total number of light particles thermalized in the early Universe using $N_{\rm eff}$. Light particles thermalized in the early Universe leave a universal contribution to $N_{\rm eff}$ that is sensitive to the freeze-out temperature and the spin of the particle. The current *Planck* measurement of $N_{\rm eff} = 2.99 \pm 0.17$ (1σ) is sensitive to particles thermalized after the QCD phase transitions. PICO's measurement with $\sigma(N_{\rm eff}) = 0.03$ (SO4), enabled by low noise levels, high resolution, and full-sky coverage, will reach back to times when the temperature of the Universe was orders of magnitude hotter than we have probed today, and a period that is still largely unexplored.

These same experimental features are advantageous not only for $N_{\rm eff}$ but for any new physics with signatures on the CMB. Of particular interest is the nature of dark matter and its interactions. PICO will place constraints that are more than one order of magnitude stronger than *Planck* for a dark matter particle of MeV mass range, which can not be probed by direct detection experiments. PICO will thus reveal important clues to the nature of the fundamental physical laws and our cosmic origins.

Secondary anisotropies in the CMB[2] provide a wealth of information on the growth and evolution of structure in our Universe. CMB lensing, the thermal and kinematic Sunyaev-Zel′dovich (SZ) effects, and extragalactic point sources all contribute significantly to the CMB intensity fluctuations on small angular scales (note that lensing is also present in polarization fluctuations). Immense progress in mapping these sources is enabled by PICO's depth, broad frequency coverage, and relatively high resolution. The all-sky, projected mass map reconstructed from CMB lensing that PICO will provide can be correlated with tracers of large-scale structure to tomographically probe the growth of structure at unprecedented SNR levels. The thermal SZ effect provides a map of the integrated free-electron pressure along the line of sight, and the peaks in this map trace the locations of all galaxy clusters in the Universe. PICO will find all the massive, virialized, galaxy clusters at any redshift. The epoch of reionization imprints information on the statistical moments of the kinematic SZ signal. The combination of these kSZ statistical moments with the cosmic-variance-limited τ measurement from PICO will provide tight constriants on the global properties of the sources responsible for reionization of the Universe.

Our understanding of magnetic fields is rooted in observations of the very local Universe: the Milky Way and nearby galaxies. Magnetic fields are observed to be a foremost agent of the Milky Way's ecology. Understanding the Milky Way's magnetic field is crucial for making progress on important issues in the astrophysics of galaxies: the dynamics and energetics of the multiphase interstellar medium; the efficiency of star formation; the acceleration and propagation of cosmic rays; and the impact of feedback on galaxy evolution. Through its detailed high-resolution polarization measurements of Galactic dust emission, PICO will produce an unprecedented data set, mapping Galactic magnetic fields and providing answers to these questions (SO7).

Learning about magnetic fields has impact beyond understanding the dynamics and evolution of galaxies. The very origin of magnetic fields in galaxies, and their possible evolution from primordial, early Universe cosmic magnetic fields is a topic of intense debate. PICO is poised to provide definitive answer as to whether early Universe magnetic fields provide the seeds for the magnetic fields observed in most current galaxies.

The magnetized ISM in the solar neighborhood presents a challenge for the investigation of cosmological signals. The signals of interest, such as CMB B-mode polarization, CMB spectral distortions, and 21cm line emission from the cosmic dawn and the reionization epoch, are obscured by Galactic dust and synchrotron emission that can be orders of magnitude brighter. PICOs detailed mapping of these signals will strongly constrain the physical properties of the ISM and thus models of dust grain composition, temperature, and emissivities (SO6). In addition, this significantly improved understanding of the physics of the ISM will feed back into improving foreground removal that is essential for supporting other PICO science goals.

The PICO deep and high resolution maps will yield a treasure trove of point sources that will be mined for years. The mission will provide a full-sky catalog of tens of thousands of extragalactic millimeter and

[2]Secondary anisotropies arise from sources other than primordial density and inflationary gravity wave (IGW) fluctuations

DRAFT

sub-millimeter point sources, which are beacons for active galactic nuclei (in the radio) and dust emission from vigorously star-forming galaxies at $z \sim 2$ and earlier (in the far-IR).

2.2 Science Objectives

2.2.1 Fundamental Physics

Gravitational waves and Inflation

• **Targets** Measurements of the CMB together with Einstein's theory of general relativity imply that the observed density perturbations must have been created long before the CMB was released, and rather remarkably even before the Universe became filled with a hot and dense plasma of fundamental particles. Understanding the mechanism generating these perturbations, which evolved to fill the Universe with structures, is one of the most important open questions in cosmology. In addition to density perturbations, this mechanism may have also produced gravitational waves that would have left a B-mode polarization signature in the CMB [3, 4]. Any detection of primordial B-mode polarization by PICO will constitute evidence for gravitational waves from the same primordial period that created the density perturbations and will open a new window onto this early epoch. Because the dynamics of gravitational waves is essentially unaffected by the plasma, they would be a pristine relic from the earliest moments of our Universe, and their properties would shed light on the mechanism that created the primordial perturbations.

Inflation, a period of nearly exponential expansion of the early Universe [5–8], is the leading paradigm explaining the origin of the primordial density perturbations [9–13]. It predicts a nearly scale invariant spectrum of primordial gravitational waves originating from quantum fluctuations [14]. Measurements of the CMB are the only foreseeable way to detect these gravitational waves.

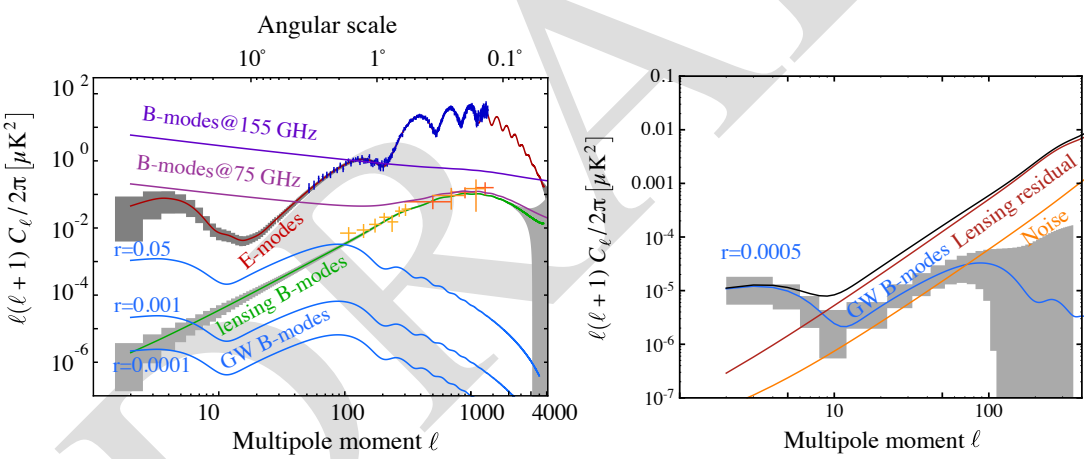

Figure 2.1: With PICO's baseline configuration we will measure the EE (left, red) and lensing BB (green) angular power spectra with high precision (grey). PICO's goal is to detect $r = 5 \times 10^{-4}\,(5\sigma)$ (right, grey). This forecast includes PICO's 80% delensing (red) and foreground separation. The baseline noise level (right, orange) allows detection of even lower levels; we expect foreground separation to limit performance. As an example we show the BB spectra of Galactic emission on the cleanest 60% of the sky at 75 and 155 GHz (left, purple). They largely dominate the cosmological signals. Also shown are measurements of lensing from current experiments (left, orange) [15–18], *Planck*'s EE measurements (left, dark blue) [19], and the BB spectrum produced by IGW with different values of r (cyan).

The strength of the signal, quantified by the tensor-to-scalar ratio r, is a direct measure of the expansion rate of the Universe during inflation. Together with the Friedmann equation, it reveals one of the most important characteristics of inflation: its energy scale.[3] A detection of r "would be a watershed discovery",

[3] In some models of inflation the one-to-one correspondence between r and the energy scale of inflation does not hold because there are additional sources of gravitational waves [20]. However, in these models the signal is highly non-Gaussian and could be distinguished from quantum fluctuations.

DRAFT

a quote from the 2010 decadal panel report [21]. The combination of data from *Planck* and the BICEP/Keck Array give the strongest constraint to date, $r < 0.06\,(95\%)$ [22]. Next decade S3 efforts strive to reach $\sigma(r) = 2 \times 10^{-3}$ [23, 24].

PICO's goal is to detect primordial gravitational waves if inflation occurred at an energy scale of at least 5×10^{15} GeV, or equivalently $r = 5 \times 10^{-4}\,(5\sigma)$ (SO1 in Table 2.2 and Figure 2.1). A detection will have profound implications for fundamental physics because it will provide evidence for a new energy scale tantalizingly close to the energy scale associated with grand unified theories, probe physics at energies far beyond the reach of terrestrial colliders, and be the first observation of a phenomenon associated with quantum gravity [25].

There are only two classes of slow-roll inflation in agreement with current data that naturally explain the observed value of the spectral index of primordial fluctuations n_s [26]. The first class is characterized by potentials of the form $V(\phi) \propto \phi^p$. This class includes many of the simplest models of inflation, some of which have already been strongly disfavored by existing observations. Select models in this class are shown as blue lines in Fig. 2.2. If the constraints on n_s tighten by about a factor of two with the central value unchanged, and the upper limit on r improves by an order of magnitude, this class would be ruled out.

The second class is characterized by potentials that approach a constant as a function of field value, either like a power law or exponentially. Two representative examples in this class are shown as the green and gray bands in Fig. 2.2. This class also includes R^2 inflation, which predicts a tensor-to-scalar ratio of $r \sim 0.004$. All models in this class with a characteristic scale in the potential that is larger than the Planck scale predict a tensor-to-scalar ratio of $r \gtrsim 0.001$.

Many microphysical models in this class possess a characteristic scale that is super-Planckian. PICO will either detect gravitational waves with high confidence or will exclude all models with a Planckian characteristic scale with high significance. But not all models have a super-Planckian characteristic scale. The Goncharov-Linde model is an example with a somewhat smaller characteristic scale. It predicts a tensor-to-scalar ratio of $r \sim 4 \times 10^{-4}$ [27], still within reach of PICO. In addition, there are models with significantly smaller values that are out of reach, but distinguishing between models with sub- and super-Planckian characteristic scales would provide much needed guidance to discriminate between classes of ideas for the earliest moments of our universe.

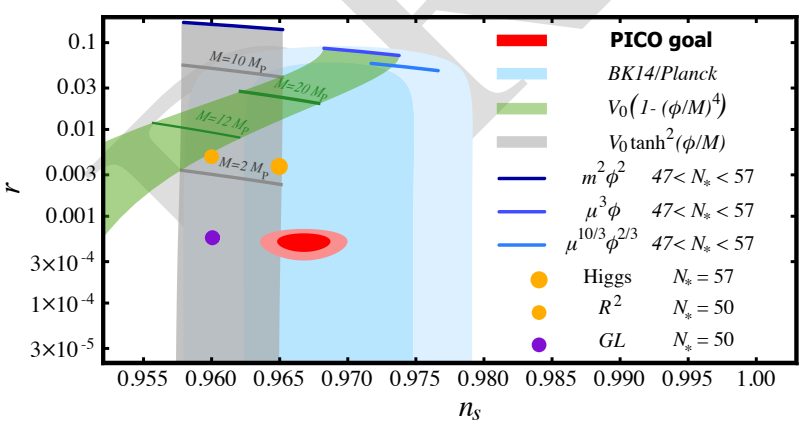

Figure 2.2: Current 1σ and 2σ limits on r and n_s (cyan) and forecasted constraints for a fiducial model with $r = 0.0005$ for PICO together with predictions for selected models of inflation. Characteristic super-Planckian scales in the potentials are marked with darker lines.

• **Observational Considerations** The *BB* angular power spectrum measured by PICO will have contributions by Galactic sources of emission and 'lensing' *B*-modes, created by gravitational lensing of *E*-modes as the CMB photons traverse the gravitational potentials throughout the Universe (Fig. 2.1). In case of an r detection, there will be two additional features due to the inflationary signal. One is the 'recombination peak' at $\ell \sim 80$ and the other is the 'reionization peak' at multipoles of $\ell \lesssim 10$.

The Galactic signals act as foregrounds and uncertainty in the characterization of these foregrounds

DRAFT

already now limits our ability to constrain r. PICO's goal for reaching $\sigma(r) = 1 \times 10^{-4}$ is driven by estimates of the efficacy of foreground separation, not noise. An analytic performance forecast accounting for PICO's statistical noise level and a foreground model that has polarized emission from two components of dust, synchrotron radiation, and correlations between synchrotron and dust emission, gives $\sigma(r) = 2 \times 10^{-5}$, five times lower than our baseline goal. Our goal is set based on end-to-end, map-based simulations, which include physical effects known to exist but not captured in the analytic forecasts; see Section 2.5.

When the tensor-to-scalar ratio $r \simeq 0.01$, the *BB* lensing and inflation spectra are comparable in magnitude at the recombination peak ($\ell \sim 80$). For lower levels of r, the lensing *B*-mode dominates, but the *B*-mode maps can be 'delensed' if the polarization maps are measured with few-arcmin resolution and sufficient depth [28, 29]. Forecasts for PICO show that at least 73% of the lensing *B*-mode power can be removed for the baseline configuration, after accounting for Galactic foreground separation. As much as 84% will be removed for the CBE and for milder foreground contamination. For measuring the recombination peak, delensing is essential to reach PICO's limits on r, and this was a driver in choosing the resolution of the instrument.

For the levels of r targeted by PICO, the *BB* reionization signal ($\ell \sim 5$) has somewhat higher level than the lensing spectrum, but the map-level foregrounds at this angular scale are at least two orders of magnitude brighter. PICO's instrument temporal stability, absence of atmospheric noise, full-sky coverage, and unmatched capability to characterize and separate foregrounds make it the most suitable instrument to measure these lowest multipoles. No S3 experiments have measured or plan to measure *B*-modes at $\ell < 40$ that reach to $\sigma(r) < 0.006$ at the lowest multipoles [30, 31].

If an inflationary *B*-mode signal is detected, it is important to characterize its entire ℓ dependence, in both the predicted reionization and recombination peaks. Furthermore, the strongest constraints on r are obtained when using all available ℓ modes. And the PICO full sky coverage will enable detection of the recombination peak in several independent patches of the sky, giving an important systematic cross-check.

• **Scalar Spectral Index and Non-Gaussianity** Models of the early Universe differ in their predictions for the scalar spectral index n_s and its scale dependence $n_{\rm run}$. PICO will improve n_s and $n_{\rm run}$ constraints by a factor of three relative to *Planck* and will thus have more discriminating power between different models.

The simplest models of inflation predict primordial fluctuations that are very nearly Gaussian. But only certain classes of multi-field inflation produce a level of non-Gaussianity large enough to exceed $f_{NL} = 1$, where f_{NL} is a parameter quantifying the level of non-Gaussianity (Fig. 2.3). PICO will probe the statistical properties of the primordial perturbations over a wide range of scales and will improve constraints on departures from Gaussianity by a factor of two to three depending on the precise form of the departure from non-Gaussianity. By cross-correlating the lensing map with large-scale structure data from LSST it may even be possible to reach a theoretically important threshold (see, e.g. [32] and references therein) and constrain local non-Gaussianity to better than $\sigma(f_{NL}) = 1$.

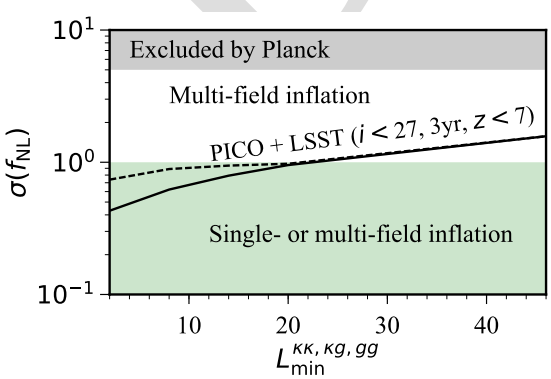

Figure 2.3: Forecasted sensitivity to the parameter describing primordial non-Gaussianity of the local type for the PICO CMB lensing map together with three years of the LSST survey, as a function of the minimal multipole used in the analysis ($f_{\rm sky} = 50\%$). A value of $\sigma(f_{\rm NL}) \simeq 1$ is a well-motivated theoretical target.

One can use correlations between large-scale structure tracers with different clustering bias factors and measure the relative difference between their clustering power spectra to effectively cancel cosmic vari-

DRAFT

ance [33, 34]; this can constrain physics that affects the biasing of objects on large scales, such as primordial local non-Gaussianity [35]. In Fig. 2.3 we show the expected constraints for the CMB lensing field as reconstructed with PICO, in cross-correlation with three years of the LSST survey. It can be seen that depending on the minimal multipole that can be used in the cross correlation, which is uncertain in both LSST and the PICO lensing map, the well-motivated theory target of $\sigma(f_{\rm NL}) \simeq 1$ [32] can be within reach. Values of $f_{\rm NL}$ at or above this level are a generic prediction of multi-field inflationary models.

Fundamental Particles: Light relics, Dark Matter, and Neutrinos

• **Light Relics** In the inflationary paradigm, the Universe was reheated to temperatures of at least 10 MeV and perhaps as high as 10^{12} GeV. At these high temperatures, even very weakly interacting or very massive particles, such as those arising in extensions of the Standard Model of particle physics, can be produced in large abundances [36, 37]. As the Universe expands and cools, the particles fall out of equilibrium, leaving observable signatures in the CMB power spectra. Through these effects the CMB is a sensitive probe of neutrino and of other particles' properties.

One particularly compelling target is the effective number of light relic particle species $N_{\rm eff}$. The canonical value with three neutrino families is $N_{\rm eff} = 3.046$. Additional light particles contribute a change $\Delta N_{\rm eff}$ that is a function only of the decoupling temperature and the effective degrees of freedom of the particle, g. The magnitude of $\Delta N_{\rm eff}$ is quite restricted, even for widely varying decoupling temperatures T_F. A range $0.027\,g \leq \Delta N_{\rm eff} \leq 0.07\,g$ corresponds to a range in T_F spanning decoupling during post-inflation reheating ($0.027g$) down to lower T_F with decoupling occurring just prior to the QCD phase transition ($0.07g$).

Information about $N_{\rm eff}$ is gleaned from the TT and EE power spectra. For an experiment like PICO, which has sufficient resolution to reach cosmic-variance-limited measurement[4] of EE up to $\ell = 2300$, the two additional most important parameters for improving constraints are the fraction of sky observed $f_{\rm sky}$ and the noise (Fig. 2.4, left). The PICO baseline will use data from 70% of the sky to constrain $\Delta N_{\rm eff} < 0.06\,(95\%)$. [5] This constraint, which is a factor of 4.7 improvement relative to *Planck* ($\Delta N_{\rm eff} < 0.28$, 95%) and will not be matched by any currently funded effort, opens up a new range of temperatures in which to detect the signature of light relic species. If no new species are detected, then the lowest temperature T_F at which any particle with spin could have fallen out of equilibrium will move up by a factor of 400 (Fig. 2.4, right).

While our theoretical target for $N_{\rm eff}$ is defined by particles that decoupled long before neutrinos did, there are a number of well-motivated scenarios in which the thermal evolution of the Standard Model is altered after the time of neutrino decoupling. These scenarios will change the relationship between $N_{\rm eff}$ as measured in the CMB relative to the value of $N_{\rm eff}$ that affects BBN and the production of helium, which is quantified through the helium fraction Y_p. For example, the decay of a thermal relic into photons after nucleosynthesis would reduce $N_{\rm eff}$ in the CMB but would could leave Y_p unaltered from its Standard Model value. PICO will make a simultaneous measurement of $N_{\rm eff}$ and Y_p with $\sigma(N_{\rm eff}) = 0.08$ and $\sigma(Y_p) = 0.005$, respectively, giving a 2% uncertainty on the value of Y_p. These uncertainties are equivalent to those available with other astrophysical measurements, but the systematic uncertainties are entirely different. Systematic uncertainties currently limit our knowledge of Y_p.

• **Dark Matter** Cosmological measurements have already confirmed the existence of one relic that lies beyond the Standard Model: dark matter. CMB experiments are effective in constraining dark matter candidates in the lower mass range, which is not available for terrestrial direct detection experiments [38, 39].

Interactions between dark matter and protons in the early Universe create a drag force between the two cosmological fluids, damping acoustic oscillations and suppressing power in density perturbations on small

[4] A measurement is cosmic-variance-limited when the measurement uncertainty is dominated by the statistics of observing the finite number of Fourier modes available in our Universe.

[5] The CMB EE and the Galactic foregrounds EE and BB spectra are comparable in level (Fig. 2.1). With 21 frequency bands PICO should be able to separate signals at the mild levels necessary for 70% of the sky.

DRAFT

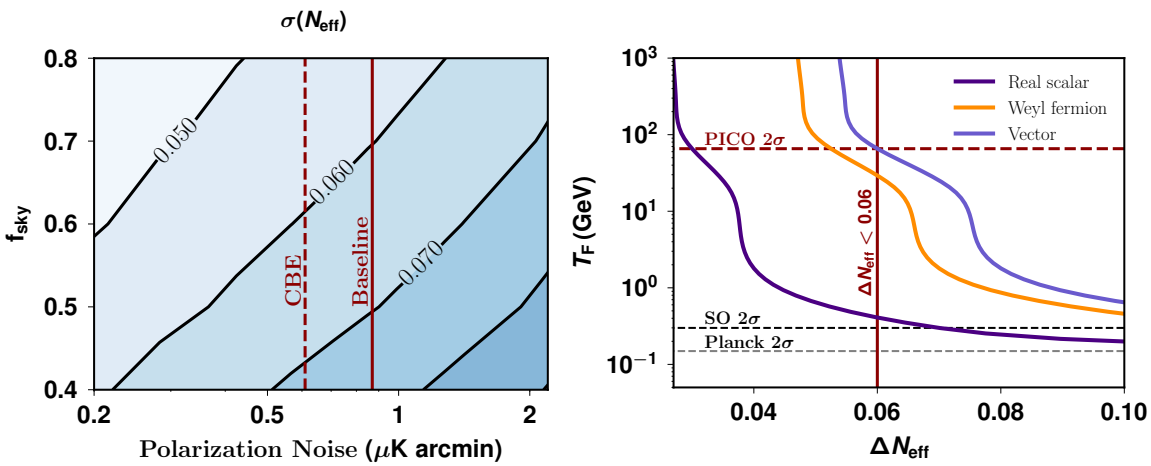

Figure 2.4: PICO will achieve a constraint $\Delta N_{\rm eff} < 0.06\,(95\%)$ (left, 1σ contours shown) in the baseline configuration (vertical solid) using its cosmic-variance-limited measurement of EE for $\ell \leq 2300$, and 21 frequency bands to utilize data over 70% of the sky ($5'$ resolution assumed) . This constraint translates to moving up the lowest decoupling temperature T_F for vector, Weyl Fermion, and scalar particles by a factor of 400, 200, and 6, respectively, relative to *Planck* (right, dash black, only T_F for vector particle is shown). We also show the projected vector particle limit for the Simons Observatory [23].

scales. As a result, the CMB temperature, polarization, and lensing power spectra are suppressed at high multipoles relative to a Universe without such drag forces. This effect has been used to search for evidence of dark matter-proton scattering over a range of masses, couplings, and interaction models [40–47], to test the possibility of an interacting dark-matter sub-component [46], and to provide consistency tests of dark matter in the context of the anomalous 21-cm signal reported by the EDGES collaboration [46, 48–50].

PICO's constraining power comes primarily from making high SNR maps of the lensing-induced deflections of polarized photons, which are discussed in Section 2.2.2. For a spin-independent velocity-independent contact-interaction, chosen as our fiducial model, PICO will improve upon *Planck*'s dark matter cross-section constraints by a factor of 25 over a broad range of candidate masses that will not be probed by direct detection experiments (Fig. 2.5, right).

Axion is another dark matter candidate that is well motivated by string theory [52], and that is consistent with straightforward extensions of the standard model of particle physics [53–55]. For an axion mass in the intermediate range $10^{-30} < m_a < 10^{-26}$ eV, current measurements constrain its fraction to be equal to or less than 2% of the total dark matter density. If 2% of the total dark content is made of axions, PICO's measurement of the TT, TE and EE spectra with additional constraints from the lensing reconstruction will give a 6σ detection, a factor of 10 improvement relative to *Planck*, profoundly shaping our understanding of the nature of dark matter and its small-scale clustering. "

• **Neutrino Mass** The origin and structure of the neutrino masses is one of the great outstanding questions about the nature of the Standard Model particles. Cosmology offers a measurement of the sum of the neutrino masses $\sum m_\nu$ through the gravitational influence of the non-relativistic cosmic neutrinos. The current measurement of $N_{\rm eff} = 2.99 \pm 0.17$ [56] already confirms the existence of these neutrinos at $> 10\sigma$ and their mass implies that they will contribute to the matter density at low redshifts. The best current mass constraint arises from a combination of *Planck* and BOSS BAO giving $\sum m_\nu < 0.12$ eV (95%) [56]. should we say 'and their minimal mass implies that they will contribute at least 3%(?) of the total matter density at low..

Cosmological measurements are primarily sensitive to the suppression of power on small scales after the neutrinos become non-relativistic, which can be measured via CMB lensing, or weak lensing in galaxy surveys. However, these measurements are limited by our knowledge of the amplitude of the primordial fluctuation power spectrum A_s because they only constrain the combination $A_s e^{-2\tau}$. Although many surveys

DRAFT

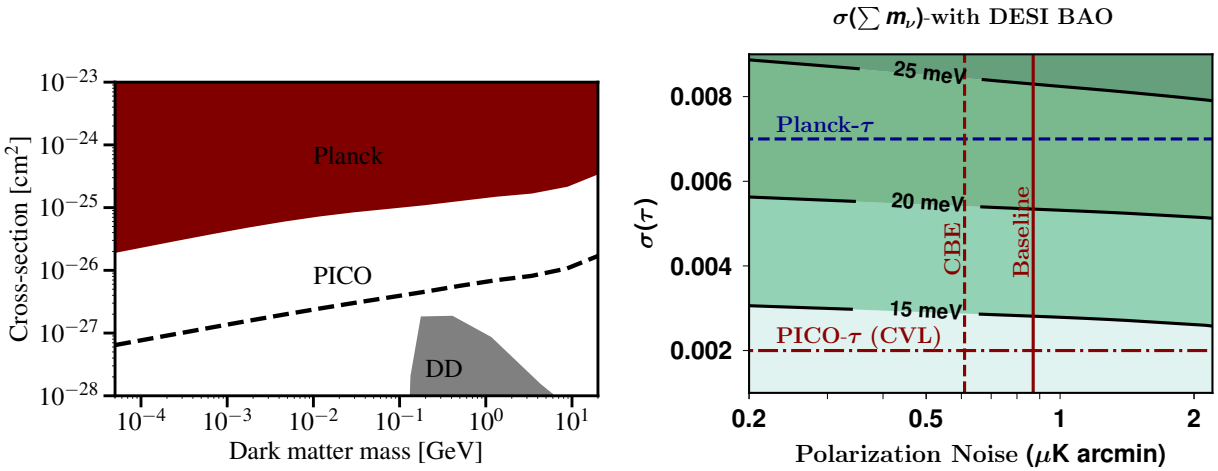

Figure 2.5: **Left:** PICO will give a factor of 25 more stringent constraint on spin-independent velocity-independent dark matter scattering cross-section (dash) relative to current *Planck* 95% confidence limit (red) [43]. Terrestrial direct detection experiments are expected to give complementary and stronger constraints, but only for the higher dark matter masses (grey) [51]. **Right:** Using cosmic-variance-limited (CVL) measurement of τ, $\sigma(\tau) = 0.002$, BAO information from DESI, and 21 frequency bands to separate foregrounds over 70% of the sky, PICO will reach $\sigma(\Sigma m_\nu) = 14$ meV giving at least 4σ detection of the minimal expected sum of neutrino masses $\Sigma m_\nu = 58$ meV.

hope to detect $\sum m_\nu$, any detection of the minimum value expected from particle physics, $\sum m_\nu = 58$ meV, at more than 2σ will require a better measurement of τ.

The best constraints on τ come from the EE spectrum at $\ell < 10$, which require measurements over the largest angular scales, and good separation of Galactic foreground sources of emission. The current limit of $\sigma(\tau) = 0.007$ is from *Planck* [57]. I notice we are quoting Planck2016; are there newer constraints With the current uncertainty in τ one is limited to $\sigma(\sum m_\nu) \gtrsim 25$ meV, after including forthcoming BAO information (Fig. 2.5, right); no other survey or cosmological probe will improve this constraint, unless a more accurate measurement of τ is made. One of the S3 experiments is attempting to measure the lowest ℓ's [30]. A space mission with its access to the entire sky and broad frequency coverage is the most suitable platform for the measurement. PICO will reach the cosmic-variance limit uncertainty on τ, $\sigma(\tau) \sim 0.002$, and will therefore reach $\sigma(\sum m_\nu) = 14$ meV when combined with measurements of BAO from DESI or Euclid [58] (PICO alone would reach $\sigma(\sum m_\nu) = 43$ meV). This measurement will give a 4σ detection of the minimum sum.

Fundamental Fields: Primordial Magnetic Fields and Cosmic Birefringence

• **Primordial Magnetic Fields** One of the long-standing puzzles in astrophysics is the origin of observed 1-10 μG galactic magnetic fields [59]. Producing such fields through a dynamo mechanism requires a primordial seed field [60]. Moreover, μG-strength fields have been observed in proto-galaxies that are too young to have gone through the number of revolutions necessary for the dynamo to work [61]. A primordial magnetic field (PMF), present at the time of galaxy formation, could provide the seed or even eliminate the need for the dynamo altogether. Specifically, a 0.1 nG field in the intergalactic plasma would be adiabatically compressed in the collapse to form a $\sim$1 μG galactic field [62]. PMFs could have been generated in the aftermath of phase transitions in the early Universe [63], during inflation [64, 65], or at the end of inflation [66]. A detection of PMFs with the CMB would be a major discovery as it would establish the magnetic field's primordial origin, signal new physics beyond standard models of particle physics and cosmology, and discriminate among different theories of the early Universe [67–69].

The current CMB bounds on PMF strength are $B_{1\mathrm{Mpc}} < 1.2$ nG at 95% CL for the scale-invariant PMF

DRAFT

spectrum [70], based on measurements of the TT, TE, EE and BB spectra.[6] The much more accurate measurement of BB by PICO would only marginally improve the PMF bound because CMB spectra scale as $B^4_{1\mathrm{Mpc}}$. However, Faraday rotation provides a signature that scales linearly with the strength of PMF [71]. It converts CMB E modes into B modes, generating mode-coupling EB and TB correlations. So far this signature was out of reach because prior experiments did not have sufficient sensitivity. Using Faraday rotation, PICO will probe PMFs as weak as 0.1 nG (1σ), a limit that already includes the effects of imperfect lensing subtraction, Galactic foregrounds [72–74], and other systematic effects. With this limit, which is a factor of five stronger than achievable with S3 experiments, PICO will conclusively rule out the purely primordial (i.e, no-dynamo driven) origin of the largest galactic magnetic fields.

• **Cosmic Birefringence** A number of well-motivated extensions of the Standard Model involve (nearly) massless axion-like pseudo-scalar fields coupled to photons via the Chern-Simons interaction term [75–78]. These couplings also generically arise within quintessence models for dark energy [77], chiral-gravity models [79], and models that produce parity-violation during inflation [80]. Regardless of the source of the parity-violating coupling, its presence may cause cosmic birefringence–a rotation of the polarization of an electromagnetic wave as it propagates across cosmological distances [77, 81, 82]. Cosmic birefringence converts primordial E-modes into B-modes, producing TB and EB cross-correlations whose magnitude depends on the statistical properties of the rotation field in the sky [83–85]. Previous studies have constrained both a uniform rotation angle as well as anisotropic rotation described by a power spectrum [85]. The current bound on a uniform angle is 30 arcmin (68%) [86], and the bound on the amplitude of a scale-invariant rotation angle spectrum is 0.11 deg^2 (95%) [87]). Using the combination of 5 bands in the $70-156$ GHz range, PICO will reduce the 95% CL bound on the uniform rotation angle by a factor of 300 to $0.1\,'$. The 95% CL bound on the amplitude of a scale-invariant rotation spectrum will be reduced by a factor of 275 to 4×10^{-4} deg^2, giving important constraints on string-theory-motivated axions [88, 89].

2.2.2 Cosmic Structure Formation and Evolution

The Formation of the First Luminous Sources A few hundred million years after the Big Bang, the neutral hydrogen gas permeating the Universe was reionized by photons emitted by the first luminous sources to have formed. The nature of these sources and the exact history of this epoch are key missing links in our understanding of structure formation (SO5).

The reionization of the Universe imprints multiple signals in the temperature and polarization of the CMB. In polarization, the most important signature is an enhancement in the EE power spectrum at large angular scales $\ell \lesssim 10$ (Fig. 2.1). This signal gives a direct measurement of the optical depth to the reionization epoch τ and thus to the mean redshift of reionization z_{re}, with very little degeneracy with other cosmological parameters (Fig. 2.6).[7] *Planck*'s determination of the optical depth to reionization $\tau = 0.054 \pm 0.007\,(1\sigma)$ has indicated that reionization concluded by $z \approx 6$, but the measurement uncertainty leaves many unanswered questions including: were the ionizing sources primarily star-forming galaxies or more exotic sources such as supermassive black holes or annihilating dark matter? What was the mean free path of ionizing photons during this epoch? What was the efficiency with which such photons were produced by ionizing sources? Did the reionization epoch extend to $z \approx$ 15-20, as has been claimed recently? [90] PICO's cosmic-variance-limited measurement of the large-scale E modes reaching $\sigma(\tau) = 0.002$ will settle some of these questions and will significantly constrain the others.

Figure 2.6 presents forecasts for reionization constraints in the $z_{re} - \Delta z_{re}$ parameter space. These are obtained from PICO's measurement of τ in combination with S3 experiments measurements of the "patchy" kinematic Sunyaev-Zel′dovich (kSZ) effect, due to the peculiar velocities of free electron bubbles around ionizing sources [91]. The figure includes curves of constant efficiency of production of ionizing photons

[6] It is conventional to quote limits on the PMF strength smoothed over a 1 Mpc region in comoving units, *i.e.* rescaled to $z = 0$: $\mathbf{B}_{\mathrm{today}} = a^2\mathbf{B}(a)$.

[7] The mean redshift to reionization is the redshift when 50% of the cosmic volume was reionized.

DRAFT

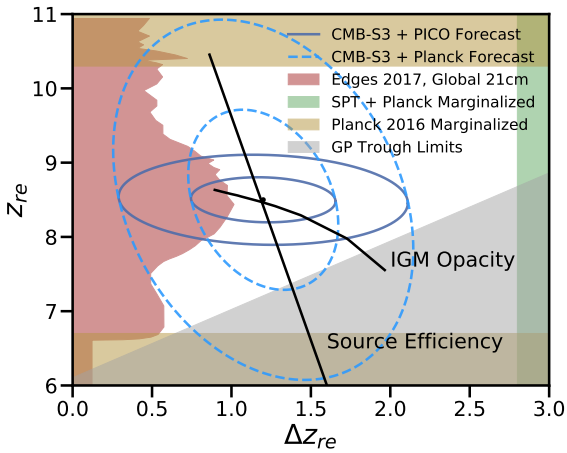

Figure 2.6: Contours of 1 and 2σ constraints on the mean redshift and duration of reionization using PICO and CMB-S3 data (solid dark blue), and comparison with *Planck* and CMB-S3 (dash light blue). Source efficiency and IGM opacity (dark lines) are two physical parameters controlling the reionization process in current models. The PICO measurements, together with higher resolution data of the kSZ effect, will significantly constrain the range of models allowed. We also include other constraints from *Planck*, EDGES, the Gunn-Peterson (GP) trough, and *Planck*+ the South Pole Telescope [56, 92–94].

in the sources, and of intergalactic-medium opacity, two parameters that quantify models of reionization. The curves shown are illustrative; families of models, that would be represented by parallel 'source efficiency' and 'IGM Opacity' lines, are allowed by current data. PICO's data will give simultaneous constraints on these physical parameters, yielding important information on the nature of the first luminous sources. For example, galaxies and quasars predict significantly different values for their IGM opacities and source efficiencies.

The process of reionization leaves specific non-Gaussian signatures in the CMB. In particular, patchy reionization induces non-trivial 4-point functions in both temperature and polarization [95, 96]. The temperature 4-point function can be used to separate reionization and late-time kSZ contributions. Combinations of temperature and polarization data can be used to build quadratic estimators for reconstruction of the patchy τ field, analogous to CMB lensing reconstruction (next Section). These estimators generally require high angular resolution, but also rely on foreground-cleaned CMB maps. PICO's data in its high-frequency bands — which have better than 2 arcmin resolution and cover frequencies that are not suitable for observations from the ground — will enable these estimators to be robustly applied to high resolution ground-based CMB data, a strong example of ground-space complementarity.

With ten independent maps of the entire sky, multiple frequency bands and ample sensitivity to remove foregrounds, PICO is uniquely suited to make the low ℓ EE-spectrum measurements that are needed to elucidate the formation of the first luminous sources. No such measurements have yet been done from the ground. Of the currently operating Stage-III experiments, one is targeting the lowest ℓ EE spectrum [97].

Lowering the uncertainty on τ is crucial for many cosmological observables of the growth of structure. As discussed in Section 2.2.1, these observables require knowledge of the amplitude of the initial fluctuations power spectrum A_s; however, the signatures of A_s and τ are degenerate in the CMB power spectra, except in the low-ℓ EE power spectrum. PICO's cosmic-variance-limited polarization measurements will break this degeneracy and thus improve constraints on the sum of neutrino masses, on dark energy, and modified gravity coming from *any* low-z growth measurement such as CMB and galaxy lensing, velocity-field measurements, redshift-space distortions, and galaxy surveys.

Probing Structure Formation via Gravitational Lensing PICO will constrain the growth of cosmic structure through multiple probes, including gravitational lensing (and cross-correlations thereof) and cluster counts. We focus here on implications of PICO CMB lensing measurements for constraints on dark energy and modified gravity (using the model-independent $\sigma_8(z)$ formalism) as well as high-redshift astrophysics.

Matter between us and the last-scattering surface deflects the path of photons through gravitational lensing, imprinting the 3-dimensional matter distribution across the volume of the Universe onto the CMB maps. The specific quantity being mapped by the data is the projected gravitational potential ϕ that is lensing the

DRAFT

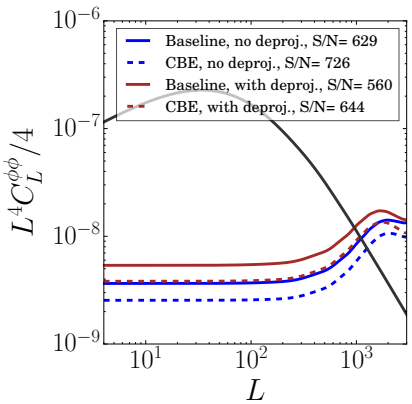

Figure 2.7: PICO will make a high SNR full sky map of the projected gravitational potential ϕ due to all matter between us and the last scattering surface at all angular scales L for which its noise (red and blue) is below the theoretically predicted power spectrum $C_L^{\phi\phi}$ (black). Noise predictions are given with (dash) and without (solid) foregrounds separation, and we include values for the SNR for the measurement of $C_L^{\phi\phi}$ for $2 \leq L \leq 1000$.

photons. From the lensing map, which receives contributions from all redshifts between us and the CMB, with the peak of the distribution at $z \simeq 2$, we infer the angular power spectrum $C_L^{\phi\phi}$ (Fig. 2.7). Both the temperature and polarization maps of the CMB, and by extension the angular power spectra, are affected by lensing.

Planck's ϕ map had SNR of $\sim$1 per L mode over a narrow range of scales, $30 < L < 50$.[8] PICO's map would represent true mapping, with SNR $\gg 1$ for each mode in the range $2 \leq L \lesssim 1000$. While *Planck* had an SNR of 40 integrated across the entire $C_L^{\phi\phi}$ power spectrum [98], PICO will give SNR of 560 and 644 for the baseline and CBE configurations, respectively; both values already account for foreground separation (Fig. 2.7).

The value of the reconstructed lensing map is immense, as has already been demonstrated with the much lower SNR map from *Planck*. The unprecedented constraints on neutrino mass, discussed on page 10, are a direct result of this deep map. Tomographic cross-correlations of the lensing map with wide-field samples of galaxies and quasars will yield constraints on structure formation, and thereby dark energy and modified gravity. This is achieved by using correlations between large-scale structure tracers with different clustering bias factors and measuring the relative difference between their clustering power spectra to effectively cancel cosmic variance [33, 34]. Using these cross-correlation techniques, it is possible to constrain the evolution of the amplitude of structure as a function of redshift. Fig. 2.8 shows constraints on the amplitude of linear structure, $\sigma_8(z)$, in several redshift bins. This is a model-independent representation of the structure growth constraints; these measurements will yield constraints on dark energy or modified gravity, in the context of specific models. The measurements can also be used for a neutrino mass constraint that is complementary to and competitive with that inferred from the CMB lensing auto-power spectrum described earlier.

In addition to cosmological constraints, PICO's lensing measurements will constrain the properties of quasars and other high-redshift astrophysics. For example, cross-correlations with quasar samples from DESI will yield a precise determination of the quasar bias (and hence host halo mass) as a function of the quasar properties, such as (non-)obscuration. Such studies are not possible with any other lensing techniques (that have been demonstrated to date), due to their sensitivity to lower redshifts.

Lensing will also be used to weigh dark matter halos hosting galaxies, quasars, and groups and clusters of galaxies. In the context of quasar analyses described above, this halo mass information is in the "one-halo" term of the cross-correlation, while the bias information is in the "two-halo" term. PICO will access both sets of information, allowing consistency tests and further tightening constraints. Detailed forecasts for halo lensing are presented in the cluster subsection below.

Constraining Structure Growth and Galaxy Formation via the Sunyaev-Zel′dovich (SZ) Effects Not all CMB photons propagate through the Universe freely; about 6% are Thomson-scattered by free electrons

[8] L refers to multipoles in the CMB lensing and galaxy clustering fields, in contrast to the use of ℓ for the CMB itself.

DRAFT

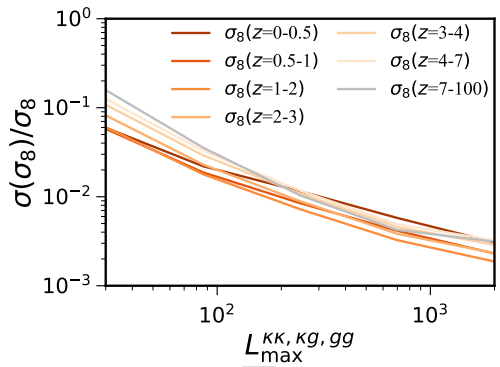

Figure 2.8: Forecasted sensitivity to the parameter describing the amplitude of structure in various redshift bins, as a function of the maximal multipole used in the analysis. Percent-level constraints on these parameters allow for stringent tests of physics beyond ΛCDM that modify the rate of growth of structure.

in the intergalactic medium (IGM) and intracluster medium (ICM). These scattering events leave a measurable imprint on CMB temperature fluctuations, which thereby contain a wealth of information about the growth of structures and the thermodynamic history of baryons. A fraction of these photons are responsible for the thermal and kinetic Sunyaev–Zel′dovich effects (tSZ and kSZ) [99, 100]. The amplitudes of the tSZ and kSZ signals are proportional to the integrated electron pressure and momentum along the line of sight, respectively. They thus contain information about the thermodynamic properties of the IGM and ICM, which are highly sensitive to astrophysical 'feedback'. Feedback is the process of energy injection into the IGM and ICM from accreting supermassive black holes, supernovae, stellar winds, and other sources. The tSZ effect will be used to measure ensemble statistics of galaxy clusters, which contain cosmological information, as well as to provide uniform cluster samples for galaxy-formation studies in dense environments.

• **Galaxy Clusters** Galaxy clusters found via the tSZ effect provide a well-defined sample with a selection function that is simple to model. Such samples of clusters are straightforward to use for cosmological inference and studies of galaxy evolution in dense environments. The tSZ-selected sample from PICO will provide all clusters with masses above $\sim 3\times10^{14}M_\odot$ (defined with respect to the radius within which the average density reaches 200 times the critical density) out to high redshifts, as long as the clusters have started to virialize. We forecast that PICO will find ∼150,000 galaxy clusters, assuming the cosmological parameters from *Planck* and applying a foreground mask, using only 70% of the sky. With redshifts provided by optical surveys and infrared follow-up observations, the PICO tSZ-selected cluster sample will be an excellent cosmological probe, with mass calibration provided by CMB halo lensing described below and optical weak lensing for clusters with $z < 1.5$.

Calibrating the masses of clusters is the most uncertain and crucial step in the cluster cosmology program, in which CMB lensing has already begun to play an important role. In this approach, known as CMB halo lensing, we focus on the small-scale effects of gravitational lensing around these objects [101–103]. The technique holds great potential for measuring halo masses out to high redshifts where gravitational lensing of galaxies (i.e., gravitational shear) no longer works because of the lack of background sources.

This is illustrated in Fig. 2.9, which shows the mass sensitivity of PICO using a spatial filter optimized for extracting the mass of halos [104]. The curves give the 1σ noise in a mass measurement through the filter as a function of redshift. Their flattening at high redshift reflects the fact that CMB lensing is sensitive over a broad range of redshifts, extending well beyond the limit of $z = 2$ shown in the figure. We see that PICO can measure the mass of individual low-mass clusters ($\sim 10^{14}\,\mathrm{M}_\odot$) over a wide redshift range, and by stacking we can determine the mean mass of much smaller halos, including those hosting individual galaxies.

Halo lensing will enable calibration of the galaxy cluster mass scale, which is critical for our cosmological analysis of PICO cluster counts, as mentioned above. From a complementarity perspective, the high-resolution, high-frequency PICO channels will play an essential role in cleaning foregrounds for high-resolution ground-based halo lensing measurements at lower frequencies, particularly those derived from the temperature-based estimator, which is most contaminated by foregrounds.

DRAFT

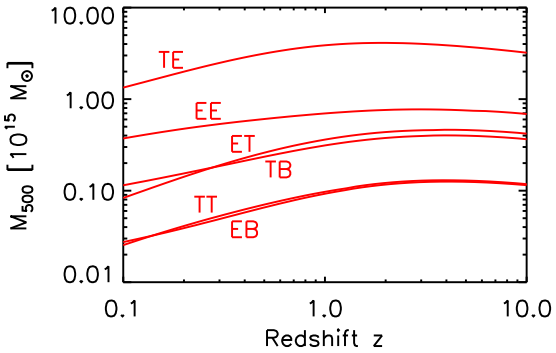

Figure 2.9: PICO sensitivity for CMB halo lensing. Curves for different CMB signal correlations give the 1σ sensitivity of an optimal mass filter [104]. The curves are flat at high redshift, demonstrating the essential property that CMB halo lensing can be probed over a very wide redshift range, and well beyond the $z = 2$ limit of the figure. For PICO, the EB and TT estimators are roughly equivalent, offering important cross-validation of measurements because the systematics are very different for temperature and polarization.

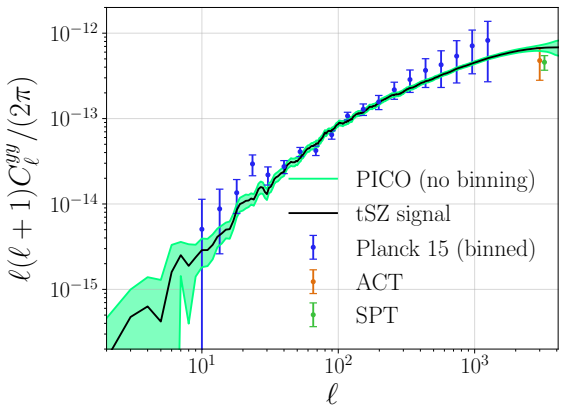

Figure 2.10: Constraints on the tSZ power spectrum from PICO and current data. A simulated tSZ power spectrum (black) is constrained at each multipole by PICO's data (1σ, green). Binning in ℓ, would increase the SNR beyond the calculated value of 1270, which is already nearly 100 times larger than from *Planck* (blue). We include current measurements by the SPT and ACT, two ground-based programs [106, 107]

• **Constraining Feedback Processes: Compton-*y* map and tSZ auto-power spectrum** In addition to finding individual clusters, multifrequency CMB data also allow the reconstruction of full-sky maps of the tSZ signal. These are called 'Compton-*y* maps'. With its extremely low noise and broad frequency coverage, which is essential for separating out other signals, PICO will yield a definitive Compton-*y* map over the full sky, with high SNR down to angular scales of a few arcminutes, which will provide strong constraints on astrophysical feedback models via cross-correlations and its own auto-power spectrum. We quantify this expectation by reconstructing the Compton-*y* field using the needlet internal linear combination (NILC) algorithm [105] applied to sky simulations generated with the *Planck* sky model, with maps at all PICO frequencies (with appropriate noise added). The error bars on the reconstructed tSZ power spectrum are shown in Fig. 2.10, in comparison to current measurements. The total SNR is 1270 for the PICO CBE configuration, with the PICO baseline configuration only $\approx 10\%$ lower. This is nearly two orders of magnitude higher SNR than *Planck*, which has already provided data with much higher SNR than ground-based experiments.

Extremely strong constraints on models of astrophysical feedback will be obtained from the analysis of the PICO *y*-map, both from its auto-power spectrum and from cross-correlations with galaxy, group, cluster, and quasar samples. Like the CMB-lensing map described above, the legacy value of the PICO *y*-map will be immense. As an example, we forecast the detection of cross-correlations between the PICO *y*-map and galaxy weak lensing maps constructed from LSST and WFIRST data. Considering the LSST 'gold' sample with a source density of 26 galaxies/arcmin^2 covering 40% of the sky, we forecast a detection of the tSZ-weak lensing cross-correlation with SNR = 3000. Cross-correlations with the galaxies themselves will be measured at even higher SNR. At this immense significance, the signal can be broken down into dozens of tomographic redshift bins, yielding a precise tracing of the evolution of thermal pressure over cosmic time. For PICO and WFIRST (assuming 45 galaxies/arcmin^2 covering 5.3% of the sky), we forecast SNR = 1100

DRAFT

for the tSZ-weak lensing cross-correlation. The WFIRST galaxy sample extends to higher redshift, and thus this high-SNR measurement will allow the evolution of the thermal gas pressure to be probed to $z \approx 2$ (the peak of the cosmic star formation history) and beyond. These transformative measurements will revolutionize our understanding of galaxy formation and evolution by distinguishing between models of feedback energy injection at high significance. Additional cross-correlations of the PICO y-map with quasar samples, filament catalogs, and other large-scale structure tracers will provide valuable information on baryonic physics that is complementary to inferences from the lensing cross-correlations described earlier. Finally, beyond Compton-y, PICO's CMB halo lensing measurements will also be a unique tool for measuring the relation between galaxies and their dark matter halos during the key epochs of cosmic star formation at $z \geq 2$, not reachable by other means. This will provide valuable insight into the role of environment on galaxy formation during the rise to and fall from the peak of cosmic star formation at $z \sim 2$.

2.2.3 Galactic Structure and Star Formation

Planck enabled an immense step forward in Galactic astrophysics [108]. With 7 full sky polarization maps at frequencies between 30 and 353 GHz and a highest resolution of $5'$, *Planck* provided entirely new and surprising data about the structure of the ISM; the data have a lasting legacy for the foreseeable future. PICO will provide an even greater leap forward, with 21 polarization maps, each much deeper than *Planck*'s, and with the highest resolution being 5 times finer (Fig. 2.11). Such a data set can only be obtained from space. While the PICO data will likely provide many new insights and surprises, we focus here on two crucially important science objectives that are integral to NASA's science goal to explore how the Universe evolved and can only be addressed by the PICO dataset. These objectives relate to the structure and evolution of the Milky Way.

(1) *Test Composition Models of Interstellar Dust:* Less than one thousandth of a millimeter in size, dust grains are intermediate in the evolution from atoms and molecules to large solid bodies such as comets, asteroids, and planets. Encoded in the composition of dust are the pathways through which grains formed and grew. Dust grains also participate directly in interstellar chemistry, e.g., by catalyzing the formation of H_2 and organic molecules on their surfaces, in ways that depend upon their chemical makeup. Thus, the composition of dust grains is an essential aspect of the chemical evolution of interstellar matter from the formation of complex molecules in space to the growth of planets. Through vastly improved spectral characterization of Galactic polarization, the PICO data will discriminate among models of Galactic dust composition to elucidate the chemical evolution of the Galaxy. The data will inform methods to separate diffuse dust emission from cosmological signals of interest (SO6).

(2) *Determine how magnetic fields affect the processes of molecular cloud and star formation:* Stars are formed through interactions between gravitational and magnetic fields, turbulence, and gas over more than four orders of magnitude of spatial scales. However, the role magnetic fields play in the large scale structure of the diffuse interstellar matter (ISM) and in the observed low star-formation efficiency has eluded answer because of dearth of data. By virtue of the strong dynamical coupling of dust and gas and the systematic alignment of dust grains with magnetic fields, PICO's dust polarization measurements will for the first time probe the large scale Galactic magnetic field with resolution to trace the role of magnetic fields through the entirety of the star formation process (SO7).

(1) Test Composition Models of Interstellar Dust

Strong extinction features at 9.7 and 18 μm indicate that much of interstellar dust is in the form of amorphous silicates while features at 2175 Å, 3.3 μm, and 3.4 μm attest to abundant hydrocarbons. It is unknown, however, whether the silicate and carbonaceous materials coexist on the same grains or whether grains of each composition grow through distinct, parallel pathways dictated by their surface chemistry.

Some data suggest that the populations are distinct. Spectropolarimetry of dust extinction reveals robust polarization in the 9.7 μm silicate feature [e.g., 111], indicating that the silicate grains are aligned with the

DRAFT

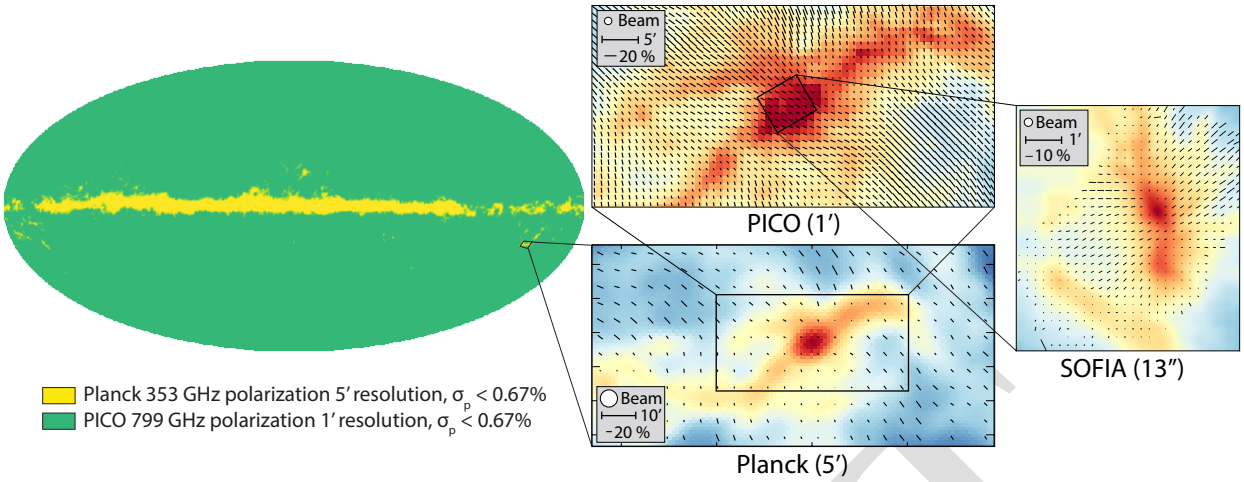

Figure 2.11: *Planck*'s 353 GHz polarization map gave a resolution of 5′ and sensitivity to polarization intensity of $\sigma_p < 0.67\%$ over a small portion of the sky (left, yellow). At 799 GHz, the PICO baseline mission will give a polarization map of the *entire sky* and with 5 times higher resolution (left, green). The *Planck* map of the Orion region overlaid with vectors that are aligned with the inferred magnetic field (lower panel), and a simulated PICO observation (upper panel) illustrate the leap in information content (vector lengths are proportional to polarization fraction). With this map, and maps at many other frequencies that *Planck* did not have, PICO will characterize Galactic magnetized turbulence at scales spanning the diffuse ISM down to dense star forming cores, which will be mapped with high-resolution polarimetry by instruments such as HAWC+/SOFIA [*109*] (right panel) and the Atacama Large Millimeter Array [ALMA, *110*].

interstellar magnetic field. In contrast, searches for polarization in the 3.4 μm carbonaceous feature have yielded only upper limits, even along sightlines where silicate polarization is observed [*112*, *113*]. These data are consistent with silicate and carbonaceous materials existing on separate grains that have different alignment properties.

At odds with the spectropolarimetric evidence from dust extinction are current measurements of the polarization fraction of the far-infrared dust emission with *Planck* [*114*] and BLASTPol [*115*]. They show little to no frequency dependence, whereas substantial frequency dependence would be expected if two components with distinct polarization properties were contributing to the total emission.

With excellent polarization sensitivity, even in diffuse regions, PICO will provide a definitive test of the two component paradigm [*116*]. In this case, the PICO baseline mission will determine the intrinsic polarization fractions of the two components to a precision of 0.03. The data will therefore validate or reject state-of-the-art dust models [e.g. *117*, Hensley & Draine, in prep], test for the presence of additional grain species with distinct polarization signatures, such as magnetic nanoparticles [*118*], and will be used as a crucial input for the foreground separation necessary to extract cosmological B-mode science.

"Anomalous Microwave Emission (AME)" is a component of Galactic emission peaking in the 20-30 GHz range that has been tentatively identified with small, rapidly-spinning dust grains.[*119*] As only upper limits have been placed on its polarization, its role as a foreground for B-mode science remains unclear. Given the present uncertainty on its physical origin and SED variability, even small levels of polarization could prove challenging. However, PICO will finely sample the AME SED with its bands at 21, 25, 30, 36, and 43 GHz. Combined with ground-based maps at lower frequencies [e.g., C-BASS *120*, at 5 GHz], PICO will efficiently separate the AME from synchrotron and free-free emission and either detect or place stringent upper limits on its polarization. Further, the enhanced frequency coverage will enable characterization of systematic changes in the AME SED with interstellar environment and thus elucidate its underlying physics.

(2) Determine how magnetic fields affect the processes of molecular cloud and star formation

DRAFT

Stars form out of dense, gravitationally unstable regions within molecular gas clouds, which themselves form through the flow of diffuse, atomic-phase gas to denser regions. Magnetic fields play an important role throughout this process.

On the largest scales, magnetized turbulence mediates the flow of the gaseous ISM from the atomic to the denser, molecular phase. Recent observations suggest that the structure of the diffuse medium is highly anisotropic, and strongly coupled to the local magnetic field [*121*–*124*]. As molecular gas clouds collapse to form stars, magnetic fields can slow the process of star formation by inhibiting movement of gas in the direction perpendicular to the field lines. Observations to date suggest that the outer envelopes of clouds can be supported against gravity by magnetic fields and turbulence, but in dense cores gravity tends to dominate, and so these dense structures can collapse to form stars [*125*]. The degree to which magnetic fields affect the formation of molecular clouds, as well as stars within these clouds, is poorly constrained, in large part due to the difficulty of making detailed maps of magnetic fields in the ISM.

• **Formation of Magnetized Molecular Clouds from The Diffuse Interstellar Medium** A comprehensive understanding of the magnetized diffuse ISM is challenging because of its diverse composition, its sheer expanse, and the multi-scale nature of the physics that shapes it. To understand how matter and energy are exchanged between the diffuse and dense media, it is essential to measure the properties of the magnetic field over more than four orders of magnitude in column density. PICO is unique in its ability to provide the necessary data. *Planck* achieved measurements of the diffuse sky at $60'$ resolution, resulting in $\sim$30,000 independent measurements of the magnetic field direction. With $1.1'$ resolution PICO will expand the number of independent polarization measurements to 86,000,000. The data will thus robustly characterize turbulent properties like the Alfvén Mach number, $\mathscr{M}_A$, across a previously unexplored regime of parameter space.

PICO's observations will complement recently completed high dynamic range neutral hydrogen surveys, such as HI4PI [*126*] and GALFA-HI [*127*], as well as planned surveys of interstellar gas, most prominently with the Square Kilometer Array (SKA) and its pathfinders. One of the open questions in diffuse structure formation is how gas flows within and between phases of the ISM. A planned all-sky absorption line survey with the forthcoming SKA-1 will increase the number of measurements of the ISM gas temperature by several orders of magnitude [*128*]. Quantitative comparisons of the ISM temperature distribution from SKA-1 and estimates of the magnetic field strength and coherence length scale from PICO will elucidate the role of magnetized turbulence in the flow of matter in the ISM from diffuse regions to regions of denser molecular gas.

• **Formation of Stars within Magnetized Molecular Clouds** The role of magnetic field in star-formation is quantified by the ratio of energy stored in magnetic and gravitational fields, and the ratio of energy stored in magnetic field and that stored in turbulence. The first ratio is parameterized through a mass-to-flux ratio μ, and the second through $\mathscr{M}_A$.

With full-sky coverage and a resolution of $1.1'$, PICO will map all molecular clouds with better than 1 pc resolution, out to a distance of 3.4 kpc. Extrapolating from the Bolocam Galactic Plane Survey [BGPS, *129*], PICO is expected to make highly detailed magnetic field maps of over 2,000 molecular clouds with thousands to hundreds of thousands of independent polarization measurements per cloud. These are the *only foreseeable* measurements that will give μ and $\mathscr{M}_A$ over a statistically significant sample of molecular clouds. *Planck*, for example, mapped only 10 nearby clouds to a similar level of detail [*130*]. A large sample of clouds is crucial because (1) dust polarization observations are sensitive to only the magnetic field projected on the plane of the sky, and therefore polarization maps will look very different for molecular clouds observed at different viewing angles; and (2) the relative importance of the magnetic field will likely be a function of cloud age and mass. By observing thousands of molecular clouds PICO will determine μ and $\mathscr{M}_A$ for different sub-classes of cloud age and mass.

Galactic Legacy Science

PICO will also produce legacy datasets that will revolutionize our understanding of how magnetic fields influence physical processes ranging from planet formation to galaxy evolution. For 10 nearby clouds,

DRAFT

Table 2.3: **Cosmological Legacy Science** include all science

Catalog	Impact	Science
1. Proto-clusters	Discover 50,000[a] mm/sub-mm proto-clusters distributed over the sky out to $z \sim 4.5$.	Probe the earliest phases of cluster evolution, well beyond the reach of other instruments; test the formation history of the most massive virialized halos; investigate galaxy evolution in dense environments.
	Current knowledge: *Planck* ACT/SPT data expected to yield a few tens.	
2. Strongly lensed galaxies	Discover 4500[a] highly magnified dusty galaxies across redshift.	Gain information about the physics governing early, $z \simeq 5$, galaxy evolution, taking advantage of magnification and extra resolution enabled by gravitational lensing; learn about dark matter sub-structure in the lensing galaxies.
	Current knowledge: 13 sources confirmed in *Planck* data; few hundred candidates in *Herschel*, SPT and ACT data.	
4. Polarized point sources	Detect 2000[b] radio and several thousand dusty galaxies in polarization.	Study the physics of jets of extragalactic sources, close to their active nuclei; determine the large-scale structure of magnetic fields in dusty galaxies; determine the importance of polarized sources as a foreground for CMB polarization science.
	Current knowledge: about 200 up to 100 GHz; 1 polarization measurement of a dusty galaxy.	

[a] Confusion (not noise) limited
[b] Noise and confusion limited

which have distances of less than 500 pc, PICO will resolve magnetic fields on scales of 0.1 pc. This is the scale of dense cores and filaments for these clouds, and thus the observations will constrain how magnetic fields on these scales influence the formation of cloud cores. By comparing the orientation of the core-scale magnetic fields with the orientation and sizes of proto-planetary disks, PICO will probe whether magnetic braking influences the growth of such disks [131, 132] and provide complementarity to higher angular resolution instruments such as ALMA [110] and SOFIA [133].

Key processes in the diffuse ISM, including heat transport [134], streaming of cosmic rays [135], and magnetic reconnection [136] are dramatically dependent on the level of magnetization. PICO addresses this with tens of millions of independent measurements of magnetic field orientation over the entire Galaxy that will enable the study the physics of how magnetic fields are generated through a combination of turbulence and large-scale gas motions [137].

Finally, PICO observations will create detailed magnetic field maps of approximately 70 nearby galaxies, with more than 100 measurements of magnetic field directions per galaxy. These observations will determine how interaction between large-scale magnetic fields, turbulence, and feedback from previous generations of star formation affect galaxy evolution and star formation efficiency.

2.3 Legacy Surveys

PICO was designed to respond to requirements posed by the 7 SOs listed in Table 2.2. It will also generate a rich catalog of hundreds of thousands of new sources consisting of proto-clusters, strongly lensed galaxies, and polarized radio and dusty galaxies. An abundance of information about galaxy and cluster evolution, dark matter, the physics of jets of active galactic nuclei, and magnetic fields of dusty galaxies will be stored in this catalog (Table 2.3). This catalog will be mined in future years through subsequent analysis and follow-up observations.

2.3.1 Early phases of galaxy evolution

PICO's catalog of high-z strongly-lensed galaxies will provide answers to major, still open issues in galaxy formation and evolution. What are the main physical mechanisms shaping the properties of galaxies [138, 139]: in situ processes, interactions, mergers, or cold flows from the intergalactic medium? And how do feedback processes work? To settle these issues we need direct information on the structure and dynamics of high-z galaxies. But these are compact, with typical sizes of 1–2 kpc [140]), corresponding to angular

DRAFT

sizes of 0.1–0.2 arcsec at $z \simeq 2$–3. Thus they are hardly resolved, even by ALMA or by HST. If they *are* resolved, high enough SNRs per resolution element are only achieved for the brightest galaxies, which are probably not representative of the general population.

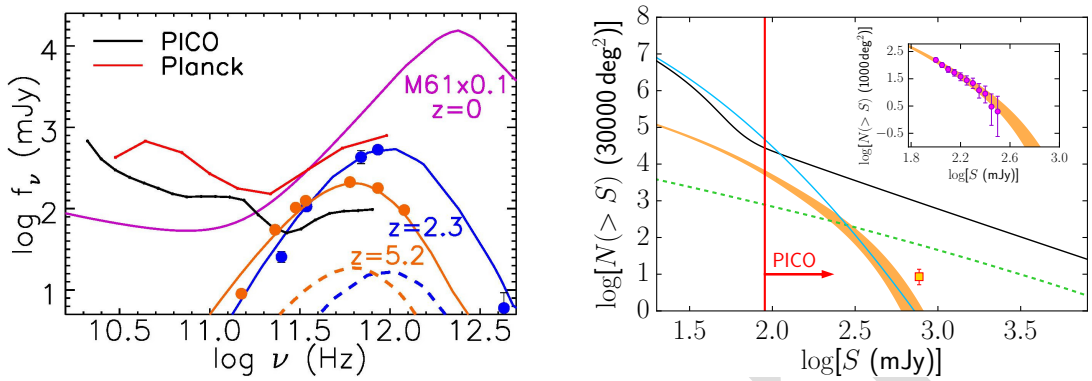

Figure 2.12: **Left:** PICO will detect thousands of new strongly lensed galaxies near the peak of their spectral energy distributions (SEDs), such as SMM J2133-0102 (blue) at $z = 2.3$ [*141*] and HLSJ091828.6+514223 (orange) at $z = 5.2$ [*142*]. The dashed lines are the SEDs pre-lensing-induced magnification. PICO's higher resolution gives point-source detection limits (black line) that are up to 10 times fainter compared to *Planck*'s 90% completeness limits (red line [*143*]). High frequency measurements ($\nu > 300$ GHz) of 30,000 low-z galaxies, like M61 (magenta, SED was scaled down by a factor of ten.), will give a census of their cold dust. **Right panel.** Integral counts of unlensed (black) and strongly lensed, high-z (orange) star-forming galaxies for 70% of the sky away from the Galactic plane at 600 GHz based on fits of *Herschel* counts (inset [*144*]). The PICO detection region (right of vertical red line) will yield a factor of 1000 increase in strongly lensed galaxies relative to *Planck* (yellow square), as well as about 50,000 proto-clusters (blue) and 2,000 radio sources (green) [*145*].

Strong gravitational lensing provides a solution to these problems. Since lensing conserves the surface brightness, the effective angular size is stretched on average by a factor of $\mu^{1/2}$, where μ is the gravitational magnification, thus substantially increasing the resolving power. A spectacular example is ALMA observations of the *Planck*-discovered, strongly lensed galaxy PLCK_G244.8+54.9 at $z \simeq 3.0$ with $\mu \simeq 30$ [*146*]. ALMA observations with a $0.1''$ resolution reached an astounding spatial resolution of 60 pc, substantially smaller than the size of a Milky Way giant molecular clouds. CO spectroscopy of this object, measuring the kinematics of the molecular gas, gave an uncertainty of 40–50 km/s. Such precision allows a high SNR detection of the predicted $\sim 1000\,\mathrm{km\,s^{-1}}$ outflows capable of sweeping the galaxy clear of gas that would otherwise be available for star formation [*147*]. In this specific case, there were no clear indications that mergers or cold flows shaped the galaxy, but similar spectroscopy of another strongly lensed galaxy at $z = 5.3$ detected a fast (800 km/s) molecular outflow due to feedback.

PICO will detect thousands of early forming galaxies whose flux densities are boosted by large factors (Fig. 2.12, right). Currently there are reports of just a few other high-z galaxies that are spatially resolved thanks to gravitational lensing, albeit with less extreme magnifications [*148*–*150*]. PICO's catalog will be transformative as it will probe the spectral energy distributions of the lensed galaxies at their peaks. Two examples of known sources are shown in the left panel of Figure 2.12. While ground-based instruments observe at frequencies up to $\log \nu = 11.45$ PICO's data will extend to the peak of the **SED!** (**SED!**), up to $\log \nu = 11.9$ (Fig. 2.12, left).

A straightforward extrapolation of the *Herschel* counts to the 70% non-Galactic sky gives a detection of 4,500 strongly-lensed galaxies with a redshift distribution peaking at $2 \lesssim z \lesssim 3$ [*144*], but extending up to $z > 5$ (Fig. 2.12, left panel).[9] If objects like the $z = 5.2$ strongly lensed galaxy HLSJ091828.6+514223 exist at higher redshifts, they will be detectable by PICO out to $z > 10$. At the 600 GHz detection limit, about 25% of all detected extragalactic sources will be strongly lensed; for comparison, at optical/near-IR and

[9]Extrapolating from achieved performance by the South Pole Telescope [**?**], we estimate that S3 experiments will detect ∼1,600 such sources, and only in the RJ part of the spectrum.

radio wavelengths, where intensive searches have been carried out for many years, the yield is only about 0.1%, that is more than two orders of magnitude lower [151]. To add to the extraordinary sub-mm lensing bonanza, the selection of PICO-detected strongly lensed galaxies will be extremely easy because of their peculiar sub-mm colors (Fig. 2.12, left panel), resulting in a selection efficiency close to 100% [152]. The survey will give the brightest objects over the entire sky, maximizing the efficiency of selecting sources for follow-up observations.

The intensive high spectral and spatial resolution follow-up campaign of this large sample will enable a leap forward in our understanding of the processes driving early galaxy evolution and open up other exciting prospects, both on the astrophysical and on the cosmological side (see for example Treu [151]).

2.3.2 Early phases of cluster evolution

PICO will open a new window for the investigation of early phases of cluster evolution, when their member galaxies were actively star forming (and dusty), but the hot inter-galactic medium (IGM) was not necessarily in place. In this phase, traditional approaches to cluster detection (X-ray and SZ surveys, and searches for galaxy red sequences) work only for the more evolved clusters, which do include hot IGM; indeed these methods have yielded only a handful of confirmed proto-clusters at $z \gtrsim 1.5$ [153].[10] *Planck* has demonstrated the power of low-resolution surveys for the study of large-scale structure [154], but its resolution was too poor to detect individual proto-clusters [145]. Studies of the high-z 2-point correlation function [145, 155] and *Herschel* images of the few sub-mm bright protoclusters detected so far, at z of up to 4 [156–158], all of which will be detected by PICO, indicate sizes of $\simeq 1'$ for the proto-cluster cores, nicely matching the PICO FWHM at the highest frequencies.

PICO will detect 50,000 proto-clusters as peaks in the high frequency maps, which are not available for ground-based instruments (Table 2.3; blue line in the right-hand panel of Fig. 2.12).[11] The redshift distribution will extend out to $z \sim 4.5$. This catalog will be augmented by 150,000 evolved clusters, detected by the SZ effect. This will constitute a breakthrough in the observational validation of the formation history of the most massive dark-matter halos, traced by clusters, a crucial test of models for structure formation. Follow-up observations will characterize the properties of member galaxies, probing galaxy evolution in dense environments and shedding light on the complex physical processes driving it.

2.3.3 Additional products of PICO surveys

PICO will yield a complete census of cold (< 20K) dust, available to sustain star formation in the nearby Universe, by detecting tens of thousands of galaxies mostly at $z \lesssim 0.1$; the **SED!** of M61 is a typical example (Fig. 2.12, left). With a statistical population, and information only available using data at frequencies above 300 GHz, we will investigate the distribution of such dust as a function of galaxy properties, such as morphology, and stellar mass.

PICO will increase by an order of magnitude the number of blazars selected at sub-mm wavelengths and will determine the SEDs of many hundreds of them up to 800 GHz and up to $z > 5$. Blazar searches are the most effective way to sample the most massive black holes at high z because of the Doppler boosting of their flux densities. PICO's surveys of the largely unexplored mm/sub-mm spectral region will also offer the possibility to discover new transient sources or events, such as blazar outbursts [159].

PICO will make a leap forward in the determination of the polarization properties of both radio sources and of dusty galaxies over a frequency range where ground-based surveys are impractical or impossible. At 320 (800) GHz it will find 1,200 (500) radio sources and 350 (15,000) dusty galaxies at flux limit down to 4 (6) mJy. These data will give information on the structure and ordering of dusty-galaxies' large-scale magnetic fields. In the case of radio sources emission at higher frequencies comes from regions closer to

[10] More high-z proto-clusters have been found by targeting the environment of tracers of very massive halos, such as radio-galaxies, QSOs, sub-mm galaxies. These searches are, however, obviously biased.

[11] Extrapolating from achieved performance by the South Pole Telescope [**?**], we estimate that S3 experiments will detect few hundred sources.

DRAFT

Characteristic	Ground	Balloon	Space
Sky coverage	Partial from single site	Partial from single flight	Full
Frequency coverage	70 GHz inaccessible[a] $\nu \geq 300$ GHz unusable limited atmospheric windows	70 GHz inaccessible[a] otherwise, almost unlimited	Unrestricted
Angular resolution at 150 GHz[b]	1.5' with 6 m telescope	6' with 1.5 m telescope	6' with 1.5 m telescope
Detector Noise	265 $\mu K_{CMB}\sqrt{s}$ [c]	124 $\mu K_{CMB}\sqrt{s}$ [c]	36 $\mu K_{CMB}\sqrt{s}$ [c]
Integration time	Unlimited	Weeks to a Month	Continuous, for years
Accessibility, repairability	Good	None. Multiple flights possible.	None

[a] 70 GHz is the frequency at which large angular scale B-mode Galactic emissions have a minimum.
[b] We give representative approximate telescope aperture values. Significantly larger apertures for balloons and in space result in higher mass, volume, and cost.
[c] Noise equivalent temperature: timestream-based median at 95 GHz from BICEP3 [167]; pre-flight expectation at 94 GHz from SPIDER [168]; at 90 GHz from PICO CBE.

Table 2.4: Relative characteristics of ground, balloon, and space platforms for experiments in the CMB bands.

the central engine, providing information on the innermost regions of the jets, close to the active nucleus.

The anisotropy of the cosmic infrared background (CIB), produced by dusty star-forming galaxies over a wide redshift range, is an excellent probe of the history of star formation across time. The *Planck* collaboration derived values of the star-formation rate out to $z \sim 4$ [160–162]). PICO's lower noise and twice the number of frequency bands will give an order of magnitude improvement on the statistical errors for parameters describing the rate of star-formation history [163]. Similar improvement will be achieved in constraining $M_{\rm eff}$, the galaxy halo mass that is most efficient in producing star-formation activity. PICO's increased sensitivity to Galactic dust polarization will enhance the separation of signals coming from the largely unpolarized CIB and polarized Galactic dust; an effective separation of signals currently limits making reliable, legacy-quality CIB maps. By providing a nearly full-sky map of matter fluctuations traced by dusty star-forming galaxies, such a set of maps could be used for delensing the CMB [164], for measuring local primordial non-Gaussianity from CIB auto-correlations [165], or for cross-correlations with CMB lensing [166].

2.4 Complementarity with Other Surveys and with Sub-Orbital Measurements

2.4.1 Complementarity with Astrophysical Surveys in the 2020s

PICO has strong complementarity with forthcoming surveys. Here we summarize areas of synergy that have been mentioned in a number of earlier sections.

Any refinement of the cosmological constraint on the sum of the neutrino masses $\sigma(\sum m_\nu) < 25\,\mathrm{meV}$ will require improving *Planck*'s measurement of the optical depth τ. In particular, this applies to all methods that rely on comparing low-redshift structures with the amplitude of the CMB at high redshift, such as galaxy clustering, weak lensing, or cluster counts. PICO therefore complements all efforts that probe the late-time structure of the Universe; combining PICO with these low-redshift observations extends the scientific reach of all these experiments well beyond what they could achieve on their own.

Reconstructing the CMB lensing ϕ map on very large angular scales, $L < 20$, requires exquisite control of systematic uncertainties over a large sky fraction, with sufficient angular resolution to perform the lensing reconstruction, and with breadth in frequency to robustly separate Galactic emissions (see Section 2.5). PICO will provide these, complementing ground-based CMB lensing reconstructions that typically observe a smaller sky fraction, with a smaller number of frequency bands, and without access to the largest angular scales. As discussed on page 13, PICO will robustly measure the lensing signal with a power spectrum SNR larger than 10 *per mode* on very large scales. Such high-significance CMB lensing measurements on the very largest scales will be useful when combined with measurements of galaxy clustering from LSST, Euclid, and SPHEREx, to search for local primordial non-Gaussianity via its scale-dependent effect on galaxy bias (see Section 2.2.1).

2.4.2 Complementarity with Sub-Orbital Measurements

Since the first CMB measurements, more than 50 years ago, important observations have been made from the ground, from balloons, and from space. Each of the CMB satellites flown to date (i.e. COBE, WMAP, and *Planck*) has relied crucially on technologies and techniques that were first proved on ground and balloon

DRAFT

flights, making these also crucial to the success of PICO. The phenomenal success of, and the immense science outcomes produced by, past space missions is a direct consequence of their relative advantages over ground and balloon platfroms, as listed in Table 2.4. In every respect, with the exception of serviceability, space has an experimental advantage. These advantages used to come with higher relative costs. However, with the advent of massive ground-based experiments this balance shifts; the costs for a CMB experiment planned for the next decade are squarely within the cost window of this Probe. We can thus point to the following general guidelines for the next decade.

When the entire sky is needed, as for fluctuations on the largest angular scales, space is by far the most suitable platform, and for the search for the IGW signal it is absolutely necessary. When broad frequency coverage is needed, space will be required to reach the ultimate limits set by astronomical foregrounds. As Fig. 2.1 and 2.13 demonstrate, Galactic emission overwhelms the IGW signal on the largest angular scales, and it is dominant even at high ℓ, potentially limiting the process of delensing that is necessary for reaching levels of $r \lesssim 0.001$. The stability offered in space cannot be matched on any other platform and translates to superb control of systematic uncertainties. There is a broad consensus within the CMB community that for levels of $r \lesssim 0.001$ the challenges in the measurement are the ability to control systematic uncertainties and to remove Galactic emissions; modern focal-plane arrays, like the one employed by PICO, have ample raw sensitivity. The PICO goal of $\sigma(r) = 1 \times 10^{-4}$ is beyond the reach of ground-based observations. However, for science requiring higher angular resolution, such as observations of galaxy clusters with ~ 1 arcmin resolution at 150 GHz, the ground has a clear advantage. An appropriately large aperture on the ground will also provide high-esolution information at lower frequencies, which may be important for separating Galactic emissions at high ℓ. A recommended plan for the next decade is therefore to pursue a space mission, and complement it with an aggressive ground-based program that will overlap in ℓ space, and will add science at the highest angular resolution, beyond the reach of a space mission.

Balloon observations have been exceedingly valuable in the past. They co-led discoveries of the temperature anisotropy and polarization, provided proving grounds for the technologies enabling the successes of COBE, WMAP and *Planck*, and trained the scientists that then led NASA's space missions. There are specific areas for which balloon missions can continue to play an important role, despite their inherently limited observing time. Balloon payload can access frequency bands above 280 GHz; currently there are no plans for any ground program to conduct observations at higher frequencies. These frequency bands will provide important, and perhaps critical information about polarized emission by Galactic dust, a foreground that is currently known to limit knowledge of the CMB signals. With flights above 99% of the atmosphere, balloon-borne observations are free from the noise induced by atmospheric turbulence, making them good platforms for observations of the low-ℓ multipoles, and for characterizing foregrounds on these very large angular scales. From a technology point of view, the near-space environment is the best available for elevating detector technologies to TRL6; and balloon platforms continue to be an excellent arena for training the scientists of tomorrow.

2.5 Signal Separation

Diffuse Milky Way emission dominates the sky's polarized intensity on the largest angular scales (Fig. 2.1 and 2.13). do they dominate EE? Is that your point? Polarized radiation arises primarily from the synchrotron emission of energetic electrons spiraling in the Galactic magnetic field, and from thermal emission from elongated interstellar dust grains partially with the local magnetic field. Although the levels of these foreground emissions decrease with decreasing angular scale, they can still be considerably brighter than the IGW peak around $\ell = 80$ when averaging over 60% of the sky. In fact, even in the cleanest, smaller patches of the sky, far from the Galactic plane and thus relatively low in Galactic emissions, their levels are expected to be substantial relative to the IGW for $r \lesssim 0.01$, and dominate it for $r \lesssim 0.001$. Separating the cosmological and Galactic emission signals (also called foreground separation) together with control of systematic uncertainties are *the* challenges facing any next-decade experiment attempting to reach these

DRAFT

levels of constraints on r.

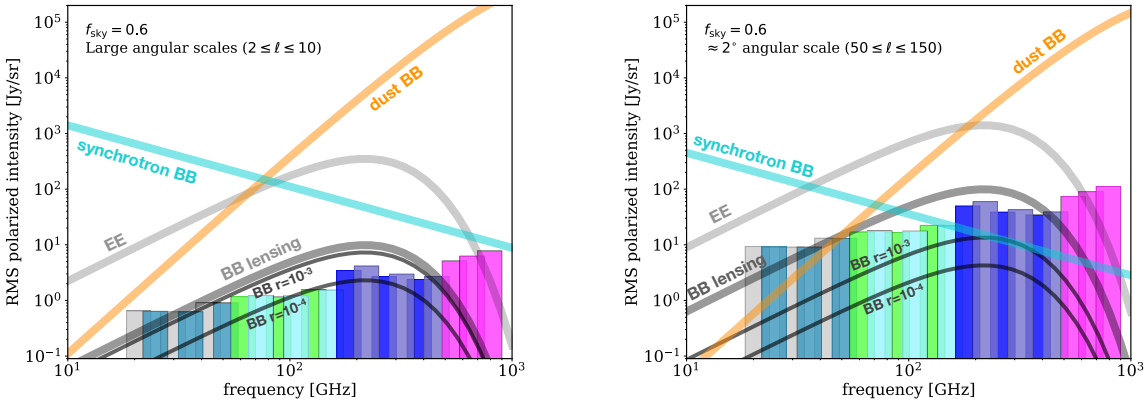

Figure 2.13: Polarization *BB* spectra of Galactic synchrotron and dust, compared to CMB polarization *EE* and *BB* spectra of different origins for two values of r and for two ranges of angular scales: large $\ell \leq 10$, corresponding to the reionization peak (left panel); and intermediate $50 \leq \ell \leq 150$, corresponding to the recombination peak (right panel). The location and sensitivity of the 21 PICO frequency channels is shown as vertical bands. The color scheme is explained in Section 3.2.

The foreground-separation challenge would be easily surmountable if the Galactic emissions were precisely characterized, or were known to have simple, fittable spectral emission laws. But neither is true. To first order, the spectrum of Galactic synchrotron emission, arising from free electrons spiraling around Galactic magnetic fields, can be modeled as a power law $I_{\rm sync} \propto \nu^{\alpha}$, with $\alpha \simeq -1$. The spectrum of Galactic dust emission, arising from emission by Galactic dust grains, can be modeled as $I_{\rm dust} \propto \nu^{\beta} B_{\nu}(T_{\rm dust})$, where $\beta \simeq 1.6$, $T_{\rm dust} \simeq 19$ K, and $B_{\nu}(T)$ is the Planck function; this is referred to as 'modified blackbody emission'. If those models were exact, then in principle, an experiment that had 6 frequency bands could determine the three emission parameters, as well as the three amplitudes corresponding to that of dust, synchrotron, and the CMB. However, recent observations have shown that neither emission law is universal, that spectral parameters vary with the region of sky [*169*–*171*], and thus that the analytic forms and parameter values given above are valid only as averages across the sky. Also, while both emission laws are well-motivated phenomenological descriptions, the fundamental physics of emissions from grains of different materials, sizes, and temperatures, and of electrons spiraling around magnetic fields implies that these laws are expected to be neither exact, nor universal.

Additional polarized foregrounds may exist. 'Anomalous microwave emission' (AME) is observed at mm wavelengths, spatially correlated with thermal dust emission, but with intensity peaking at frequencies near 30 GHz. While not known to be polarized, even a small (0.1%) fractional polarization would be an appreciable foreground for $\sigma(r) \lesssim 0.001$. Astrophysical emission from CO lines at mm wavelengths, and even weak polarization of radio and infrared sources at shorter wavelengths, could also complicate polarized signal separation [*172*, *173*].

PICO will dramatically improve sensitivity to inflationary B-modes. The improved sensitivity requires concurrent improvements in foreground separation. Simple foreground models, suitable for the current generation of CMB measurements, will fail at the higher PICO sensitivity. For example, the *Planck* modified blackbody model assumes that interstellar dust emits at a single temperature, which is clearly an approximation to the more complicated emission along lines of sight spanning hundreds of parsecs. Several publications have demonstrated that fitting complicated temperature profiles using a simple one- or two-temperature model will bias the fitted CMB signal at levels $\delta r \lesssim 10^{-3}$, large compared to the PICO goal [*174*–*178*].

Foreground uncertainties, and the level of fidelity required in their characterization, also compel new approaches to the way we assess and forecast the performance of a future experiment. We can no longer

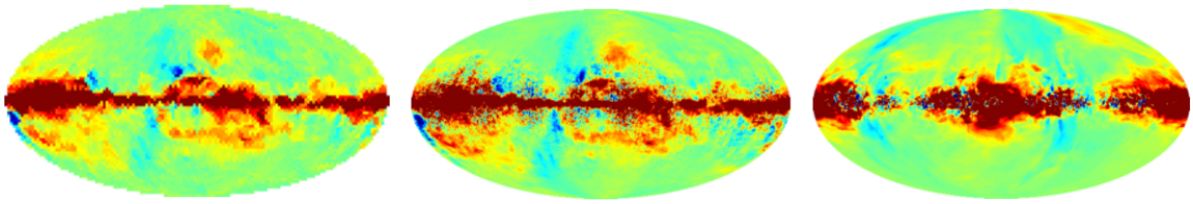

Figure 2.14: Foreground maps: *Planck* real sky (left) at 143 GHz, models at 155 GHz from PySM (middle) [179] and Galactic MHD simulations (right).

impose specific models upon the data; rather, the data collected should provide information to constrain Galactic emissions with sufficient accuracy. Two broad techniques are available. Parametric models use the frequency dependence of the data in each line of sight to determine the effective frequency dependence of foreground emission. Since the CMB spectrum is well determined, measurements with sufficiently broad frequency coverage can distinguish foreground emission from the CMB component using their different spectral dependences. Non-parametric techniques, in contrast, rely on the fact that CMB emission is uncorrelated with the foregrounds and these methods use both spatial and frequency correlations within a spatial/frequency data cube to separate CMB from foreground components. Simulated data assess the efficacy of both techniques as a function of increasing complexity for the assumed foreground emission.

To investigate the capacity of PICO to address this foreground-separation problem, we use the approach that has become the 'gold standard' in the community. In this approach we simulate sky maps that are constrained by available data, but otherwise have a mixture of foreground properties. We 'observe' these maps just like a realistic experiment will do, and then apply foreground separation techniques to separate the Galactic and CMB emission. We also provide forecasts using different techniques which use analytic calculations to estimate the efficacy of foreground separation, or others in which the simulated sky map is assumed to follow specific Galactic emission models, which are then fitted.

2.5.1 PICO Foreground Separation Methodology

For assessing the efficacy of foreground separation with PICO we used eight different full-sky models. All models were broadly consistent with available data and uncertainties from WMAP and *Planck*. The range of models included one test case that had a very simple realization of foregrounds, and others with varying degree of complexity, including spectral parameters varying spatially and along the line of sight, anomalous microwave emission up to 2% polarized, dust polarization that rotates slightly as a function of frequency because of projection effects, or dust spectral energy distributions that depart from a simple modified blackbody. All foreground maps were generated at native resolution of 6.8 arcmin pixels [180]. They were generated using PySM and/or PSM codes [179, 181]. Distinctly different realizations of the sky are allowed by current data, as demonstrated by Fig. 2.14.

For each of the eight models, we added CMB signals in both intensity and polarization, matching a ΛCDM universe. The *BB*-lensing signal matched the level of 85% delensing forecasted for PICO. Each of these sky models had 100 different realization of the PICO CBE noise levels; 50 realizations had no IGW signal; and 50 others had a level of $r = 0.003$. The sky models were analyzed with a variety of techniques, which were based on the two broad categories described above.

Analytic forecasts were based on a Fisher information-matrix approach [182] and included foreground separation using a parametric maximum-likelihood method, assuming that the foreground spectral indices are constant on patches of size 15° across.

2.5.2 Results and Discussion

There is evidence that at levels of $r \simeq 0.001$ the combination of PICO's sensitivity and broad frequency coverage are effective in foreground removal. Fig. 2.15 shows a result from the gold-standard process described above for one of the sky models and with an input IGW of $r = 0.003$. Residual foregrounds are below the cosmological signal over the important low ℓ range, where foregrounds are strongest. The residual

DRAFT

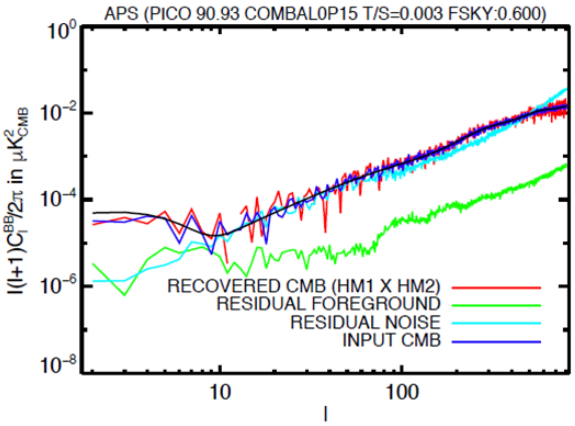

Figure 2.15: Power spectrum of residual *BB* foregrounds (green) has lower level than both the input CMB (blue) and the recovered CMB (red) which match well each other, and the underlying cosmological model (black) after foreground separation with the NILC algorithm. This exercise assumed use of 60% of the sky.

spectra would likely be lower when analysis is carried out on only 50 or 40% of the sky, rather than the 60% used here.

Our results validate the need for a broad frequency coverage with a strong lever arm on Galactic emission outside of the primary CMB bands. Fig. 2.16 shows that removing several of PICO's frequency bands, particularly those that monitor dust and synchrotron at high and low frequencies, respectively, significantly biases the extracted *BB* power spectrum, especially at the lowest multipoles.

There is other evidence that PICO could reach its stated target of $\sigma(r) = 0.0001$. Map-based simulations that were carried out for the forthcoming CMB-S4 experiment have shown that it can reach levels of $\sigma(r) = 0.0005$ in small, 3%-size, clean patches of the sky. The PICO noise level per sky pixel is similar to that of CMB-S4, but PICO will have *full* sky coverage and thus access to *all* the clean patches available. Data from *Planck* indicate that there are approximately ten patches as clean, or cleaner than those used for the CMB-S4 analysis, indicating that PICO's $\sigma(r)$ could be about three times more stringent. This scaling is very conservative because it only assumes CMB-S4's much narrower breadth of frequency coverage and its seven bands; it neglects PICOs much stronger rejection of foregrounds with 21 bands and up to 800 GHz. We note that if there *is* a detection of the IGW signal with $r = 0.001$, PICO will make it with high significance in multiple independent patches of the sky.

Results from the Fisher-based analytic calculations give $\sigma(r) = 9 \times 10^{-5}$, and indicate a very small foreground residual with an $r_{eff} = 9 \cdot 10^{-7}$.

While our results are encouraging, as they suggest that PICO's frequency coverage and sensitivity will be adequate for this level of r, more work should be invested to gain complete confidence. This work includes: running numerous realizations of different sky models, and analyzing them with various approaches; optimizing sky masks; and using combination of techniques to handle large, intermediate, and small angular scale foregrounds differently.

from Draine: Why no mention of free-free when discussing Galactic foregrounds? We of course do not expect the free-free to be polarized, but it is a significant contribution to total intensity, and component separation needs to take it into account.

2.6 Systematic Uncertainties

Some of the PICO science goals require detecting extremely faint signals. The most ambitious goal is to detect the signal characterizing an inflationary gravitational wave with $r \geq 3 \times 10^{-}4\,(3\sigma)$, through a B-mode polarization peak signal $\lesssim$ 10nK in amplitude at $\ell = 80$. It has long been recognized that exquisite control of systematic uncertainties will be required for any experiment attempting to reach these levels, and it is widely accepted that the stability provided aboard a space platform makes it best suited to control systematic uncertainties compared to other platforms. This is one of the most compelling reasons to observe the CMB from space. As WMAP and *Planck* demonstrated, an L2 orbit offers excellent stability, as well as

DRAFT

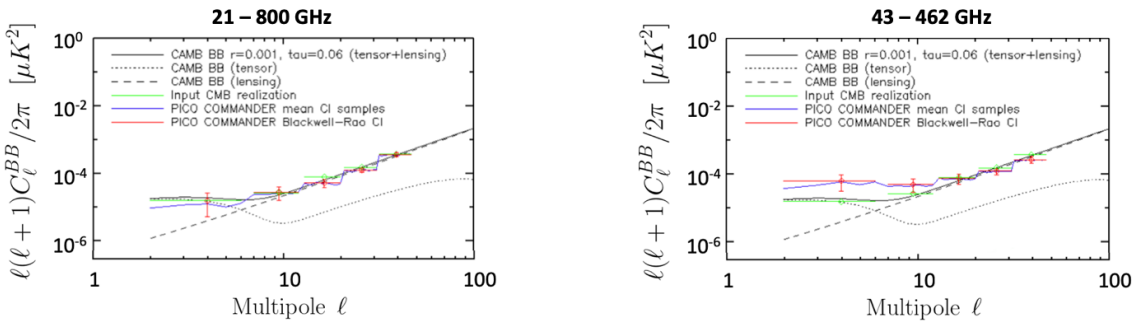

Figure 2.16: Left: foreground removal with all of PICO's 21 frequency bands recovers the input *BB* power spectrum (green) without any bias (red) using the Commander algorithm on the *Planck* sky model (with 4° pixels, and 50% sky fraction). Right: running the same algorithm on the same sky without several of the lowest and highest bands produces an output spectrum (red) that is biased relative to the input (green) at low multipoles. The bias would be interpreted as higher value of r relative to the model input (solid black) with $r = 0.001$ (dots) and lensing (dash lines).

flexibility in the choice of scan strategy. PICO takes advantage of an L2 orbit, using a rotating spacecraft (at 1 rpm) whose spin axis precesses with a 10 hour period, thus scanning the sky in a way that is crosslinked on many time scales and at many angles, without interference from the Sun, Earth, or Moon; this reduces the effects of low frequency excess noise without additional modulation. The redundancy of observations allows the checking of consistency of results and an improved ability to calibrate and to correct systematic errors in post-processing analysis.

A rich literature investigates the types of systematic errors due to the environment, the instrumentation, observation strategies, and data analysis that confound polarization measurements by creating a bias or an increased variance [*183*–*185*]. Every measurement to date has reached a systematic error limit, and many sophisticated techniques have been advanced to mitigate systematics, finding both new technological solutions and new analysis techniques. As an example, BICEP systematics limited it to r=0.1[*186*] while through additional effort within the program, BICEP2 achieved a systematics limit of r=6×10^{-3}[*187*]). In the near term, the ground-based and suborbital CMB community will continue to develop new techniques in handling systematics, particularly in developing the CMB-S4 project.

All prior on-orbit measurements of CMB polarization were limited by systematic errors until an in-depth study of the systematics was performed allowing a post-processing data analysis to suppress them [*19*, *57*, *188*]. Particularly we note figure 3 of Ref.[*19*] which quantifies *Planck*'s systematic error limits on the polarization power spectral measurements. Recently studied space missions, such as EPIC-IM, LiteBird and *CORE*, have placed systematic error mitigation at the forefront of the case for their mission and have developed tools and strategies for estimating and mitigating these[*189*–*191*].

Systematic effects are coupled with the spacecraft scan strategy, and the details of the data analysis pipeline. Thus, end-to-end simulation of the experiment is an essential tool, including realistic instabilities and non-idealities of the spacecraft, telescope, and instrument, as well as folding in data post-processing techniques used to mitigate the systematic effects.

2.6.1 List of Systematics

The systematic errors faced by PICO can be categorized into three broad categories: 1) intensity-to-polarization leakage; 2) stability; and 3) straylight. These are listed in Table 2.5 and were prioritized for further study using a risk factor incorporating the working group's assessment of how mission-limiting the effect is, how well these effects are understood by the community and whether mitigation techniques exist.

The three highest risk systematic errors were studied further and are discussed in subsections below. The PICO team used simulation and analysis tools developed for *Planck* [*192*] and *CORE*, adapting them for

PICO.

Name	Risk	Effect	
Leakage			
Polarization angle calibration	5	$E \to B$	Sect. 2.6.2.
Bandpass mismatch	4	$T \to$P, $E \to B$	
Beam mismatch	4	$T \to$P, $E \to B$	Sect. 2.6.2
Time response accuracy and stability	4	$T \to$P, $E \to B$	
Readout cross-talk	4	spurious P	
Chromatic beam shape	4	spurious P	
Gain mismatch	3	$T \to$P	
Cross-polarization	3	$E \to B$	
Stability			
Gain stability	5	$T \to$P, $E \to B$	Sect. 2.6.3
Pointing jitter	3	$T \to$P, $E \to B$	
Straylight			
Far sidelobes	5	spurious P	Sect. 2.6.4.
Other			
Residual correlated noise (1/f, cosmic ray hits)	3	increased variance	

Table 2.5: Potential systematic errors anticipated in PICO's measurement of CMB polarization. Each source of systematic errors was given a rating of the risk that it will dominate the B-mode measurement. A risk level of 5 indicates that a systematic effect is highly significant because it is design-driving, has limited past experiments, and/or isn't well understood. A risk level of 4 indicates a systematic that is either known to be large but is understood reasonably well, or a smaller effect that requires precise modeling. A risk level of 3 indicates that we expect the effect to be small, but it is not necessarily well understood enough that modeling it needs to be done in detail in a mission Phase A study. We have investigated the systematics with risk levels of 5 via simulations.

2.6.2 Absolute polarization angle calibration

The measured CMB polarization can be rotated due to (1) a birefringent primordial Universe, or a Faraday rotation due a primordial magnetic field [193]; (2) birefringent foregrounds, or interaction with the Galactic magnetic field; (3) systematic effects in the instrument, and in particular an error in the direction of polarization measured by each detector. While the first two sources create a rotation that may depend on scale, position and/or frequency, the latter depends mainly on the detector itself.

A rotation α of the direction of polarization mixes the Q and U Stokes parameters via $Q \pm iU \longrightarrow e^{\mp i2\alpha}(Q \pm iU)$ and thus mixes the power spectra and their correlations, as illustrated in Fig. 2.17.

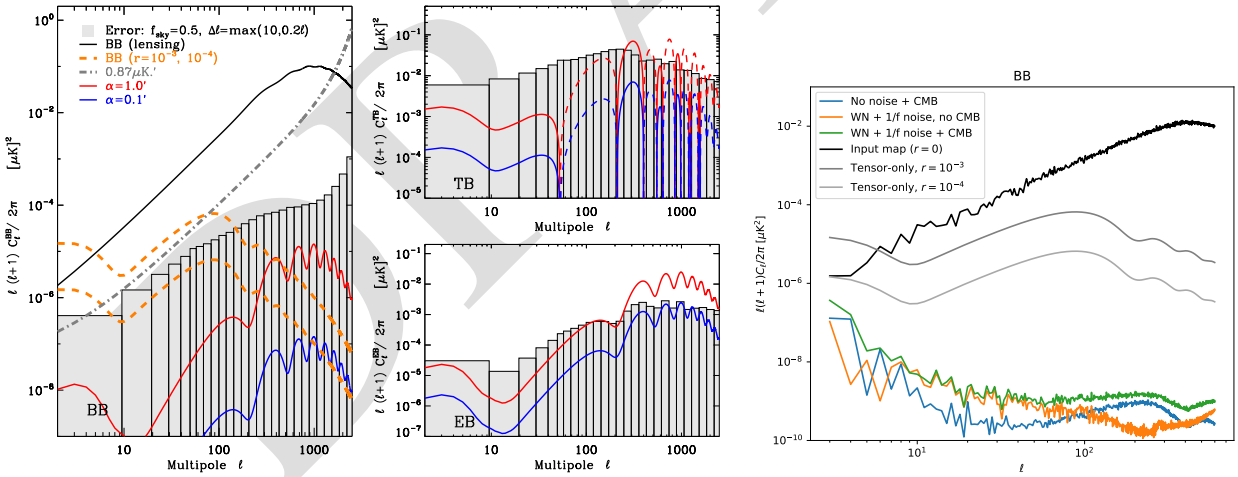

Figure 2.17: Left and center: Spurious power due to a rotation of the angle of polarization, assuming the *Planck* 2018 ΛCDM model [56] with $\tau = 0.054$ and expected PICO noise performance, assuming removal of 85% of the lensing power. Right: residual power after removal of temporal gain drifts using the dipole.

The most recent constraints on cosmological birefringence [194] were limited by uncertainties on the detector orientations. In *Planck*, the detectors were characterized pre-launch to $\pm 0.9^\circ$ (rel.) $\pm 0.3^\circ$ (abs.) [195]. For PICO, the relative rotation of the detectors will be measured to a few $0.1'$ using the CMB, but the overall rotation is unlikely to be known pre-launch to better than *Planck*. Known polarized sources, such as the Crab Nebula, are not characterized well enough independently to serve as calibrators; Aumont et al. [196] show that the current uncertainty of 0.33° on the Crab polarization orientation, limits a B-mode

DRAFT

measurement to $r \sim 0.01$, far from PICO's target.

In the absence of other systematics and foregrounds, a polarization rotation error α of $10'$ degrades the uncertainty of r by 30%, while EB, TB, and BB spectra can measure a rotation α at 3σ when $\alpha = 0.07, 0.2$ and $0.9'$, respectively, on perfectly delensed maps, and $0.25, 0.9$, and $4.5'$ on raw maps.

In principle, the technique of using the TB and EB spectra can measure a global polarization rotation error at levels (around $0.1'$) below those affecting r measurements in BB ($> 1'$). However, a future mission should simulate additional aspects of this issue, such as delensing, the interaction with foregrounds, and $1/f$ noise in simulating and assessing the impact of an angle-calibration error.

2.6.3 Gain Stability

Photometric calibration is the process of converting the raw output of the receivers into astrophysical units via the characterization of the "gain factor" $G(t)$ for each receiver, which we allow to vary with time. In space, $G(t)$ can be measured using the CMB dipole. For the PICO concept study, we evaluated the impact of noise in the estimation of $G(t)$ using the tools developed for the *Planck*/LFI instrument and the CORE mission proposal. The quality of the estimate depends on the noise level of the receivers, but also on the details of the scanning strategy. To analyze the impact of calibration uncertainties on PICO, we performed the following analysis. Firstly, we simulated the observation of the sky, assuming four receivers, the nominal scanning strategy, and $1/f$ noise. The simulated sky contained CMB anisotropies, plus the CMB dipole. Then we ran the calibration code to fit the dipole against the raw data simulated during the first step. We again simulated the observation of the sky, this time using the values of G computed during the second step, which contain errors due to the presence of noise and the CMB signal.

The presence of large-scale Galactic emission features can bias the estimation of calibration factors. Ideally, a full data-analysis pipeline would pair the calibration step with the component-separation step, following a schema similar to *Planck*/LFI's final data processing [197]: the calibration code is followed by a component-separation analysis, and these two steps are iterated until the solution converges.

Results of the simulation (neglecting foregrounds) are shown as power spectrum residuals in Fig. 2.17. We estimate the gain fluctuations to better than 10^{-4} when solving for the gain every 40 hours (4 precession periods). The scanning strategy employed by PICO allows for a much better calibration than was possible for *Planck*, thanks to the much faster precession.

2.6.4 Far-Sidelobe Pickup

Measurement of each detector's response to signals off axis, which tends to be weak (–80dB less than the peak response) but spread over a very large solid angle, is difficult to do pre-launch, and may not even be done accurately after launch. Nonetheless, this far sidelobe can couple bright Galactic signals from many tens of degrees off-axis and confuse it with polarized signal from the CMB off the Galactic plane. To evaluate this systematic error, GRASP software[12] was used to compute the PICO telescope's response over the full sky. The computed full-sky beams showed features peaking at about -80 dB of the on-axis beam. This full-sky beam was convolved with a polarized Galactic signal and a one-year PICO mission scan using the simulation pipeline; this preliminarily shows that the far sidelobe pickup must be reduced by 90% to keep the sidelobe signal from appreciably increasing the variance on the B-mode power measurement. This reduction can be achieved by adjusting the instrument design or by modeling, measuring, and removing the sidelobe pickup during data analysis.

2.6.5 Key Findings

Properly modeling, engineering for, and controlling the effects of systematic errors in a next-generation CMB probe is critical. As of today, we conclude that there is a clear path to demonstrate that state-of-the-art technology and data processing can take advantage of the L2 environment and control systematic errors to a level that enables the science goals of PICO. In particular we note the following points:

- The raw sensitivity of the instrument should include enough margin that data subsets can indepen-

[12] https://www.ticra.com

DRAFT

dently achieve the science goals. This allows testing of the results in the data analysis and additional data cuts, if needed.

- For PICO mission, a physical optics model of the telescope should be developed, enabling full-sky beam calculations, which should be validated as much as possible on the ground. This will be needed to characterize and remove far-sidelobe pickup seen during the mission.
- NASA's support of ground-based and suborbital CMB missions will mitigate risk to a future space mission such as PICO by continuing to develop analysis techniques and technology for the reduction of systematic errors.
- In the PICO mission's phase A, a complete end-to-end system-level simulation software facility should be developed to assist the team in setting requirements and conducting trade-offs between subsystem requirements while realistically accounting for post-processing mitigation. Any future CMB mission is likely to have similar orbit and scan characteristics to those of PICO, thus there is an opportunity for NASA and the CMB community to invest in further development of this capability now.
- Low frequency excess noise (also called 1/f noise) should be studied in detail as part of a simulation effort to set detailed detector and systems level requirements. The systematics simulations performed here show that PICO's science goals can be achieved with no additional modulation and assuming current state-of-the-art levels of low frequency noise (a total knee frequency of 20 mHz) based on demonstrated TES performance, and system-level residuals achieved by *Planck*.

2.7 Measurement Requirements

The set of physical parameters and observables that derive from the PICO science objectives place requirements on the depth of the mission, the fraction of sky the instrument scans, the frequency range the instrument probes and the number of frequency bands, the angular resolution provided by the reflectors, and the specific pattern with which PICO will observe the sky. We discuss each of these aspects in turn now.

• **Depth** We quantify survey depth in terms of the RMS fluctuations that would give a signal-to-noise ratio of 1 in a sky pixel that is $1'$ on a side. Depth in any frequency band is determined by detector sensitivity, the number of detectors in the focal plane, the sky area covered, and the duration of the mission. The science objective driving the depth requirement is SO1, the search for the IGW signal, which requires a combined depth of 0.87 μK $\cdot$ arcmin. This requirement is a combination of the low-level of the signal, the need to separate the various signals detected in each band, and the need to detect and subtract systematic effects to anticipated levels. The CBE value is 0.61 μK $\cdot$ arcmin coming from a realistic estimate of detector noise, and giving 40% margin on mission performance.

• **Sky Coverage** There are several science goals driving a full-sky survey for PICO. The term 'full-sky' here refers to the entire area of sky available after separating other astrophysical sources of confusion. In practice this implies an area of 50-70% of the full sky for probing non-Galactic signals, and the rest of the sky for achieving the Galactic science goals. There are five main goals, each driving different mission requirements.

(1) Probing the optical depth to the epoch of reionization (STM SO5) requires full sky coverage as the signal peaks in the EE power spectrum on angular scales of 20° to 90°. Measuring this optical depth to limits imposed by the statistics of the small number of available ℓ modes is crucial for minimizing the error on the neutrino-mass measurement.

(2) If $r \neq 0$, the BB power spectrum due to IGW (STM SO1) has local maxima on large angular scales (20° to 90°, $2 \leq \ell \leq 10$), and around 1° ($\ell \simeq 80$). A detection would strongly benefit from confirmation at *both* angular scales – a goal that is beyond the capabilities of ground-based instruments – and, for the $\ell = 80$ peak, *in several independent patches of the sky*, a goal PICO will achieve, but that is currently not planned for any next-decade instrument.

(3) The PICO constraint on N_{eff} (STM SO4) requires a determination of the EE power spectrum to limits

imposed by the statics of available ℓ modes. Full sky coverage is required to achieve this limit.
(4) Achieving the targeted neutrino mass limits (STM SO3), giving two independent 4σ constraints on the minimal sum of 58 meV, requires a lensing map, and cluster counts from as large a sky fraction as possible.
(5) PICO's survey of the Galactic plane and regions outside of it is essential to achieving its Galactic structure and star-formation science goals (SO6, 7).

• **Frequency Bands** The multitude of astrophysical signals that PICO will characterize determine the frequency range and number of bands that the mission uses. The IGW signal peaks in the frequency range between 30 and 300 GHz. However, Galactic signals, which are themselves signals PICO strives to characterize, are a source of confusion for the IGW. The Galactic signals and the IGW are separable using their spectral signatures. Simulations indicate that 21 bands, each with 25% bandwidth, that are spread across the range of 20 - 800 GHz can achieve the separation at the level of fidelity required by PICO.

Additionally, characterization of the Galactic signals, specifically the make-up of Galactic dust (SO6), requires spectral characterization of Galactic dust in frequencies between 100 and 800 GHz.

• **Resolution** Several science objectives require an aperture of 1.5 m and the resolution per frequency listed in Table 2.2. To reach $\sigma(r) = 1 \times 10^{-4}$ we will need to 'delens' the E- and B-mode maps, as describe in Sections 2.2.1 and 2.2.2. Delensing is achieved with a map that has a native resolution of 2-3 arcminutes at frequencies between 100 and 300 GHz. Similar resolution is required to meet the constraints on the number of light relics (SO4), which will be extracted from the EE power spectrum at multipoles $100 \lesssim \ell \lesssim 2500$. The process of delensing may be affected by other signals, primarily that due to Galactic dust. It is thus required to map Galactic dust to at least the same resolution as at 300 GHz. Higher resolution is mandated by SO6 and 7, which require resolution of $1'$ at 800 GHz. We have thus chosen to implement diffracted-limited resolution between 20 and 800 GHz.

• **Sky Scan Pattern** Control of polarization systematics uncertainties at anticipated levels is enabled by: (1) making I, Q, and U Stokes-parameter maps of the entire sky from each independent detector; and (2) by enabling sub-percent absolute gain calibration of the detectors through observations of the CMB dipole. With these requirements we chose a sky scan pattern that enables each detector to scan a given pixel of the sky in a multitude of directions, satisfying requirement (1). The scan we chose also gives strong CMB dipole signals in every rotation of the spacecraft throughout the lifetime of the mission, satisfying requirement (2).

DRAFT

3 Instrument

PICO meets all of its science-derived instrument requirements (STM) with a single instrument: an imaging polarimeter with 21 frequency bands centered between 21 and 799 GHz. The instrument is built around an all-aluminum two-reflector Dragone-style telescope (§ 3.1) with an internal aperture stop between the primary and secondary. The focal plane is populated by 12,996 transition edge sensor (TES) bolometers (§ 3.2) read out using a time-domain multiplexing scheme (§ 3.3). The instrument employs a single science observing mode: fixed rotation-rate imaging while scanning the sky.

A V-groove radiator assembly provides passive cooling (§ 3.4.3). The instrument is configured inside the shadow of the V-grooves, thermally and optically shielded from the Sun. The sun shadow cone depicted in Fig. 3.1 is 29°. The angle to the Sun during the survey, $\alpha = 26°$ (§ 4.1.2 and Fig. 4.1), is supplemented with a margin of 3° to account for the radius of the sun (0.25°), pointing control error, design margin, and alignment tolerances.

The V-groove assembly is attached to the bipod struts that support the instrument structural ring. The ring supports the primary reflector and telescope box 'Telescope box' is not a good terminology; telescope refers to all reflectors. suggest to change to 'cold box'; will need to change the label in the Figure. The telescope box contains the actively cooled components (§ 3.4.1, § 3.4.2), including the secondary reflector, the focal plane, and sub-kelvin adiabatic refrigerator structures. Just inside the box, a thermal liner serves as a cold optical baffle and aperture stop.

During the survey, the instrument is spun at 1 rpm (§ 4.1.2). Spacecraft control is simplified by mounting the instrument on a spinning spacecraft module, while a larger non-spinning module houses most spacecraft subsystems (§ 4.3). Instrument elements that act as heat sources are accommodated on the spinning module of the spacecraft. Instrument integration and test (I&T) is described in § 3.5.

3.1 Telescope

PICO telescope design is driven by a combination of science requirements and physical volume limits. The science requirements are: a large diffraction-limited field of view (DLFOV) sufficient to support $\sim 10^4$ detectors, arcminute resolution at 800 GHz, low spurious polarization, and low sidelobe response. All requirements are met with PICO's 1.4 m aperture modified open-Dragone design (Fig. 3.2). There are no moving parts in the PICO optical system. we should take figure 19 out. It is not useful for the decadal panel. Can give reference to the Young etal. paper.

this entire paragraph is not necessary More than 30 years ago Dragone analyzed the performance of several off-axis systems and found solutions with low cross-polarization at the center of the field of view and with stigmatism, or astigmatism and coma, canceled to first order [*198*–*200*]. A number of recent suborbital CMB instruments have used off-axis systems, and several began design optimization with systems based on designs by Dragone [*201*–*203*].

The PICO optical design was selected following a trade study examining cross-Dragone, Gregorian Dragone, and open-Dragone designs [*204*]. We chose the open-Dragone because both the cross- and open-Dragone systems can accommodate the focal plane size required, while the Gregorian can not [*205*], and because the open-Dragone is more compact and does not require more massive baffles that the cross-Dragone would require to overcome its sidelobes. The initial open-Dragone design has been modified by adding an aperture stop and adding corrections to the primary and secondary reflectors to enlarge the diffraction limited field of view. The detailed geometric parameterization of the PICO optical design is described in [*204*].

The two reflectors (270 cm × 205 cm primary and 160 cm × 158 cm secondary) are all-aluminum to minimize complexity. The highest frequency (900 GHz) sets the surface accuracy requirement of the reflectors to $\sim \lambda/14 = 24\,\mu$m. The focal ratio is 1.42. The primary is maintained at ambient temperature. A cold stop, between the primary and secondary reflectors, and the secondary reflector are actively cooled. The slightly concave focal surface, which has a radius of curvature of 4.55 m, is telecentric to within 0.12° across the entire FOV.

DRAFT

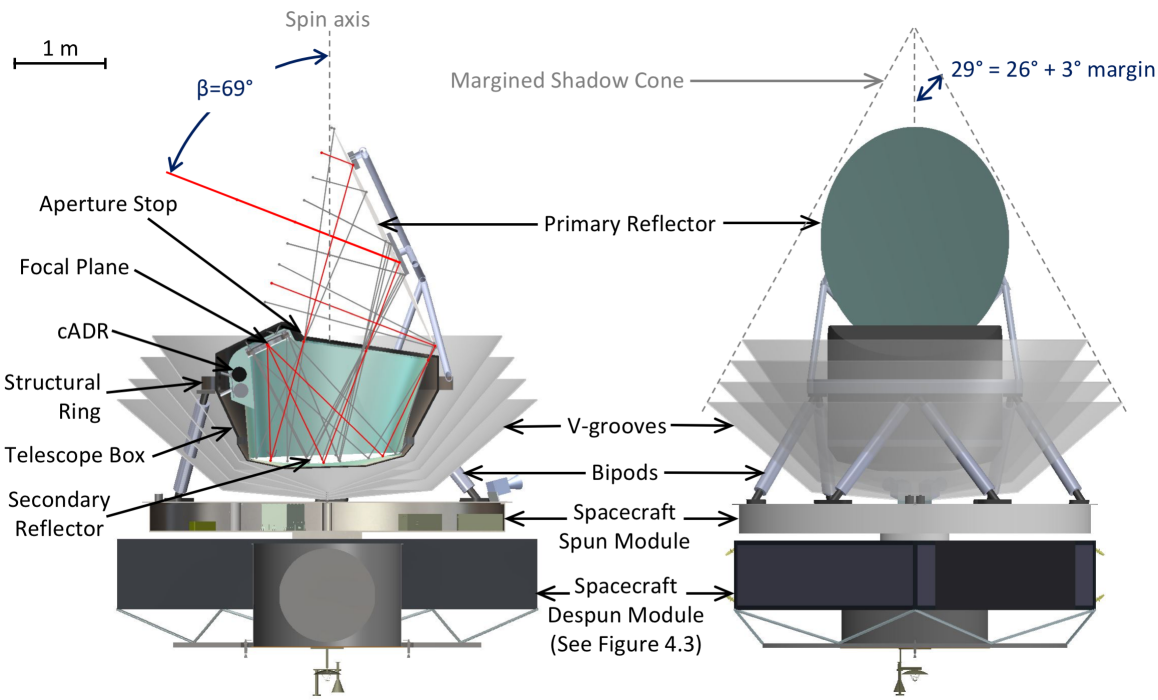

Figure 3.1: Detailed PICO instrument configuration. There are no moving or deployed parts. The spacecraft spun module accommodates warm instrument components: the 4 K cooler compressor and drive electronics, the sub-K cooler drive electronics, and the detector warm readout electronics.

Stray light analysis of the PICO open-Dragone design using GRASP confirms that the focal plane is protected from direct view of the sky, and that spillover past the primary is suppressed by 80 dB relative to the main lobe for both co-pol and cross-pol beams.

replaced the entire red text below with the orange text above. Stray light analysis of the PICO open-Dragone design using GRASP confirms that the focal plane is protected from direct view of the sky (an advantage relative to the cross-Dragone system), that spillover past the primary is suppressed by 80 dB relative to the main lobe for both co-pol and cross-pol beams. Relative to the cross-Dragone, an open-Dragone also has a smaller f-number, so the volume constrained by the shadow cone can accommodate a larger effective aperture. The smaller f-number also reduces the physical focal plane size (for the same number of pixels), reducing focal plane mass and consequently the heat lift requirements on the active coolers (§ 3.4).

PICO's initial open-Dragone design follows Granet's method [*206*], with f/1.42. An actively cooled circular aperture stop is added between the primary and secondary reflectors to reduce detector noise and shield the focal plane from stray radiation. Distortions are then added to the primary and secondary reflectors according to Dragone's published prescription [*200*] to eliminate coma and increase the DLFOV. The detailed geometric parameterization of the PICO optical design is described in [*204*].

replaced all the material below, with what's above The PICO open-Dragone design follows Granet's method [*206*], with f/1.42. An actively cooled circular aperture stop is added between the primary and secondary reflectors to reduce detector noise and shield the focal plane from stray radiation. Distortions are then added to the primary and secondary reflectors according to Dragone's published prescription [*200*] to eliminate coma and increase the DLFOV. The detailed geometric parameterization of the PICO optical design is described in [*204*].

DRAFT

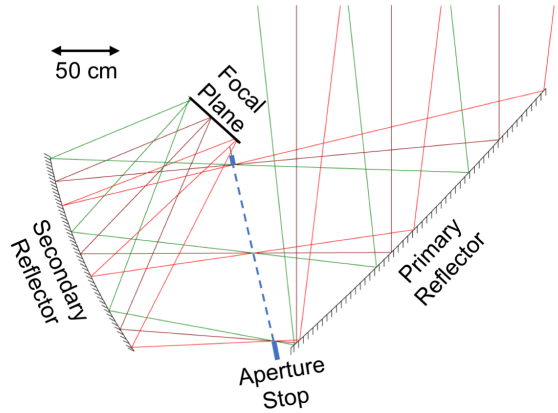

Figure 3.2: The optical system is compact. this figure is not necessary

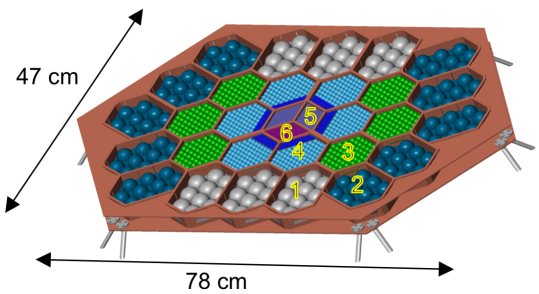

Figure 3.3: PICO focal plane. Detectors are fabricated on six types of tiles (shown numbered and colored to match first column in Table 3.1). The wafers are located on the focal plane such that higher frequency bands, which require better optical performance, are placed nearer to the center.

The two reflectors (270 cm × 205 cm primary and 160 cm × 158 cm secondary) are all-aluminum to minimize complexity. The highest frequency (900 GHz) sets the surface accuracy requirement of the reflectors to $\sim \lambda/14 = 24\,\mu$m.

The slightly concave focal surface, which has a radius of curvature of 4.55 m, is telecentric to within 0.12° across the entire FOV. This results in a defocus of 0.1 mm at the edge of a flat 10 cm detector wafer, adding an RMS wavefront error of less than 3 μm, which is negligible relative to PICO's shortest wavelength.

3.2 Focal plane

PICO's focal plane is populated by an imaging array of transition edge sensor (TES) bolometers observing in 21 overlapping 25%-wide frequency bands with band centers ranging from 21 to 799 GHz. Polarization is measured by differencing the signals from pairs of polarization-sensitive bolometers. A conceptual layout of the PICO focal plane is shown in Fig. 3.3 and detailed in Table 3.1.

Modern mm/sub-mm detectors are photon-noise limited, so the primary approach to increase sensitivity is to increase the number of detectors. The PICO focal plane has 12,996 detectors, 175 times the number flown on the *Planck* mission, providing a breakthrough increase in sensitivity with a comparably sized telescope. This breakthrough is enabled by development and demonstration in suborbital projects, which now commonly use field arrays of $\sim 10^4$ detectors. For example, SPT-3G is currently observing with ... and by the time PICO will enter phaseA the Simmons Observatory will have ... include citations.

3.2.1 Low-frequency detectors

The majority of the PICO focal plane is populated with multichroic pixels (MCPs) [*207*, *208*], which make optimal use of the focal plane area by feeding several photometric bands from a common broad-band antenna

DRAFT

Tile type	N_{Tile}	Pixels / Tile	Pixel type	Bandcenters [GHz]	Sampling Rate [Hz]
1	6	10	A	21, 30, 43	45
2	10	10	B	25, 36, 52	55
3	6	61	C	62, 90, 129	136
4	6	85	D	75, 108, 155	163
		80	E	186, 268, 385	403
5	2	450	F	223, 321, 462	480
6	1	220	G	555	917
		200	H	666	
		180	I	799	

Table 3.1: PICO makes efficient use of the focal area with multichroic pixels (three bands per pixel, § 3.2.1). The sampling rate is based on the smallest beam (Table 3.2), with 3 samples per FWHM at a scan speed $(360^\circ/\mathrm{min})\sin(\beta = 69^\circ) = 336^\circ/\mathrm{min}$.

that is polarization sensitive. PICO has three bands, and thus there are six bolometers per pixel.

Several competing optical coupling technologies have matured over the past ten years using horn-coupling [209], antenna-array coupling [210], and sinuous antenna/lenslet-coupling [211], delivering high optical efficiency over more than an octave of bandwidth I don't think this is correct. The antenna-array is not giving octave of bandwidth. It is not a multi-color option. not sure that the horn-coupling is giving an octave. Need to check. Pixel size, number, and spacing is relatively agnostic to the coupling scheme, so multiple options are open to PICO (technology maturation plan described in § 5.2.1). I am not sure this is what we want to say. For all of these schemes, niobium microstrips mediate the signals between the antenna and detectors, and partition the wide continuous bandwidth into narrow channels using integrated micro-machined filter circuits [212].

3.2.2 High-frequency detectors

PICO's highest three frequency channels are beyond the Niobium superconducting band-gap, rendering microstrip filters a poor solution for defining the optical passband. In this regime, PICO instead measures a single band with each pixel using feedhorn-coupled polarization-sensitive bolometers. Radiation is coupled through horns directly to an absorber. TES bolometers detect the incident power. The waveguide cut-off defines the lower edge of the band, and quasi-optical metal-mesh filters define the upper edge. Numerous experiments have successfully used similar approaches [213–215]. The technology maturation required for PICO is described in § 5.2.1. is there any tech maturation? we need to point to Planck and Herschel here.

3.2.3 Sensitivity

We developed an end to end noise model of the PICO instrument to predict full mission sensitivity (Table 3.2) and provide a metric by which to evaluate mission design trades. The model considers four noise sources per bolometer: photon, phonon, TES Johnson, and readout (from both cold and warm readout electronics). To validate our calculations, we compared two independent software packages that have been validated through use on several current CMB instruments. The calculations agreed within 1% for both individual noise terms and for overall mission noise.

Laboratory experiments have demonstrated that TES detectors can be made background limited in the low loading environment they would experience at L2 is that true? reference? need to be careful. not sure that's been done for our loading levels. may need to cite Planck and spider For PICO, the primary contributor to noise is the optical load. The sources of optical load are the CMB, reflectors, aperture stop, and low pass filters. The CMB and stop account for the majority of the optical load at all frequencies. The CMB gives more than half the load in the middle and upper bands of the multichroic pixels, but the stop dominates the load in the lowest band of each pixel. A detailed description of the PICO noise model is

DRAFT

Band Center [GHz]	Beam FWHM [arcmin]	CBE Bolo NET ($\mu K_{CMB}\sqrt{s}$)	N_{bolo}	CBE Array NET ($\mu K_{CMB}\sqrt{s}$)	Required (Baseline) Array NET ($\mu K_{CMB}\sqrt{s}$)	Baseline Polarization Map Depth	
						μK_{CMB} - arcmin	Jy/sr
21	38.4	112.2	120	12.0	17.0	23.9	8.3
25	32.0	103.0	200	8.4	11.9	18.4	10.9
30	28.3	59.4	120	5.7	8.0	12.4	11.8
36	23.6	54.4	200	4.0	5.7	7.9	12.9
43	22.2	41.7	120	4.0	5.6	7.9	19.5
52	18.4	38.4	200	2.8	4.0	5.7	23.8
62	12.8	69.2	732	2.7	3.8	5.4	45.4
75	10.7	65.4	1020	2.1	3.0	4.2	58.3
90	9.5	37.7	732	1.4	2.0	2.8	59.3
108	7.9	36.2	1020	1.1	1.6	2.3	77.3
129	7.4	27.8	732	1.1	1.5	2.1	96.0
155	6.2	27.5	1020	0.9	1.3	1.8	119.1
186	4.3	70.8	960	2.0	2.8	4.0	433.1
223	3.6	84.2	900	2.3	3.3	4.5	604.2
268	3.2	54.8	960	1.5	2.2	3.1	433.4
321	2.6	77.6	900	2.1	3.0	4.2	577.8
385	2.5	69.1	960	2.3	3.2	4.5	429.1
462	2.1	132.6	900	4.5	6.4	9.1	551.1
555	1.5	657.8	440	23.0	32.5	45.8	1580
666	1.3	2212	400	89.0	125.8	177.2	2075
799	1.1	10430	360	525.9	743.8	1047	2884
		Total	12,996	0.43	0.61	0.87	

Table 3.2: PICO measures in 21 broad overlapping frequency bands with band centers (ν_c) from 21 GHz to 799 GHz and bandwidth $\Delta\nu/\nu_c = 25\,\%$. The beams are single mode, with FWHM sizes of $6.2' \times (155\,\mathrm{GHz}/\nu_c)$. The Current Best Estimate (CBE) per-bolometer sensitivity is background limited (§ 3.2.3). The total number of bolometers for each band is equal to (number of tiles) $\times$ (pixels per tile) $\times$ (2 polarizations per pixel), from Table 3.1. Array sensitivity assumes 90 % detector operability, and meets the requirements of the baseline mission with $> 40\,\%$ margin. The map depth assumes 5 yr of full sky survey at 95 % survey efficiency, except the 25 and 30 GHz frequency bands, which are conservatively excluded during 4 hr/day Ka-band (26 GHz) telecom periods (§ 4.2).

Component	T Req'd	T CBE	Active heat lift		
			Req'd per model	Capability today	Projected capability
Primary reflector	< 40 K	17 K	N/A (radiatively cooled)		
Secondary reflector	< 8 K	4.5 K	42 mW total at 4.5 K		> 100 mW (§3.4.2, Figure 3.5)
Aperture stop	4.5 K				
cADR heat rejection	4.5 K				
Focal plane enclosure and filter	1.0 K	1.0 K	0.36 mW	1.0 mW	
Focal plane	0.1 K	0.1 K	5.7 uW	16 uW	

Table 3.3: Projected cooler heat lift capabilities offer > 100 % margin, complying with community best practices [221]. The cADR lift capability at 1 K and 0.1 K is from a Goddard quote. Both NGAS and Ball project > 100 mW lift capability at 4.5 K using higher compression-ratio compressors currently in development (§ 3.4.2). The required loads were calculated using Thermal Desktop. Reference [222] was used to estimate the thermal conductive loads through mechanical supports. In addition to the listed components, the total 4.5 K heat load includes the intercept on the focal plane mechanical supports.

available in [204]; small differences with Table 3.2 are due to refinements of the component temperatures. The sensitivity model assumes white noise at all frequencies. removed the additional sentences; calibration uncertainties and systematics are *never* part of a sensitivity model. If we want to make this comment, which is a valid comment, it should be made elsewhere.

Sub-orbital submillimeter experiments have demonstrated TES detectors that are stable to at least as low as 20 mHz [216], meeting PICO's requirements for the proposed scan strategy (§ 4.1.2).

3.3 Detector readout

Suborbital experiment teams over the past ten years have chosen to use voltage biased TESs because their current readout scheme lends itself to SQUID-based multiplexing. Multiplexing reduces the number of wires to the cryogenic stages and thus the total thermal load that the cryocoolers must dissipate. This approach also simplifies the instrument design. In the multiplexing circuitry, SQUIDs function as low-noise amplifiers and cryogenic switches. The current baseline for PICO is to use a time-domain multiplexer (TDM), which assigns each detector's address in a square matrix of simultaneously read columns, and sequentially cycles through each row of the array [217]. The PICO baseline architecture uses a matrix of 128 rows and 102 columns, requiring some technology maturation (§ 5.2.2). The thermal loading on the cold stages from the wire harnesses is subdominant to conductive loading through the mechanical support structures. Redundant warm electronics boxes perform detector readout and instrument housekeeping using commercially available ASICs. The readout electronics compress the data before delivering it to the spacecraft. PICO detectors produce a total of 6.1 Tbits/day assuming 16 bits/sample, sampling rates from Table 3.1, and bolometer counts from Table 3.2. Suborbital work has demonstrated 6.2× compression of similar data [218]. *Planck* HFI typically achieved 4.7× compression in flight [219, 220]. PICO conservatively assumes 4×.

3.4 Thermal

The PICO focal plane is maintained at 0.1 K (§ 3.4.1), a temperature that simplifies TES bolometer design given the low optical loads expected. The *Planck*-HFI focal plane was also maintained at 0.1 K. To minimize detector ~~shot~~ noise due to instrument thermal radiation, the aperture stop and reflectors are cooled using both active and radiative cooling (§ 3.4.2, § 3.4.3). All thermal requirements are met with robust margins (Table 3.3).

3.4.1 cADR Sub-K Cooling

A multi-stage continuous Adiabatic Demagnetization Refrigerator (cADR) cools the PICO focal plane to 0.1 K and the surrounding enclosure, filter, and readout components to 1 K. The cADR employs three refrigerant assemblies operating sequentially to absorb heat from the focal plane at 0.1 K and reject it to 1 K. Additionally, the cADR employs two assemblies operating sequentially to absorb this rejected heat at 1 K,

DRAFT

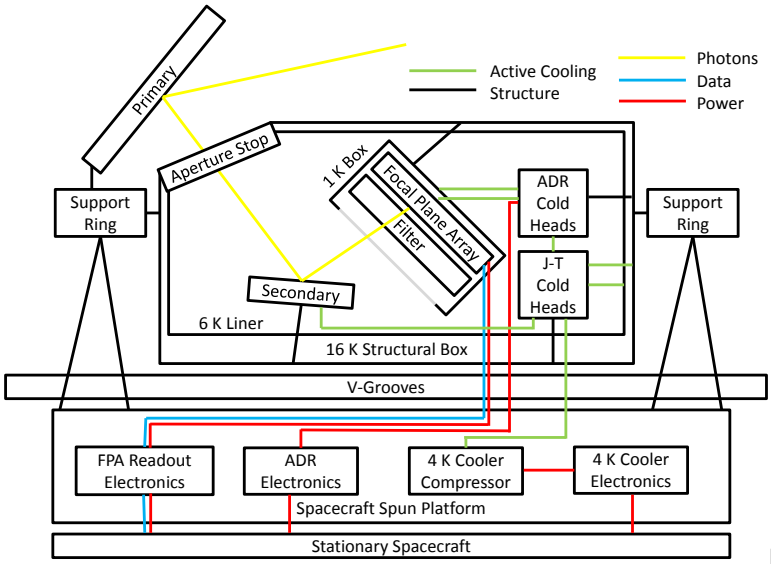

Figure 3.4: PICO instrument block diagram. Active coolers provide cooling to the focal plane, its box, the secondary reflector, and the thermal liner that acts as a cold aperture stop. Data from the focal plane flows to (redundant, cross-strapped) warm readout electronics on the spun module of the spacecraft bus.

cool other components to 1 K, and reject heat at 4.5 K. This configuration provides continuous cooling with small temperature variations at both the 0.1 K and 1 K. Heat straps connect the two cADR cold sinks to multiple points on the focal plane assembly, which has high thermal conductance paths built in, to provide spatial temperature uniformity and stability during operation. Heat loads in the range of 20 μW at 0.1 K and 1 mW at 1 K (time-average) are within the capabilities of current cADRs developed by GSFC [223, 224]. The PICO sub-K loads are estimated at less than half of this capability.

3.4.2 4 K Cooler

A cryocooler system similar to that used on JWST to cool the MIRI detectors [225, 226] removes the heat rejected from the cADR and cools the aperture stop and secondary reflector to 4.5 K. Both NGAS (which provided the MIRI coolers) and Ball Aerospace have developed such coolers under the NASA-sponsored Advanced Cryocooler Technology Development Program [227]. NGAS and Ball use slightly different but functionally-equivalent hardware approaches. A 3-stage precooler (acoustic Stirling by NGAS or mechanical Stirling by Ball) provides $\sim$ 16 K precooling to a separate circulated-gas loop driven by a similar compressor modified for DC flow. The circulated-gas loop utilizes Joule–Thomson (J-T) expansion, further cooling the gas to 4.5 K. The entire precooler assembly and the J-T circulator compressor are located on the warm spacecraft, with relatively short tubing lengths conducting the gas flow from the precooling point to the J-T expansion point. All waste heat rejected by the cooler compressors and drive electronics is transferred to the spacecraft heat rejection system. Unlike JWST, the PICO cooler does not require deployment of the remote cold head.

The J-T expansion point is located close to the cADR heat rejection point, thereby providing the lowest temperature to the cADR. Subsequent to cooling the cADR, the gas flow intercepts conducted heat to the focal plane enclosure, then cools the aperture stop and the secondary reflector before returning in counterflow to the circulation compressor. Model-based projections indicate that the coolers delivered for MIRI could meet the PICO 4.5 K heat lift requirement with $> 100\,\%$ margin with minimal changes: the replacement of the ^{4}He gas used for MIRI with ^{3}He, plus resizing of the gas counterflow heat exchangers to take advantage of the ^{3}He

It is highly likely that a better solution will be available before Phase A. NGAS and Ball are actively working on increasing the flow rate and compression ratio of the J-T compressor, which should result in significantly higher system efficiency, and in greater heat-lift margin above the PICO requirement. These improvements entail the implementation of well-known techniques (standard thermal engineering). The

DRAFT

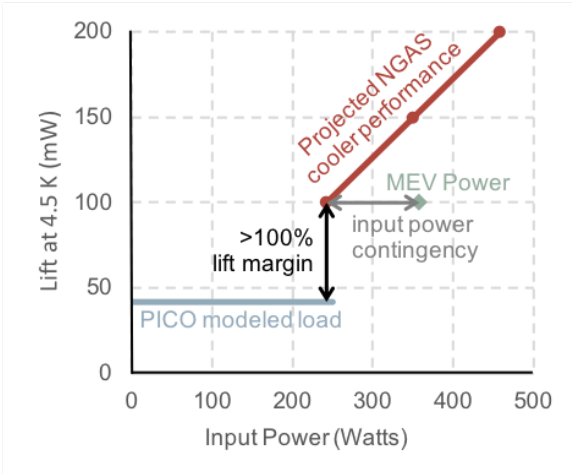

Figure 3.5: Projected performance of the NGAS cooler using a multi-stage compressor and ^{4}He [226] meets PICO's requirements with $> 100\,\%$ margin. PICO conservatively carries additional input power contingency on the efficiency of the cooler.

NGAS multi-stage J-T compressor has completed PDR-level development, and is expected to reach CDR level well before needed for PICO. Projected performance is shown in Fig. 3.5. The Ball approach started with a larger compressor, required less modification to achieve comparable performance, and eliminated the cold bypass-precooling valve that was problematic for MIRI. The Ball approach uses ^{3}He, while the NGAS approach uses ^{4}He. Both employ re-optimized gas heat exchangers (trivial engineering changes).

3.4.3 Radiative cooling

A set of four V-groove radiators provides passive cooling. The outermost of the four V-groove shields shadows the interior shields from the Sun. The V-grooves radiate to space, each reaching successively cooler temperatures. The V-groove assembly is mechanically supported from the spacecraft bus by attachment to the low-conductance bipod struts that also carry the mechanical loads of the structural ring (Fig. 3.1). The V-groove assembly provides a cold radiative environment to the primary reflector, structural ring, and telescope box, so radiative loads on those elements are smaller than the conductive loads through the mechanical support structures.

3.5 Instrument integration and test

PICO Instrument I&T planning benefits greatly from heritage experience with the *Planck* HFI instrument [228].

PICO will screen detector wafer performance prior to selection of flight wafers and focal plane integration. The cADR and 4 K cryocooler will be qualified prior to delivery. The relative alignment of the two reflectors under thermal contraction will be photogrammetrically verified in a thermal vacuum (TVAC) chamber.

PICO will integrate the flight focal plane assembly and flight cADR in a dedicated sub-kelvin cryogenic testbed. Noise, responsivity, and FPU temperature stability will be characterized using a representative optical load for each frequency band (temperature-controlled blackbody). Polarimetric and spectroscopic calibration will be performed.

The focal plane will be integrated with the reflectors and structures, and alignment verified photogrammetrically at cold temperatures in a TVAC chamber. The completely integrated observatory will be tested in TVAC to measure parasitic optical loading from the instrument, noise, microphonics and radio-frequency interference (RFI).

4 Design reference mission

DRAFT

4.1 Concept of operations

The PICO concept of operations is similar to that of the successful *WMAP* [229] and *Planck* [230] missions. After launch, PICO cruises to a halo orbit around the Earth–Sun L2 Lagrange point (§ 4.1.1). En route, a 2-week decontamination period is followed by instrument cooldown. After in-orbit checkout is complete, PICO begins the science survey.

PICO has a single science observing mode, surveying the sky continuously for 5 years using a pre-planned repetitive survey pattern (§ 4.1.2). Instrument data are compressed and stored on-board, then returned to Earth in daily 4-hr Ka-band science downlink passes (concurrent with science observations). Because PICO is observing relatively static Galactic, extragalactic, and cosmological targets, there are no requirements for time-critical observations or data latency. Presently, there are no plans for targets of opportunity or guest observer programs during the prime mission. The PICO instrument does not require cryogenic consumables (as the *Planck* mission did), permitting consideration of mission extension beyond the prime mission.

4.1.1 Mission design and launch

PICO performs its science survey from a halo orbit around the Earth–Sun L2 Lagrange point. Predecessor missions *Planck* and *WMAP* both operated in L2 orbits.

L2 orbits provide favorable survey geometry (relative to Earth orbits) by mitigating viewing restrictions imposed by terrestrial and lunar stray light. The PICO orbit around L2 is small enough to ensure than the Sun–Probe–Earth (SPE) angle is less than 15°. This maintains the telescope boresight $> 70°$ away from the Earth (Fig. 4.1, $70° = 180° - \alpha - \beta - \mathrm{SPE}$). High data rate downlink to the Deep Space Network (DSN) is available from L2 using near-Earth Ka bands. L2 provides a stable thermal environment, simplifying thermal control. The PICO orbit exhibits no post-launch eclipses.

NASA requires that Probes be compatible with an Evolved Expendable Launch Vehicle (EELV). For the purpose of this study, the Falcon 9 [231] is used as the reference vehicle. Fig. 4.2 shows PICO configured for launch in a Falcon 9 fairing. PICO's launch mass is well within the Falcon 9 capability.

Insertion to the halo manifold and associated trajectory correction maneuvers (TCMs) require $150\,\mathrm{m\,s^{-1}}$ of total Δv by the spacecraft. The orbital period is ~ 6 months. Orbit maintenance requires minimal propellant (statistical $\Delta v \sim 2\,\mathrm{m\,s^{-1}\,year^{-1}}$). There are no disposal requirements for L2 orbits, but spacecraft are customarily decommissioned to heliocentric orbit.

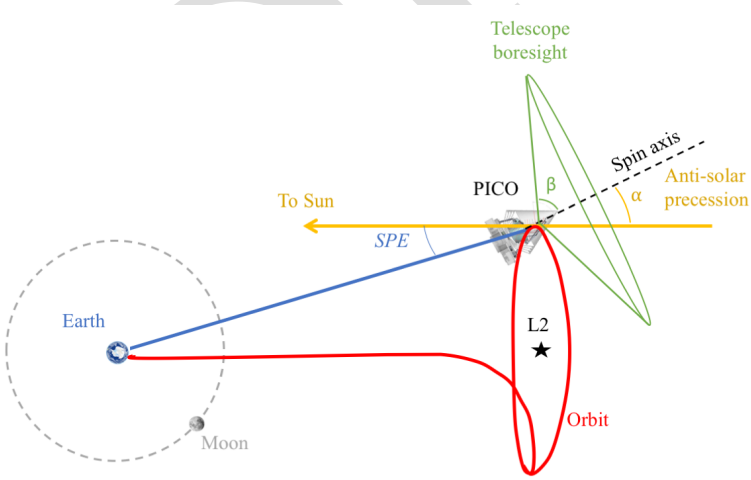

Figure 4.1: PICO surveys by continuously spinning the instrument about a precessing axis.

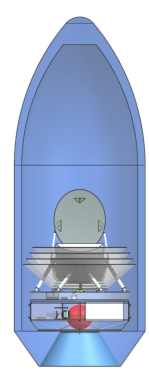

Figure 4.2: PICO is compatible with the Falcon 9.

4.1.2 Survey design

PICO utilizes a highly repetitive scan strategy to map the full sky. During the survey, PICO spins with a period $T_{\rm spin} = 1$ min about a spin axis oriented $\alpha = 26^\circ$ from the anti-solar direction (Fig. 4.1). This spin axis is forced to precess about the anti-solar direction with a period $T_{\rm prec} = 10$ hr. The telescope boresight is oriented at an angle $\beta = 69^\circ$ away from the spin axis. This β angle is chosen such that $\alpha + \beta > 90^\circ$, enabling mapping of all ecliptic latitudes. The precession axis tracks with the Earth in its yearly orbit around the Sun, so this scan strategy maps the full sky (all ecliptic longitudes) within 6 months.

PICO's $\alpha = 26^\circ$ is chosen to be substantially larger than the *Planck* mission's α angle (7.5°) to mitigate systematic effects by scanning across each sky pixel with a greater diversity of orientations [232]. Increasing α further would decrease the sun-shadowed volume available for the optics and consequently reduce the telescope aperture size. A deployable sun shade was considered, but not baselined.

The instrument spin rate, selected through a trade study, matches that of the Planck mission. The study balanced low-frequency ($1/f$) noise subtraction (improves with spin rate) against implementation cost and heritage, pointing reconstruction ability (anti-correlated with spin rate), and data volume (linearly correlated with spin rate). The $\ell = 2$ quadrupole power spectral mode appears in the data timestream at $2\ell \sin(\beta)/T_{\rm spin} = 60$ mHz [**?**]. Detector noise is stable down to these frequencies (§ 3.2.3). A destriping mapmaker applied in data post-processing effectively operates as a high-pass filter, as demonstrated by *Planck* [233]. PICO's spin axis precession frequency is $> 400\times$ faster than that of *Planck*, greatly reducing the effects of any residual $1/f$ noise by spreading the effects more isotropically across pixels.

4.2 Ground segment

The PICO Mission Operations System (MOS) and Ground Data System (GDS) can be built with extensive reuse of standard tools. The PICO concept of operations is described in § 4.1.2. There are no time critical events, and no driving data latency requirements. Routine orbit maintenance activities are required roughly every three months (§ 4.1.1). The payload consists of a single instrument with a single science observing mode (a repetitive survey pattern, § 4.1.2).

All space-ground communications, ranging, and tracking are performed by the Deep Space Network (DSN) 34 m Beam Wave Guide (BWG). X-band is used to transmit spacecraft commanding, return engineering data, and provide navigation information. Ka-band is used for high rate return of science data (150 Mb/s transfer; 130 Mb/s information rate after CCSDS encoding). The instrument produces 6.1 Tb/day, which is compressed to 1.5 Tb/day (§ 3.3). Daily 4 hr DSN passes return PICO data in 3.1 hr, with the remaining 0.9 hr available as needed for retransmission or missed-pass recovery.

4.3 Spacecraft

The PICO spacecraft bus meets all performance requirements with margin. It is designed for a minimum lifetime of 5 years in the L2 environment. Mission critical elements are redundant. Flight spares, engineering models and prototypes appropriate to Class B are budgeted.

The aft end of the spacecraft (the "de-spun module") is comprised of six equipment bays that house standard components (Fig. 4.3). The instrument and V-grooves are mounted on bipods from the spacecraft "spun module," which contains hosted instrument elements (Fig. 3.1). A spin motor drives the spun module at 1 rpm to support the science survey requirements (§ 4.1.2). Reaction wheels on the despun module cancel the angular momentum of the spun module and provide three-axis control (§ 4.3.1).

The bipods that mechanically support the instrument are thermally insulating. The passively radiating V-groove assembly thermally isolates the instrument from solar radiation and from the bus (§ 3.4.3). Like *Planck* [230], the V-grooves are manufactured using honeycomb material. Additional radiators on the spun and despun spacecraft modules ($\sim 1\,{\rm m}^2$ each) reject heat dissipated by spacecraft subsystems and hosted instrument elements.

PICO's avionics are dual-string with standard interfaces. Solid state recorders provide three days of science data storage (ensuring robustness to missed telecom passes).

DRAFT

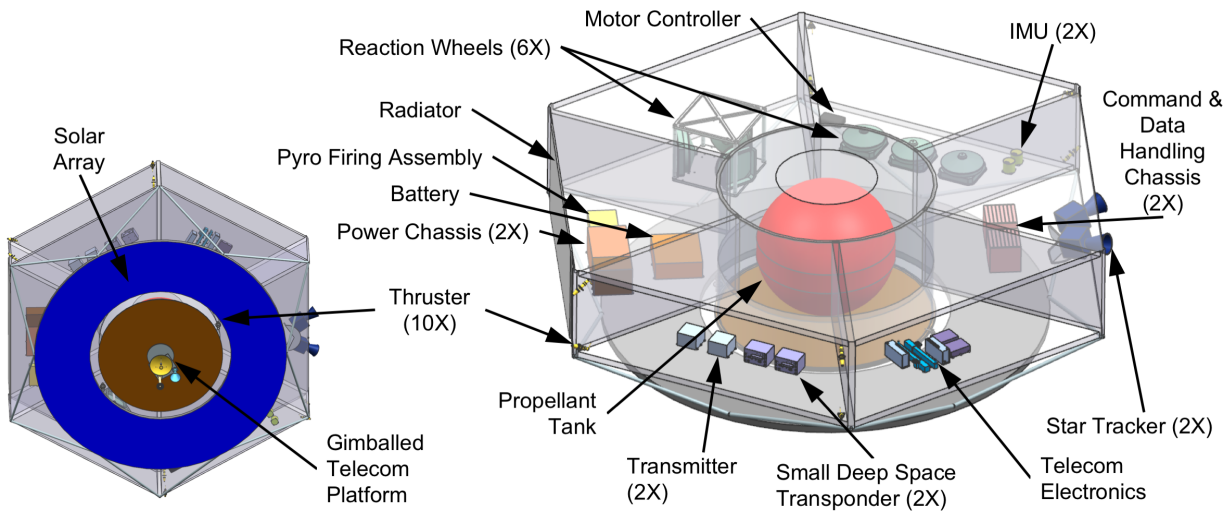

Figure 4.3: Modular equipment bays provide easy access to all components in the spacecraft de-spun module and enable parallel integration of spacecraft subsystems.

PICO employs a fully redundant Ka- and X-band telecommunications architecture. The Ka-band system uses a 0.3 m high-gain antenna to support a science data downlink information rate of 130 Mb/s to a 34 m BWG DSN ground station with a link margin of 4.8 dB. The X-band system provides command and engineering telemetry communication through all mission phases using medium and low gain antennas. Amplifiers, switches, and all three antennas are on a gimballed platform, enabling Ka and X-band downlink concurrent with science observations.

Solar cells on the aft side of the bus provide positive power (with contingency) for all mission power modes after launch. The driving mode is telecom concurrent with science survey. Unused area in the solar array plane affords significant margin for growth (Fig. 4.3). A Li-ion battery provides power during the launch phase. The heritage power electronics are dual-string.

The propulsion design is a simple monoprop blow-down hydrazine system with standard redundancy. Two aft-pointed 22 N thrusters provide Δv and attitude control for TCMs and orbit maintenance. Eight 4 N thrusters provide momentum management and backup attitude control authority.

4.3.1 Attitude determination and control

PICO uses a zero net angular momentum control architecture with heritage from the SMAP mission [234]. PICO's instrument spin rate (1 rpm) matches that of the *Planck* mission, but the precession of the spin axis is much faster (10 hr vs 6 months), and the precession angle much larger (26° vs 7.5°). These differences make the spin-stabilized *Planck* control architecture impractical because of the amount of torque required to drive precession.

The PICO 1 rpm instrument spin rate is achieved and maintained using a spin motor. The spin motor drive electronics provide the coarse spin rate knowledge used for controlling the spin rate to meet the ± 0.1 rpm requirement.

Three reaction wheel assemblies (RWAs) are mounted parallel to the instrument spin axis and spin opposite to the instrument to achieve zero net angular momentum and keep the despun module three-axis stabilized. The spin axis is precessed using three RWAs mounted normal to the spin axis in a triangle configuration. Each set of three RWAs is sized such that two could perform the required function, providing single fault tolerance.

Spin axis pointing and spin rate knowledge are achieved and maintained using star tracker and inertial

measurement unit (IMU) data. The attitude determination system is single-fault tolerant, with two IMUs each on the spun and despun modules, and two star trackers each on the spun and despun modules. Two sun sensors on the despun module are used for safe-mode contingencies and instrument Sun avoidance. All attitude control and reconstruction requirements are met, including spin axis control < 60 arcmin with < 1 arcmin/min stability, and reconstructed pointing knowledge < 10 arcsec (each axis, 3σ).

5 Technology maturation

PICO's detector and readout technologies have already been substantially matured through complimentary suborbital experiments, and can be developed by the APRA and SAT programs to NASA's Technology Readiness Level (TRL) 5 before Phase A (October 2023). The 4 K cryocooler baselined by PICO requires only standard thermal engineering (§ 3.4.2).

5.1 Current state of technologies

PICO builds off of the heritage of the *Planck* HFI instrument. The white noise of the *Planck* NTD-Ge bolometers was background-limited in all channels [235] with a $1/f$ knee at 200–300 mHz [236]. Since *Planck*, numerous suborbital experiments have used monolithically fabricated TES bolometers and multiplexing schemes to field instruments with thousands of detectors per camera.

Sentence 2 and onward do not support sentence 1. Need to discuss.

Suggest to change the heading below

5.1.1 Optical Coupling and Detectors

suggest the rephrase the text below to make it more readable for the uninitiated. Moved sentences around to make argument more logical. And clarified the issue with detectors. Suborbital teams have successfully demonstrated a variety of schemes to couple the incident free-space electromagnetic radiation onto detectors, including horns with ortho-mode transducers (OMTs), lithographed antenna arrays, and sinuous antennas under lenslets (Fig. 5.1). In all of these schemes the radiation is coupled through on-wafer transmission lines to bolometric transition-edge sensor detectors. Experiments on the ground and balloons are implementing these technologies with many of PICO's observing bands between 30 GHz and 270 GHz (Table 5.1). SPT-3G is using the PICO-baselined three-color pixel design to deploy 16,260 detectors covering 90–150–220 GHz add reference. Advanced ActPol has successfully deployed two-color pixels add reference. All of these detector arrays have been packaged into modules and focal plane units in working cameras representative of the PICO integration. The experiments have achieved background-limited performance in both ground and balloon instruments.

To date, suborbital experiments have achieved statistical map depths of $3\,\mu\mathrm{K}_{\mathrm{CMB}}$ arcmin on degree-scaled modes over small parts of the sky, approaching what PICO will achieve over the entire sky. Suborbital experiments have also demonstrated systematic control to this level through full-pipeline simulations and null-test analysis (jackknife tests). Moreover, laboratory tests and in-flight data from balloons suggest that these TES bolometers are more naturally robust against cosmic rays than the individual NTD-Ge bolometers used in Planck. Cosmic ray glitches have fast recovery times and low coincidence rates [237]. what did this paragraph want to say? not clear. what does that have to do with the title of the section?

PICO's 555–799 GHz channels (above the Niobium band gap) will use direct absorber bolometers. Ground and balloon experiments have deployed focal planes with hundreds of horn-coupled spiderweb bolometers. SPT-Pol deployed dual-polarized versions of direct absorber horn-coupled bolometers. *Planck* used this style of bolometer, but with NTD-Ge thermistors instead of TESes (Fig. 5.2). Filled arrays of detectors such as Backshort Under Ground (BUG) bolometers are also an option for these channels. The status of these efforts is summarized in Table 5.1. why are we showing the Planck detectors when we should show Herschel for the higher frequency bands?

DRAFT

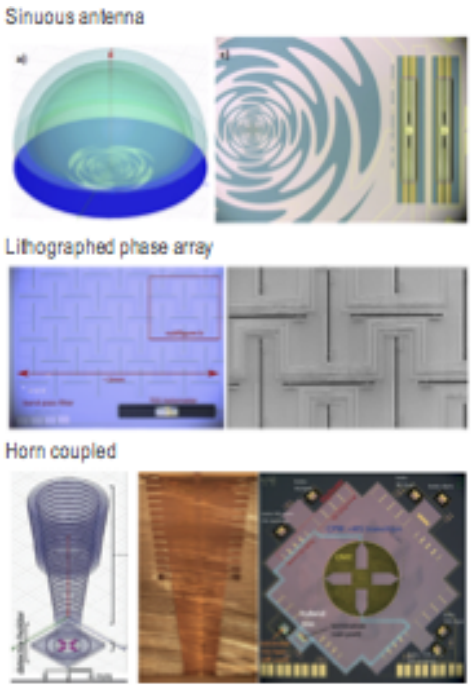

Figure 5.1: Multiple demonstrated optical coupling schemes are available to PICO. Images from CMB-S4 Technology Book [238].

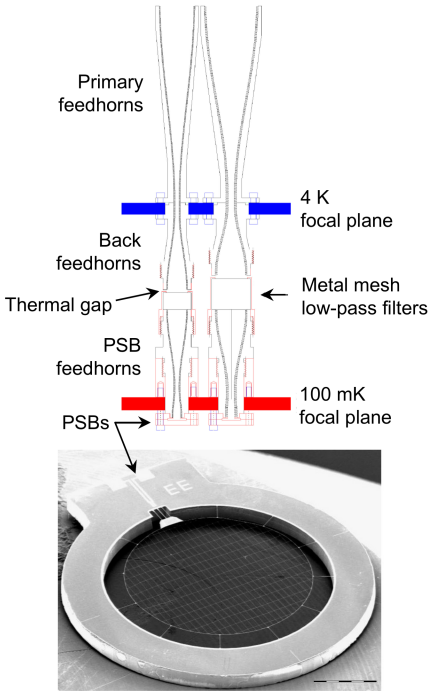

Figure 5.2: Direct-absorbing dual-polarized detectors and coupling horns used in *Planck* for 143–343 GHz bands.

5.1.2 Readout electronics status

More than ten experiments have used TDM readout. SCUBA2 on JCMT has 10,000 pixels, nearly as many detectors as planned for PICO [239]. we must also say something about FDM and μmux. We can't ignore these technologies.

5.2 Development plan

5.2.1 Detector development

The baseline PICO instrument requires three-color dual-polarized antenna-coupled bolometers covering bands from 21 to 462 GHz and single-color dual-polarized direct-absorbing bolometers from 555 to 799 GHz (§ 3.2.1, and Table 3.1). The developments required to enable the PICO baseline design are:

- extension of antenna-coupled bolometers down to 21 GHz and up to 462 GHz;
- demonstration of three-color pixels across that spectrum, with characterization of beam properties and associated systematics;
- construction of high frequency direct absorbing arrays and laboratory testing; and
- beam line and 100 mK testing to simulate the cosmic ray environment at L2.

The extension to lower frequencies requires larger antennas and therefore control of film properties and lithography over larger areas. Scaling to higher frequencies forces tighter critical dimensions and materials tend to exhibit higher losses. These challenges require tight control of cleanliness and full understanding of process parameters.

The sinuous antenna has the bandwidth to service three-colors per pixel, whereas horns and antenna arrays have only been used for two, so some version of the sinuous antenna will likely be needed to realize three-color pixels. However, the sinuous antenna couples to states that "wobble" log-periodically with frequency. There are potential solutions to this in the focal plane design, analysis, and free parameters of the antenna geometry. These will need to be explored subject to the uniformity and packing density constraints

DRAFT

Table 5.1: Multiple active suborbital efforts are advancing technologies relevant to PICO.

Project	Type	Polarized	Mono-lithic	$\nu_{c,\,Low}$ [GHz]	$\nu_{c,\,High}$ [GHz]	Colors per pixel	N_{bolo}	Significance	Reference
PICO low frequency	**Probe**	**Yes**	**Yes**	**21**	**462**	**Three**	**11,796**		**§3.2.1**
SPT-3G	Ground	Yes	Yes	90	220	Three	16,260	Trichroic	(Anderson 2018)
Advanced ACT-pol	Ground	Yes	Yes	27	230	Two	3,072	Dichroic	(Simon 2018)
BICEP/Keck	Ground	Yes	Yes	90	270	One	5,120	50nK-deg	(BICEP2&Keck 2018)
Berkeley, Caltech, NIST	Lab	Yes	Yes	30	270	Two	NA	Band coverage	
SPIDER	Balloon	Yes	Yes	90	150	One	2,400	Stable to 10mHz	(Rahlin 2014)
PICO high frequency	**Probe**	**Yes**	**Yes**	**555**	**799**	**One**	**1,200**		**§3.2.2**
Planck HFI	Flight	143-343 GHz	No	143	857	One	48	TRL 9 absorbing bolometers	(Planck HFI Core Team 2011)
SPT-SZ	Ground	No	Yes	90	220	One	840	Monolithic array TESes	
SPT-pol-90	Ground	Yes	No	90	90	One	180	Dual pol absorbing TESes	

present at the extreme spectral bands. Systematics studies for field demonstrations will be particularly important. The PICO concept is robust to any challenges in developing three-color pixels; § 5.3 describes an option to descope to two-color pixels.

Planck demonstrated the architecture of horns coupled to direct absorbing bolometers. For PICO's high frequency detectors, this only needs to be generalized to dual polarized arrays. The greatest remaining challenge is the low risk development of a packaging design. Such prototyping could culminate in a field demonstration, best performed in a balloon.

So far, cosmic ray tests and in-flight analysis of TES bolometers are encouraging [237]. The CMB community can retire residual risk with 100 mK testing where the array heat sinking may be weaker, and beam-line tests to help control for background glitch rates.

A plan to accomplish all required development is described in Table 5.2.

5.2.2 Readout electronics development

PICO's sensitivity requirements dictate the use of $\sim 13,000$ transition edge sensor bolometers, requiring a highly multiplexed system. The PICO baseline design calls for time division multiplexing with 128 switched rows per readout column (TDM-128$\times$), which exceeds that of Advanced ACTPol's recently demonstrated TDM-66$\times$ [217]. The leap to TDM-128$\times$ requires:

- development of fast-switched room temperature electronics;
- system engineering of room temperature to cryogenic row select cabling to ensure sufficiently fast row switch settling times; and
- demonstration of TDM-128$\times$ SQUID aliased noise below PICO detector sensitivity requirements.

A plan to accomplish the required development is described in Table 5.2.

5.3 Technology descopes

A descope from three-color to two-color pixels remains a viable alternative should the three-color technology not mature as planned. Descope studies suggest that a PICO-size focal plane using two-color pixels at the lower frequencies and the baseline one-color pixels at the higher frequencies would contain 8,840 detectors (compared to the baseline 12,966) and map in 19 colors (baseline 21). Because horns have a 2.3 : 1 bandwidth, each of the two bands in a pixel has 35% bandwidth (compared to the baseline 25%), which compensates for pixel count, resulting in the same 0.61 μK_{CMB} arcmin aggregate map depth (Table 3.2), but with coarser spectral resolution.

DRAFT

Table 5.2: PICO technologies can be developed to TRL 5 prior to a 2023 Phase A start using the APRA and SAT programs.

Task	Current status	Milestone A	Milestone B	Milestone C	Current Funding	Required Funding	Date TRL5 achieved
3-color arrays ν<90 GHz	See Table 5.1	Field demo of 30-40 GHz (2020)	Lab demos 20-90 GHz (2022)		APRA & SAT funds	$2.5M over 4 yr (1 APRA +1 SAT)	2022
3-color arrays ν>220 GHz		Field demo of 150-270 GHz (2021)	Lab demos 150-460 GHz (2022)		APRA & SAT funds	$3.5M over 4 yr (2 SATs)	2022
Direct absorbing arrays ν>550 GHz		Design & prototype of arrays (2021)	Lab demo of 555 GHz (2022)	Lab demo 799 GHz (2023)	None	$2M over 5 yr (1 SAT)	2023
Cosmic ray studies	250 mK w/ sources	100 mK tests with sources (2021)	Beamline tests (2023)		APRA & SAT funds	$0.5-1M over 5 yr (part of 1 SAT)	NA
Fast readout electronics	MUX66 demo	Engineering and Fab of electronics (2020)	Lab demo (2021)	Field demo (2023)	No direct funds	$2.5M over 5 yr (1 SAT)	2023
System engineering/ 128x MUX demo	MUX66 demo	Design of cables (2020)	Lab demo (2021)	Field demo (2023)	No direct funds		

5.4 Enhancing technologies

The following technologies are neither required nor assumed by the PICO baseline concept. They represent opportunities to extend scientific capabilities or simplify engineering.

PICO baselines TDM readout because of its relative maturity and demonstrated sensitivity and stability in relevant science missions. Lab tests of Frequency Domain Multiplexing (FDM) suggest comparable performance with higher multiplexing factors and lower loads on cryogenic stages relative to TDM. Suborbital experiments such as SPT-3G have used frequency division multiplexing (FDM) to readout focal planes comparable in size to PICO.

Microwave frequency SQUID multiplexing can increase the multiplexing density and reduce the number of lines between the 4K and ambient temperature stages [240, 241]. Kinetic Inductance Detectors (KIDs) and Thermal KIDs (TKIDs) can further reduce the wire count, obviate the SQUIDs, and dramatically simplify integration by performing multiplexing on the same substrate as the detectors themselves [242, 243]. The cost to develop these technologies is $3–4M/year, with a high chance of reaching TRL-5 before Phase A.

6 Project management, heritage, risk, and cost

6.1 PICO Study Participants

The PICO study was open to the entire mm/sub-mm science community and included more than 150 scientists. Seven working groups were led by members of PICO's Executive Committee, which met weekly under the leadership of PI Shaul Hanany. More than 60 people participated in-person in two community workshops (November 2017 and May 2018).

The PICO engineering concept definition package was generated by Team X (the JPL concurrent design lab). The Team X study was supported by inputs from a JPL engineering team and Lockheed Martin.

The full list of study report contributors and endorsers follows the cover page.

6.2 Project management plan

PICO benefits from the experience of predecessor missions such as *Planck* and *WMAP*, as well as many years of investment in technology development and a multitude of suborbital experiments. In addition to demonstrated science and engineering capabilities, this heritage has developed a community of people with

DRAFT

the expertise required to field a successful mission.

This study assumes mission management by JPL with a Principal Investigator leading a single science team. A Project Manager provides project oversight for schedule, budget, and deliverables. A Project Systems Engineer leads systems engineering activities and serves as the Engineering Technical Authority. A Mission Assurance Manager serves as the Independent Technical Authority. The PICO mission development schedule is shown in Fig. 6.1.

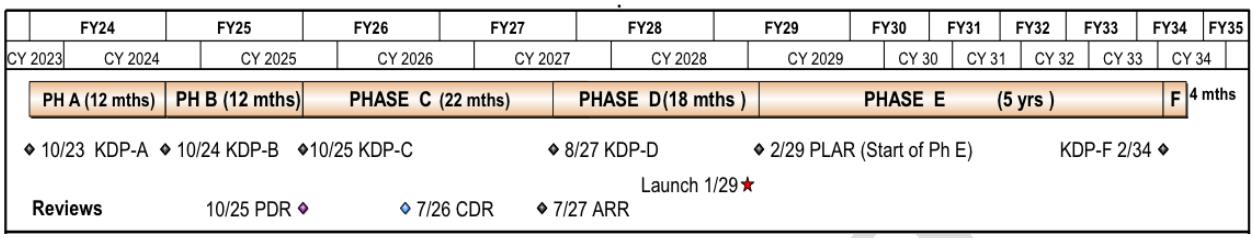

Figure 6.1: The PICO baseline schedule is based on historical actuals from similarly-sized missions such as Juno and SMAP.

Probes are medium-class missions, similar in cost scope to NASA's New Frontiers missions, which are Category 1 and Risk Classification A or B, with Phase A–D costs capped at $\sim$ \$850M (not including the launch vehicle). JPL is well-prepared to manage Probe missions, having managed the Juno New Frontiers mission (launched 2011) and also the development of the medium-class *Spitzer* Space Telescope (launched 2003). JPL delivered the bolometric detectors for the *Planck* HFI instrument (launched 2009). Presently, JPL is managing NEOCam, a Discovery class infrared space telescope.

The PICO spacecraft provider will be selected during mission formulation. Multiple organizations are capable of providing a spacecraft bus to meet PICO's requirements. Lockheed Martin contributed to the PICO concept study, leveraging their experience with New Frontiers missions Juno and OSIRIS-REx.

6.3 Heritage

The successful *Planck* mission provides science heritage for PICO. Technical heritage traces to multiple missions.

Because PICO observes in the mm/sub-mm regime, the surface accuracy requirement for the reflectors is relatively easy to meet. PICO's reflectors are similar to *Planck*'s, but somewhat larger (270 cm $\times$ 205 cm primary vs. 189 cm $\times$ 155 cm) [244]. *Herschel* observed at wavelengths more demanding than PICO's and was larger (350 cm diameter primary) [245].

The heritage of the PICO detectors and readout electronics (§ 3.2, § 3.3) is described in § 5.1.

PICO's detectors are cooled by a cADR (3.4.1) with requirements that are within the capabilities of current cADRs developed by Goddard Space Flight Center. These systems have been applied to several JAXA missions, including Hitomi [224].

PICO's 4 K cryocooler (§ 3.4.2) is a direct extension of the JWST MIRI design [225, 226]. PICO benefits from a simpler and more reliable implementation of the J-T system than was required for MIRI, in that no deployment of cooling lines is required, and all flow valving is performed on the warm spacecraft. Cooling multiple independent points with a J-T loop has been demonstrated on *Planck* with the JPL-supplied 18 K cooler [246].

Structures similar to PICO's V-groove assembly (§ 3.4.3) are a standard approach for passive cooling first described more than thirty years ago [247]. The JWST mission will deploy a 22 m $\times$ 10 m V-groove sun shield. PICO's relatively modest 4.5 m diameter V-groove assembly fits inside the launch vehicle fairing. Because it does not require deployment, PICO has baselined a simple honeycomb material construction like that successfully flown by the *Planck* mission [246, 248].

DRAFT

Most requirements on the PICO spacecraft are well within typical ranges and can be met with standard high heritage systems (§ 4.3). PICO's spin architecture and data volume requirements are less typical, and discussed below.

The PICO zero-momentum control architecture (§ 4.3.1) has heritage from the SMAP mission. PICO has a slower spin rate and less cancelled angular momentum than SMAP. SMAP requires 359 Nms to cancel the momentum of a 6 m instrument antenna spun at 14.6 rpm [234]. The PICO launch mass (including contingency) is similar to the *Planck* launch mass. If we assume *Planck* moments of inertia [249], the PICO spun elements would have an angular momentum of 210 Nms at 1 rpm. This is conservative because, unlike *Planck*, the entire PICO observatory does not spin.

Though PICO's data volume is notable by current standards, it is already enveloped by missions in development. PICO produces 6.1 Tb/day of raw data which is compressed to 1.5Tb/day (§ 3.3). PICO downlinks data daily, but baselines storage of 3 days of (compressed) data to mitigate missed telecom passes. This requires 4.5 Tb of onboard storage, in family with the 3.14 Tb solid state recorder currently in use by Landsat 8 and much smaller than the 12 Tbit flash memory planned for NISAR [250]. The PICO baseline 150 Mb/s Ka-band data downlink is an existing DSN catalog service (DSN 2015). The TESS mission presently downlinks data to the DSN using Ka-band at 100 Mb/s. The baseline PICO mission generates $\sim 2,200$ Tb of raw (uncompressed) data per year, less than the $\sim 6,800$ Tb/year currently returned by Landsat 8 and $\sim 9,300$ Tb/yr planned by NISAR [250].

6.4 Risk assessment

6.4.1 Pre-mission risks

Technology development (§ 5) is performed prior to the beginning of mission development, and is outside of the mission cost (per NASA direction), so associated risks do not represent threats to the cost of mission development. Rather, they represent risks to the availability of the described baseline mission. A technology-related mission descope is described in § 5.3.

6.4.2 Development risks

PICO's healthy contingencies, margins, and reserves provide flexibility to address risks realized during mission development. PICO carries $> 40\,\%$ instrument sensitivity margin (Table 3.2), $> 100\,\%$ heat lift margin (Table 3.3), 43 % system power contingency, 31 % payload mass contingency, and 27 % spacecraft mass contingency. The Falcon 9 launch capability (for ocean recovery) exceeds PICO's total launch mass (including contingency) by a $\sim 50\,\%$ margin. The PICO budget includes 30 % cost reserves for Phases A–D (§ 6.5).

During mission development the Project Systems Engineer continually assesses risks, tracks progress toward retiring them, and updates mitigations. Mitigations for a few top risks identified during this study are described below.

Thermal risk can be mitigated through extensive thermal modeling and review in Phase A, and design for early test verification. Risks associated with the instrument spin architecture can be mitigated by engaging JPL engineers who were involved in the SMAP mission. Detector delivery schedule risk can be mitigated by beginning fabrication early in the project life cycle and fabricating a generous number of detector wafers to ensure adequate yield. Risks associated with the integration and test of a cryogenic instrument can be mitigated through advanced planning and allocation of appropriate schedule and schedule margin.

6.4.3 Operations risks

The PICO design meets the requirements associated with the NASA Class B risk classification. For Class B missions, essential spacecraft and instrument functions are typically fully redundant. This increases mission cost, but significantly reduces the risk of mission failure during operations.

The PICO mission utilizes a single instrument with a single observing mode mapping the sky using a repetitive survey pattern. The mission does not require any time-critical activities. The observatory fits in to the launch vehicle fairing in its operational configuration, so no hardware deployments are required. The

DRAFT

telescope does not require a cover (nor the associated mission-critical cover release).

The spacecraft incorporates a fault protection system for anomaly detection and resolution. The Sun-pointed, command receptive, thermally stable safe-mode attitude allows ground intervention for fault resolution without time constraints. PICO's high degree of hardware redundancy and onboard fault protection ensure spacecraft safety in the event of unforeseen failures and faults.

Science data analysis, including foreground separation (§ **??**) and systematics control (§ **??**) are discussed in the science section (§ **??**).

6.5 Mission cost

The cost section is excluded from this draft release.

DRAFT

References

[1] A. Mennella, M. Bersanelli, R. C. Butler, A. Curto, F. Cuttaia, R. J. Davis, J. Dick, M. Frailis, S. Galeotta, A. Gregorio, H. Kurki-Suonio, C. R. Lawrence, S. Leach, J. P. Leahy, S. Lowe, D. Maino, N. Mandolesi, M. Maris, E. Martínez-González, P. R. Meinhold, G. Morgante, D. Pearson, F. Perrotta, G. Polenta, T. Poutanen, M. Sandri, M. D. Seiffert, A.-S. Suur-Uski, D. Tavagnacco, L. Terenzi, M. Tomasi, J. Valiviita, F. Villa, R. Watson, A. Wilkinson, A. Zacchei, A. Zonca, B. Aja, E. Artal, C. Baccigalupi, A. J. Banday, R. B. Barreiro, J. G. Bartlett, N. Bartolo, P. Battaglia, K. Bennett, A. Bonaldi, L. Bonavera, J. Borrill, F. R. Bouchet, C. Burigana, P. Cabella, B. Cappellini, X. Chen, L. Colombo, M. Cruz, L. Danese, O. D'Arcangelo, R. D. Davies, G. de Gasperis, A. de Rosa, G. de Zotti, C. Dickinson, J. M. Diego, S. Donzelli, G. Efstathiou, T. A. Enßlin, H. K. Eriksen, M. C. Falvella, F. Finelli, S. Foley, C. Franceschet, E. Franceschi, T. C. Gaier, R. T. Génova-Santos, D. George, F. Gómez, J. González-Nuevo, K. M. Górski, A. Gruppuso, F. K. Hansen, D. Herranz, J. M. Herreros, R. J. Hoyland, N. Hughes, J. Jewell, P. Jukkala, M. Juvela, P. Kangaslahti, E. Keihänen, R. Keskitalo, V.-H. Kilpia, T. S. Kisner, J. Knoche, L. Knox, M. Laaninen, A. Lähteenmäki, J.-M. Lamarre, R. Leonardi, J. León-Tavares, P. Leutenegger, P. B. Lilje, M. López-Caniego, P. M. Lubin, M. Malaspina, D. Marinucci, M. Massardi, S. Matarrese, F. Matthai, A. Melchiorri, L. Mendes, M. Miccolis, M. Migliaccio, S. Mitra, A. Moss, P. Natoli, R. Nesti, H. U. Nørgaard-Nielsen, L. Pagano, R. Paladini, D. Paoletti, B. Partridge, F. Pasian, V. Pettorino, D. Pietrobon, M. Pospieszalski, G. Prézeau, M. Prina, P. Procopio, J.-L. Puget, C. Quercellini, J. P. Rachen, R. Rebolo, M. Reinecke, S. Ricciardi, G. Robbers, G. Rocha, N. Roddis, J. A. Rubino-Martín, M. Savelainen, D. Scott, R. Silvestri, A. Simonetto, P. Sjoman, G. F. Smoot, C. Sozzi, L. Stringhetti, J. A. Tauber, G. Tofani, L. Toffolatti, J. Tuovinen, M. Türler, G. Umana, L. Valenziano, J. Varis, P. Vielva, N. Vittorio, L. A. Wade, C. Watson, S. D. M. White, and F. Winder, "Planck early results. III. First assessment of the Low Frequency Instrument in-flight performance," *Astron. Astrophys.*, vol. 536, p. A3, Dec. 2011.

[2] Planck HFI Core Team, P. A. R. Ade, N. Aghanim, R. Ansari, M. Arnaud, M. Ashdown, J. Aumont, A. J. Banday, M. Bartelmann, J. G. Bartlett, E. Battaner, K. Benabed, A. Benoît, J.-P. Bernard, M. Bersanelli, R. Bhatia, J. J. Bock, J. R. Bond, J. Borrill, F. R. Bouchet, F. Boulanger, T. Bradshaw, E. Bréelle, M. Bucher, P. Camus, J.-F. Cardoso, A. Catalano, A. Challinor, A. Chamballu, J. Charra, M. Charra, R.-R. Chary, C. Chiang, S. Church, D. L. Clements, S. Colombi, F. Couchot, A. Coulais, C. Cressiot, B. P. Crill, M. Crook, P. de Bernardis, J. Delabrouille, J.-M. Delouis, F.-X. Désert, K. Dolag, H. Dole, O. Doré, M. Douspis, G. Efstathiou, P. Eng, C. Filliard, O. Forni, P. Fosalba, J.-J. Fourmond, K. Ganga, M. Giard, D. Girard, Y. Giraud-Héraud, R. Gispert, K. M. Górski, S. Gratton, M. Griffin, G. Guyot, J. Haissinski, D. Harrison, G. Helou, S. Henrot-Versillé, C. Hernández-Monteagudo, S. R. Hildebrandt, R. Hills, E. Hivon, M. Hobson, W. A. Holmes, K. M. Huffenberger, A. H. Jaffe, W. C. Jones, J. Kaplan, R. Kneissl, L. Knox, G. Lagache, J.-M. Lamarre, P. Lami, A. E. Lange, A. Lasenby, A. Lavabre, C. R. Lawrence, B. Leriche, C. Leroy, Y. Longval, J. F. Macías-Pérez, T. Maciaszek, C. J. MacTavish, B. Maffei, N. Mandolesi, R. Mann, B. Mansoux, S. Masi, T. Matsumura, P. McGehee, J.-B. Melin, C. Mercier, M.-A. Miville-Deschênes, A. Moneti, L. Montier, D. Mortlock, A. Murphy, F. Nati, C. B. Netterfield, H. U. Nørgaard-Nielsen, C. North, F. Noviello, D. Novikov, S. Osborne, C. Paine, F. Pajot, G. Patanchon, T. Peacocke, T. J. Pearson, O. Perdereau, L. Perotto, F. Piacentini, M. Piat, S. Plaszczynski, E. Pointecouteau, R. Pons, N. Ponthieu, G. Prézeau, S. Prunet, J.-L. Puget, W. T. Reach, C. Renault, I. Ristorcelli, G. Rocha, C. Rosset, G. Roudier, M. Rowan-Robinson, B. Rusholme, D. Santos, G. Savini, B. M. Schaefer, P. Shellard, L. Spencer, J.-L. Starck, P. Stassi, V. Stolyarov, R. Stompor, R. Sudiwala, R. Sunyaev, J.-F. Sygnet, J. A. Tauber, C. Thum, J.-P. Torre, F. Touze, M. Tristram, F. van Leeuwen, L. Vibert, D. Vibert, L. A. Wade, B. D. Wandelt, S. D. M. White, H. Wiesemeyer, A. Woodcraft, V. Yurchenko, D. Yvon, and A. Zacchei, "Planck early results. IV. First assessment of the High Frequency Instrument in-flight performance," *Astron. Astrophys.*, vol. 536, p. A4, Dec. 2011.

[3] U. Seljak and M. Zaldarriaga, "Signature of gravity waves in polarization of the microwave background," *Phys. Rev. Lett.*, vol. 78, pp. 2054–2057, 1997.

[4] M. Kamionkowski, A. Kosowsky, and A. Stebbins, "A Probe of primordial gravity waves and vorticity," *Phys. Rev. Lett.*, vol. 78, pp. 2058–2061, 1997.

[5] A. H. Guth, "The Inflationary Universe: A Possible Solution to the Horizon and Flatness Problems," *Phys. Rev.*, vol. D23, pp. 347–356, 1981, [Adv. Ser. Astrophys. Cosmol.3,139(1987)].

[6] A. D. Linde, "A New Inflationary Universe Scenario: A Possible Solution of the Horizon, Flatness, Homogeneity, Isotropy and Primordial Monopole Problems," *Phys. Lett.*, vol. 108B, pp. 389–393, 1982, [Adv. Ser. Astrophys. Cosmol.3,149(1987)].

[7] A. Albrecht and P. J. Steinhardt, "Cosmology for Grand Unified Theories with Radiatively Induced Symmetry Breaking," *Phys. Rev. Lett.*, vol. 48, pp. 1220–1223, 1982, [Adv. Ser. Astrophys. Cosmol.3,158(1987)].

[8] A. A. Starobinsky, "A New Type of Isotropic Cosmological Models Without Singularity," *Phys. Lett.*, vol. B91, pp. 99–102, 1980, [,771(1980)].

[9] V. F. Mukhanov and G. V. Chibisov, "Quantum Fluctuations and a Nonsingular Universe," *JETP Lett.*, vol. 33, pp. 532–535, 1981, [Pisma Zh. Eksp. Teor. Fiz.33,549(1981)].

[10] A. H. Guth and S. Y. Pi, "Fluctuations in the New Inflationary Universe," *Phys. Rev. Lett.*, vol. 49, pp. 1110–1113, 1982.

[11] S. W. Hawking, "The Development of Irregularities in a Single Bubble Inflationary Universe," *Phys. Lett.*, vol. 115B, p. 295, 1982.

DRAFT

[12] A. A. Starobinsky, "Dynamics of Phase Transition in the New Inflationary Universe Scenario and Generation of Perturbations," *Phys. Lett.*, vol. 117B, pp. 175–178, 1982.

[13] J. M. Bardeen, P. J. Steinhardt, and M. S. Turner, "Spontaneous Creation of Almost Scale - Free Density Perturbations in an Inflationary Universe," *Phys. Rev.*, vol. D28, p. 679, 1983.

[14] A. A. Starobinsky, "Spectrum of relict gravitational radiation and the early state of the universe," *JETP Lett.*, vol. 30, pp. 682–685, 1979, [,767(1979)].

[15] The Polarbear Collaboration: P. A. R. Ade, Y. Akiba, A. E. Anthony, K. Arnold, M. Atlas, D. Barron, D. Boettger, J. Borrill, S. Chapman, Y. Chinone, M. Dobbs, T. Elleflot, J. Errard, G. Fabbian, C. Feng, D. Flanigan, A. Gilbert, W. Grainger, N. W. Halverson, M. Hasegawa, K. Hattori, M. Hazumi, W. L. Holzapfel, Y. Hori, J. Howard, P. Hyland, Y. Inoue, G. C. Jaehnig, A. H. Jaffe, B. Keating, Z. Kermish, R. Keskitalo, T. Kisner, M. Le Jeune, A. T. Lee, E. M. Leitch, E. Linder, M. Lungu, F. Matsuda, T. Matsumura, X. Meng, N. J. Miller, H. Morii, S. Moyerman, M. J. Myers, M. Navaroli, H. Nishino, A. Orlando, H. Paar, J. Peloton, D. Poletti, E. Quealy, G. Rebeiz, C. L. Reichardt, P. L. Richards, C. Ross, I. Schanning, D. E. Schenck, B. D. Sherwin, A. Shimizu, C. Shimmin, M. Shimon, P. Siritanasak, G. Smecher, H. Spieler, N. Stebor, B. Steinbach, R. Stompor, A. Suzuki, S. Takakura, T. Tomaru, B. Wilson, A. Yadav, and O. Zahn, "A Measurement of the Cosmic Microwave Background B-mode Polarization Power Spectrum at Sub-degree Scales with POLARBEAR," *Ap. J.*, vol. 794, p. 171, Oct. 2014.

[16] R. Keisler, S. Hoover, N. Harrington, J. W. Henning, P. A. R. Ade, K. A. Aird, J. E. Austermann, J. A. Beall, A. N. Bender, B. A. Benson, L. E. Bleem, J. E. Carlstrom, C. L. Chang, H. C. Chiang, H.-M. Cho, R. Citron, T. M. Crawford, A. T. Crites, T. de Haan, M. A. Dobbs, W. Everett, J. Gallicchio, J. Gao, E. M. George, A. Gilbert, N. W. Halverson, D. Hanson, G. C. Hilton, G. P. Holder, W. L. Holzapfel, Z. Hou, J. D. Hrubes, N. Huang, J. Hubmayr, K. D. Irwin, L. Knox, A. T. Lee, E. M. Leitch, D. Li, D. Luong-Van, D. P. Marrone, J. J. McMahon, J. Mehl, S. S. Meyer, L. Mocanu, T. Natoli, J. P. Nibarger, V. Novosad, S. Padin, C. Pryke, C. L. Reichardt, J. E. Ruhl, B. R. Saliwanchik, J. T. Sayre, K. K. Schaffer, E. Shirokoff, G. Smecher, A. A. Stark, K. T. Story, C. Tucker, K. Vanderlinde, J. D. Vieira, G. Wang, N. Whitehorn, V. Yefremenko, and O. Zahn, "Measurements of Sub-degree B-mode Polarization in the Cosmic Microwave Background from 100 Square Degrees of SPTpol Data," *Ap. J.*, vol. 807, p. 151, Jul. 2015.

[17] T. Louis, E. Grace, M. Hasselfield, M. Lungu, L. Maurin, G. E. Addison, P. A. R. Ade, S. Aiola, R. Allison, M. Amiri, E. Angile, N. Battaglia, J. A. Beall, F. de Bernardis, J. R. Bond, J. Britton, E. Calabrese, H.-m. Cho, S. K. Choi, K. Coughlin, D. Crichton, K. Crowley, R. Datta, M. J. Devlin, S. R. Dicker, J. Dunkley, R. Dünner, S. Ferraro, A. E. Fox, P. Gallardo, M. Gralla, M. Halpern, S. Henderson, J. C. Hill, G. C. Hilton, M. Hilton, A. D. Hincks, R. Hlozek, S. P. P. Ho, Z. Huang, J. Hubmayr, K. M. Huffenberger, J. P. Hughes, L. Infante, K. Irwin, S. Muya Kasanda, J. Klein, B. Koopman, A. Kosowsky, D. Li, M. Madhavacheril, T. A. Marriage, J. McMahon, F. Menanteau, K. Moodley, C. Munson, S. Naess, F. Nati, L. Newburgh, J. Nibarger, M. D. Niemack, M. R. Nolta, C. Nuñez, L. A. Page, C. Pappas, B. Partridge, F. Rojas, E. Schaan, B. L. Schmitt, N. Sehgal, B. D. Sherwin, J. Sievers, S. Simon, D. N. Spergel, S. T. Staggs, E. R. Switzer, R. Thornton, H. Trac, J. Treu, C. Tucker, A. Van Engelen, J. T. Ward, and E. J. Wollack, "The Atacama Cosmology Telescope: two-season ACTPol spectra and parameters," *JCAP*, vol. 6, p. 031, Jun. 2017.

[18] P. A. R. Ade *et al.*, "Improved Constraints on Cosmology and Foregrounds from BICEP2 and Keck Array Cosmic Microwave Background Data with Inclusion of 95 GHz Band," *Phys. Rev. Lett.*, vol. 116, p. 031302, 2016.

[19] Planck Collaboration, Y. Akrami, F. Arroja, M. Ashdown, J. Aumont, C. Baccigalupi, M. Ballardini, A. J. Banday, R. B. Barreiro, N. Bartolo, S. Basak, R. Battye, K. Benabed, J.-P. Bernard, M. Bersanelli, P. Bielewicz, J. J. Bock, J. R. Bond, J. Borrill, F. R. Bouchet, F. Boulanger, M. Bucher, C. Burigana, R. C. Butler, E. Calabrese, J.-F. Cardoso, J. Carron, B. Casaponsa, A. Challinor, H. C. Chiang, L. P. L. Colombo, C. Combet, D. Contreras, B. P. Crill, F. Cuttaia, P. de Bernardis, G. de Zotti, J. Delabrouille, J.-M. Delouis, F.-X. Désert, E. Di Valentino, C. Dickinson, J. M. Diego, S. Donzelli, O. Doré, M. Douspis, A. Ducout, X. Dupac, G. Efstathiou, F. Elsner, T. A. Enßlin, H. K. Eriksen, E. Falgarone, Y. Fantaye, J. Fergusson, R. Fernandez-Cobos, F. Finelli, F. Forastieri, M. Frailis, E. Franceschi, A. Frolov, S. Galeotta, S. Galli, K. Ganga, R. T. Génova-Santos, M. Gerbino, T. Ghosh, J. González-Nuevo, K. M. Górski, S. Gratton, A. Gruppuso, J. E. Gudmundsson, J. Hamann, W. Handley, F. K. Hansen, G. Helou, D. Herranz, E. Hivon, Z. Huang, A. H. Jaffe, W. C. Jones, A. Karakci, E. Keihänen, R. Keskitalo, K. Kiiveri, J. Kim, T. S. Kisner, L. Knox, N. Krachmalnicoff, M. Kunz, H. Kurki-Suonio, G. Lagache, J.-M. Lamarre, M. Langer, A. Lasenby, M. Lattanzi, C. R. Lawrence, M. Le Jeune, J. P. Leahy, J. Lesgourgues, F. Levrier, A. Lewis, M. Liguori, P. B. Lilje, M. Lilley, V. Lindholm, M. López-Caniego, P. M. Lubin, Y.-Z. Ma, J. F. Macías-Pérez, G. Maggio, D. Maino, N. Mandolesi, A. Mangilli, A. Marcos-Caballero, M. Maris, P. G. Martin, E. Martínez-González, S. Matarrese, N. Mauri, J. D. McEwen, P. D. Meerburg, P. R. Meinhold, A. Melchiorri, A. Mennella, M. Migliaccio, M. Millea, S. Mitra, M.-A. Miville-Deschênes, D. Molinari, A. Moneti, L. Montier, G. Morgante, A. Moss, S. Mottet, M. Münchmeyer, P. Natoli, H. U. Nørgaard-Nielsen, C. A. Oxborrow, L. Pagano, D. Paoletti, B. Partridge, G. Patanchon, T. J. Pearson, M. Peel, H. V. Peiris, F. Perrotta, V. Pettorino, F. Piacentini, L. Polastri, G. Polenta, J.-L. Puget, J. P. Rachen, M. Reinecke, M. Remazeilles, A. Renzi, G. Rocha, C. Rosset, G. Roudier, J. A. Rubiño-Martín, B. Ruiz-Granados, L. Salvati, M. Sandri, M. Savelainen, D. Scott, E. P. S. Shellard, M. Shiraishi, C. Sirignano, G. Sirri, L. D. Spencer, R. Sunyaev, A.-S. Suur-Uski, J. A. Tauber, D. Tavagnacco, M. Tenti, L. Terenzi, L. Toffolatti, M. Tomasi, T. Trombetti, J. Valiviita, B. Van Tent, L. Vibert, P. Vielva, F. Villa, N. Vittorio, B. D. Wandelt, I. K. Wehus, M. White, S. D. M. White, A. Zacchei,

DRAFT

and A. Zonca, "Planck 2018 results. I. Overview and the cosmological legacy of Planck," *ArXiv e-prints*, Jul. 2018.

[20] R. Namba, M. Peloso, M. Shiraishi, L. Sorbo, and C. Unal, "Scale-dependent gravitational waves from a rolling axion," *JCAP*, vol. 1601, no. 01, p. 041, 2016.

[21] C. for a Decadal Survey of Astronomy and Astrophysics, *New Worlds, New Horizons in Astronomy and Astrophysics*. National Academy Press, 2010.

[22] K. Array, BICEP2 Collaborations, :, P. A. R. Ade, Z. Ahmed, R. W. Aikin, K. D. Alexander, D. Barkats, S. J. Benton, C. A. Bischoff, J. J. Bock, R. Bowens-Rubin, J. A. Brevik, I. Buder, E. Bullock, V. Buza, J. Connors, J. Cornelison, B. P. Crill, M. Crumrine, M. Dierickx, L. Duband, C. Dvorkin, J. P. Filippini, S. Fliescher, J. Grayson, G. Hall, M. Halpern, S. Harrison, S. R. Hildebrandt, G. C. Hilton, H. Hui, K. D. Irwin, J. Kang, K. S. Karkare, E. Karpel, J. P. Kaufman, B. G. Keating, S. Kefeli, S. A. Kernasovskiy, J. M. Kovac, C. L. Kuo, N. A. Larsen, K. Lau, E. M. Leitch, M. Lueker, K. G. Megerian, L. Moncelsi, T. Namikawa, C. B. Netterfield, H. T. Nguyen, R. O'Brient, R. W. Ogburn, IV, S. Palladino, C. Pryke, B. Racine, S. Richter, A. Schillaci, R. Schwarz, C. D. Sheehy, A. Soliman, T. St. Germaine, Z. K. Staniszewski, B. Steinbach, R. V. Sudiwala, G. P. Teply, K. L. Thompson, J. E. Tolan, C. Tucker, A. D. Turner, C. Umilta, A. G. Vieregg, A. Wandui, A. C. Weber, D. V. Wiebe, J. Willmert, C. L. Wong, W. L. K. Wu, H. Yang, K. W. Yoon, and C. Zhang, "BICEP2 / Keck Array x: Constraints on Primordial Gravitational Waves using Planck, WMAP, and New BICEP2/Keck Observations through the 2015 Season," *ArXiv e-prints*, Oct. 2018.

[23] The Simons Observatory Collaboration, P. Ade, J. Aguirre, Z. Ahmed, S. Aiola, A. Ali, D. Alonso, M. A. Alvarez, K. Arnold, P. Ashton, and et al., "The Simons Observatory: Science goals and forecasts," *ArXiv e-prints*, Aug. 2018.

[24] H. Hui, P. A. R. Ade, Z. Ahmed, R. W. Aikin, K. D. Alexander, D. Barkats, S. J. Benton, C. A. Bischoff, J. J. Bock, R. Bowens-Rubin, J. A. Brevik, I. Buder, E. Bullock, V. Buza, J. Connors, J. Cornelison, B. P. Crill, M. Crumrine, M. Dierickx, L. Duband, C. Dvorkin, J. P. Filippini, S. Fliescher, J. Grayson, G. Hall, M. Halpern, S. Harrison, S. R. Hildebrandt, G. C. Hilton, K. D. Irwin, J. Kang, K. S. Karkare, E. Karpel, J. P. Kaufman, B. G. Keating, S. Kefeli, S. A. Kernasovskiy, J. M. Kovac, C.-L. Kuo, K. Lau, N. A. Larsen, E. M. Leitch, M. Lueker, K. G. Megerian, L. Moncelsi, T. Namikawa, C. B. Netterfield, H. T. Nguyen, R. O'Brient, R. W. Ogburn, S. Palladino, C. Pryke, B. Racine, S. Richter, R. Schwarz, A. Schillaci, C. D. Sheehy, A. Soliman, T. St. Germaine, Z. K. Staniszewski, B. Steinbach, R. V. Sudiwala, G. P. Teply, K. L. Thompson, J. E. Tolan, C. Tucker, A. D. Turner, C. Umilta, A. G. Vieregg, A. Wandui, A. C. Weber, D. V. Wiebe, J. Willmert, C. L. Wong, W. L. K. Wu, E. Yang, K. W. Yoon, and C. Zhang, "BICEP Array: a multi-frequency degree-scale CMB polarimeter," in *Millimeter, Submillimeter, and Far-Infrared Detectors and Instrumentation for Astronomy IX*, ser. Society of Photo-Optical Instrumentation Engineers (SPIE) Conference Series, vol. 10708, Jul. 2018, p. 1070807.

[25] L. M. Krauss and F. Wilczek, "Using Cosmology to Establish the Quantization of Gravity," *Phys. Rev.*, vol. D89, no. 4, p. 047501, 2014.

[26] Planck Collaboration, N. Aghanim, Y. Akrami, M. Ashdown, J. Aumont, C. Baccigalupi, M. Ballardini, A. J. Banday, R. B. Barreiro, N. Bartolo, S. Basak, R. Battye, K. Benabed, J.-P. Bernard, M. Bersanelli, P. Bielewicz, J. J. Bock, J. R. Bond, J. Borrill, F. R. Bouchet, F. Boulanger, M. Bucher, C. Burigana, R. C. Butler, E. Calabrese, J.-F. Cardoso, J. Carron, A. Challinor, H. C. Chiang, J. Chluba, L. P. L. Colombo, C. Combet, D. Contreras, B. P. Crill, F. Cuttaia, P. de Bernardis, G. de Zotti, J. Delabrouille, J.-M. Delouis, E. Di Valentino, J. M. Diego, O. Doré, M. Douspis, A. Ducout, X. Dupac, S. Dusini, G. Efstathiou, F. Elsner, T. A. Enßlin, H. K. Eriksen, Y. Fantaye, M. Farhang, J. Fergusson, R. Fernandez-Cobos, F. Finelli, F. Forastieri, M. Frailis, E. Franceschi, A. Frolov, S. Galeotta, S. Galli, K. Ganga, R. T. Génova-Santos, M. Gerbino, T. Ghosh, J. González-Nuevo, K. M. Górski, S. Gratton, A. Gruppuso, J. E. Gudmundsson, J. Hamann, W. Handley, D. Herranz, E. Hivon, Z. Huang, A. H. Jaffe, W. C. Jones, A. Karakci, E. Keihänen, R. Keskitalo, K. Kiiveri, J. Kim, T. S. Kisner, L. Knox, N. Krachmalnicoff, M. Kunz, H. Kurki-Suonio, G. Lagache, J.-M. Lamarre, A. Lasenby, M. Lattanzi, C. R. Lawrence, M. Le Jeune, P. Lemos, J. Lesgourgues, F. Levrier, A. Lewis, M. Liguori, P. B. Lilje, M. Lilley, V. Lindholm, M. López-Caniego, P. M. Lubin, Y.-Z. Ma, J. F. Macías-Pérez, G. Maggio, D. Maino, N. Mandolesi, A. Mangilli, A. Marcos-Caballero, M. Maris, P. G. Martin, M. Martinelli, E. Martínez-González, S. Matarrese, N. Mauri, J. D. McEwen, P. R. Meinhold, A. Melchiorri, A. Mennella, M. Migliaccio, M. Millea, S. Mitra, M.-A. Miville-Deschênes, D. Molinari, L. Montier, G. Morgante, A. Moss, P. Natoli, H. U. Nørgaard-Nielsen, L. Pagano, D. Paoletti, B. Partridge, G. Patanchon, H. V. Peiris, F. Perrotta, V. Pettorino, F. Piacentini, L. Polastri, G. Polenta, J.-L. Puget, J. P. Rachen, M. Reinecke, M. Remazeilles, A. Renzi, G. Rocha, C. Rosset, G. Roudier, J. A. Rubiño-Martín, B. Ruiz-Granados, L. Salvati, M. Sandri, M. Savelainen, D. Scott, E. P. S. Shellard, C. Sirignano, G. Sirri, L. D. Spencer, R. Sunyaev, A.-S. Suur-Uski, J. A. Tauber, D. Tavagnacco, M. Tenti, L. Toffolatti, M. Tomasi, T. Trombetti, L. Valenziano, J. Valiviita, B. Van Tent, L. Vibert, P. Vielva, F. Villa, N. Vittorio, B. D. Wandelt, I. K. Wehus, M. White, S. D. M. White, A. Zacchei, and A. Zonca, "Planck 2018 results. VI. Cosmological parameters," *arXiv e-prints*, Jul. 2018.

[27] A. B. Goncharov and A. D. Linde, "Chaotic Inflation in Supergravity," *Phys. Lett.*, vol. 139B, pp. 27–30, 1984.

[28] U. Seljak and C. M. Hirata, "Gravitational lensing as a contaminant of the gravity wave signal in the CMB," *Phys. Rev. D.*, vol. 69, no. 4, p. 043005, Feb. 2004.

[29] K. M. Smith, D. Hanson, M. LoVerde, C. M. Hirata, and O. Zahn, "Delensing CMB polarization with external datasets," *JCAP*, vol. 6, p. 014, Jun. 2012.

[30] D. J. Watts, B. Wang, A. Ali, J. W. Appel, C. L. Bennett, D. T. Chuss, S. Dahal, J. R. Eimer, T. Essinger-Hileman, K. Harring-

DRAFT

ton, G. Hinshaw, J. Iuliano, T. A. Marriage, N. J. Miller, I. L. Padilla, L. Parker, M. Petroff, K. Rostem, E. J. Wollack, and Z. Xu, "A Projected Estimate of the Reionization Optical Depth Using the CLASS Experiment's Sample Variance Limited E-mode Measurement," *Ap. J.*, vol. 863, p. 121, Aug. 2018.

[31] J. Lazear, P. A. R. Ade, D. Benford, C. L. Bennett, D. T. Chuss, J. L. Dotson, J. R. Eimer, D. J. Fixsen, M. Halpern, G. Hilton, J. Hinderks, G. F. Hinshaw, K. Irwin, C. Jhabvala, B. Johnson, A. Kogut, L. Lowe, J. J. McMahon, T. M. Miller, P. Mirel, S. H. Moseley, S. Rodriguez, E. Sharp, J. G. Staguhn, E. R. Switzer, C. E. Tucker, A. Weston, and E. J. Wollack, "The Primordial Inflation Polarization Explorer (PIPER)," in *Millimeter, Submillimeter, and Far-Infrared Detectors and Instrumentation for Astronomy VII*, ser. *Proceedings of SPIE*, vol. 9153, Jul. 2014, p. 91531L.

[32] M. Alvarez, T. Baldauf, J. R. Bond, N. Dalal, R. de Putter, O. Doré, D. Green, C. Hirata, Z. Huang, D. Huterer, D. Jeong, M. C. Johnson, E. Krause, M. Loverde, J. Meyers, P. D. Meerburg, L. Senatore, S. Shandera, E. Silverstein, A. Slosar, K. Smith, M. Zaldarriaga, V. Assassi, J. Braden, A. Hajian, T. Kobayashi, G. Stein, and A. van Engelen, "Testing Inflation with Large Scale Structure: Connecting Hopes with Reality," *ArXiv e-prints*, Dec. 2014.

[33] U. Seljak, "Extracting Primordial Non-Gaussianity without Cosmic Variance," *Physical Review Letters*, vol. 102, no. 2, p. 021302, Jan. 2009.

[34] M. Schmittfull and U. Seljak, "Parameter constraints from cross-correlation of CMB lensing with galaxy clustering," *Phys. Rev. D.*, vol. 97, no. 12, p. 123540, Jun. 2018.

[35] N. Dalal, O. Doré, D. Huterer, and A. Shirokov, "Imprints of primordial non-Gaussianities on large-scale structure: Scale-dependent bias and abundance of virialized objects," *Phys. Rev. D.*, vol. 77, no. 12, p. 123514, Jun. 2008.

[36] G. Steigman, "Cosmology confronts particle physics." *Annual Review of Nuclear and Particle Science*, vol. 29, pp. 313–338, 1979.

[37] M. Bolz, A. Brandenburg, and W. Buchmuller, "Thermal production of gravitinos," *Nucl. Phys.*, vol. B606, pp. 518–544, 2001, [Erratum: Nucl. Phys.B790,336(2008)].

[38] M. S. Madhavacheril, N. Sehgal, and T. R. Slatyer, "Current Dark Matter Annihilation Constraints from CMB and Low-Redshift Data," *Phys. Rev.*, vol. D89, p. 103508, 2014.

[39] D. Green, P. D. Meerburg, and J. Meyers, "Aspects of Dark Matter Annihilation in Cosmology," *ArXiv e-prints*, Apr. 2018.

[40] X. Chen, S. Hannestad, and R. J. Scherrer, "Cosmic microwave background and large scale structure limits on the interaction between dark matter and baryons," *ArXiv Astrophysics e-prints*, Feb. 2002.

[41] K. Sigurdson, M. Doran, A. Kurylov, R. R. Caldwell, and M. Kamionkowski, "Dark-matter electric and magnetic dipole moments," *Phys. Rev. D.*, vol. 70, no. 8, p. 083501, Oct. 2004.

[42] C. Dvorkin, K. Blum, and M. Kamionkowski, "Constraining Dark Matter-Baryon Scattering with Linear Cosmology," *Phys. Rev.*, vol. D89, no. 2, p. 023519, 2014.

[43] V. Gluscevic and K. K. Boddy, "Constraints on Scattering of keV-TeV Dark Matter with Protons in the Early Universe," *Physical Review Letters*, vol. 121, no. 8, p. 081301, Aug. 2018.

[44] K. K. Boddy and V. Gluscevic, "First Cosmological Constraint on the Effective Theory of Dark Matter-Proton Interactions," *ArXiv e-prints*, Jan. 2018.

[45] W. L. Xu, C. Dvorkin, and A. Chael, "Probing sub-GeV dark matter-baryon scattering with cosmological observables," *Phys. Rev. D.*, vol. 97, no. 10, p. 103530, May 2018.

[46] K. K. Boddy, V. Gluscevic, V. Poulin, E. D. Kovetz, M. Kamionkowski, and R. Barkana, "A Critical Assessment of CMB Limits on Dark Matter-Baryon Scattering: New Treatment of the Relative Bulk Velocity," *ArXiv e-prints*, Jul. 2018.

[47] T. R. Slatyer and C.-L. Wu, "Early-Universe constraints on dark matter-baryon scattering and their implications for a global 21 cm signal," *Phys. Rev. D.*, vol. 98, no. 2, p. 023013, Jul. 2018.

[48] R. Barkana, "Possible interaction between baryons and dark-matter particles revealed by the first stars," *Nature*, vol. 555, pp. 71–74, Mar. 2018.

[49] J. D. Bowman, A. E. E. Rogers, R. A. Monsalve, T. J. Mozdzen, and N. Mahesh, "An absorption profile centred at 78 megahertz in the sky-averaged spectrum," *Nature*, vol. 555, pp. 67–70, Mar. 2018.

[50] E. D. Kovetz, V. Poulin, V. Gluscevic, K. K. Boddy, R. Barkana, and M. Kamionkowski, "Tighter Limits on Dark Matter Explanations of the Anomalous EDGES 21cm Signal," *ArXiv e-prints*, Jul. 2018.

[51] B. J. Kavanagh, "Earth scattering of superheavy dark matter: Updated constraints from detectors old and new," *Phys. Rev. D.*, vol. 97, no. 12, p. 123013, Jun. 2018.

[52] A. Arvanitaki, S. Dimopoulos, S. Dubovsky, N. Kaloper, and J. March-Russell, "String axiverse," *Phys. Rev. D.*, vol. 81, no. 12, p. 123530, Jun. 2010.

[53] R. D. Peccei and H. R. Quinn, "CP conservation in the presence of pseudoparticles," *Physical Review Letters*, vol. 38, pp. 1440–1443, Jun. 1977.

[54] S. Weinberg, "A new light boson?" *Physical Review Letters*, vol. 40, pp. 223–226, Jan. 1978.

[55] F. Wilczek, "Problem of strong P and T invariance in the presence of instantons," *Physical Review Letters*, vol. 40, pp. 279–282, Jan. 1978.

DRAFT

[56] Planck Collaboration, N. Aghanim, Y. Akrami, M. Ashdown, J. Aumont, C. Baccigalupi, M. Ballardini, A. J. Banday, R. B. Barreiro, N. Bartolo, S. Basak, R. Battye, K. Benabed, J.-P. Bernard, M. Bersanelli, P. Bielewicz, J. J. Bock, J. R. Bond, J. Borrill, F. R. Bouchet, F. Boulanger, M. Bucher, C. Burigana, R. C. Butler, E. Calabrese, J.-F. Cardoso, J. Carron, A. Challinor, H. C. Chiang, J. Chluba, L. P. L. Colombo, C. Combet, D. Contreras, B. P. Crill, F. Cuttaia, P. de Bernardis, G. de Zotti, J. Delabrouille, J.-M. Delouis, E. Di Valentino, J. M. Diego, O. Doré, M. Douspis, A. Ducout, X. Dupac, S. Dusini, G. Efstathiou, F. Elsner, T. A. Enßlin, H. K. Eriksen, Y. Fantaye, M. Farhang, J. Fergusson, R. Fernandez-Cobos, F. Finelli, F. Forastieri, M. Frailis, E. Franceschi, A. Frolov, S. Galeotta, S. Galli, K. Ganga, R. T. Génova-Santos, M. Gerbino, T. Ghosh, J. González-Nuevo, K. M. Górski, S. Gratton, A. Gruppuso, J. E. Gudmundsson, J. Hamann, W. Handley, D. Herranz, E. Hivon, Z. Huang, A. H. Jaffe, W. C. Jones, A. Karakci, E. Keihänen, R. Keskitalo, K. Kiiveri, J. Kim, T. S. Kisner, L. Knox, N. Krachmalnicoff, M. Kunz, H. Kurki-Suonio, G. Lagache, J.-M. Lamarre, A. Lasenby, M. Lattanzi, C. R. Lawrence, M. Le Jeune, P. Lemos, J. Lesgourgues, F. Levrier, A. Lewis, M. Liguori, P. B. Lilje, M. Lilley, V. Lindholm, M. López-Caniego, P. M. Lubin, Y.-Z. Ma, J. F. Macías-Pérez, G. Maggio, D. Maino, N. Mandolesi, A. Mangilli, A. Marcos-Caballero, M. Maris, P. G. Martin, M. Martinelli, E. Martínez-González, S. Matarrese, N. Mauri, J. D. McEwen, P. R. Meinhold, A. Melchiorri, A. Mennella, M. Migliaccio, M. Millea, S. Mitra, M.-A. Miville-Deschênes, D. Molinari, L. Montier, G. Morgante, A. Moss, P. Natoli, H. U. Nørgaard-Nielsen, L. Pagano, D. Paoletti, B. Partridge, G. Patanchon, H. V. Peiris, F. Perrotta, V. Pettorino, F. Piacentini, L. Polastri, G. Polenta, J.-L. Puget, J. P. Rachen, M. Reinecke, M. Remazeilles, A. Renzi, G. Rocha, C. Rosset, G. Roudier, J. A. Rubiño-Martín, B. Ruiz-Granados, L. Salvati, M. Sandri, M. Savelainen, D. Scott, E. P. S. Shellard, C. Sirignano, G. Sirri, L. D. Spencer, R. Sunyaev, A.-S. Suur-Uski, J. A. Tauber, D. Tavagnacco, M. Tenti, L. Toffolatti, M. Tomasi, T. Trombetti, L. Valenziano, J. Valiviita, B. Van Tent, L. Vibert, P. Vielva, F. Villa, N. Vittorio, B. D. Wandelt, I. K. Wehus, M. White, S. D. M. White, A. Zacchei, and A. Zonca, "Planck 2018 results. VI. Cosmological parameters," *ArXiv e-prints*, Jul. 2018.

[57] Planck Collaboration, N. Aghanim, M. Ashdown, J. Aumont, C. Baccigalupi, M. Ballardini, A. J. Banday, R. B. Barreiro, N. Bartolo, S. Basak, R. Battye, K. Benabed, J.-P. Bernard, M. Bersanelli, P. Bielewicz, J. J. Bock, A. Bonaldi, L. Bonavera, J. R. Bond, J. Borrill, F. R. Bouchet, F. Boulanger, M. Bucher, C. Burigana, R. C. Butler, E. Calabrese, J.-F. Cardoso, J. Carron, A. Challinor, H. C. Chiang, L. P. L. Colombo, C. Combet, B. Comis, A. Coulais, B. P. Crill, A. Curto, F. Cuttaia, R. J. Davis, P. de Bernardis, A. de Rosa, G. de Zotti, J. Delabrouille, J.-M. Delouis, E. Di Valentino, C. Dickinson, J. M. Diego, O. Doré, M. Douspis, A. Ducout, X. Dupac, G. Efstathiou, F. Elsner, T. A. Enßlin, H. K. Eriksen, E. Falgarone, Y. Fantaye, F. Finelli, F. Forastieri, M. Frailis, A. A. Fraisse, E. Franceschi, A. Frolov, S. Galeotta, S. Galli, K. Ganga, R. T. Génova-Santos, M. Gerbino, T. Ghosh, J. González-Nuevo, K. M. Górski, S. Gratton, A. Gruppuso, J. E. Gudmundsson, F. K. Hansen, G. Helou, S. Henrot-Versillé, D. Herranz, E. Hivon, Z. Huang, S. Ilic, A. H. Jaffe, W. C. Jones, E. Keihänen, R. Keskitalo, T. S. Kisner, L. Knox, N. Krachmalnicoff, M. Kunz, H. Kurki-Suonio, G. Lagache, J.-M. Lamarre, M. Langer, A. Lasenby, M. Lattanzi, C. R. Lawrence, M. Le Jeune, J. P. Leahy, F. Levrier, M. Liguori, P. B. Lilje, M. López-Caniego, Y.-Z. Ma, J. F. Macías-Pérez, G. Maggio, A. Mangilli, M. Maris, P. G. Martin, E. Martínez-González, S. Matarrese, N. Mauri, J. D. McEwen, P. R. Meinhold, A. Melchiorri, A. Mennella, M. Migliaccio, M.-A. Miville-Deschênes, D. Molinari, A. Moneti, L. Montier, G. Morgante, A. Moss, S. Mottet, P. Naselsky, P. Natoli, C. A. Oxborrow, L. Pagano, D. Paoletti, B. Partridge, G. Patanchon, L. Patrizii, O. Perdereau, L. Perotto, V. Pettorino, F. Piacentini, S. Plaszczynski, L. Polastri, G. Polenta, J.-L. Puget, J. P. Rachen, B. Racine, M. Reinecke, M. Remazeilles, A. Renzi, G. Rocha, M. Rossetti, G. Roudier, J. A. Rubiño-Martín, B. Ruiz-Granados, L. Salvati, M. Sandri, M. Savelainen, D. Scott, G. Sirri, R. Sunyaev, A.-S. Suur-Uski, J. A. Tauber, M. Tenti, L. Toffolatti, M. Tomasi, M. Tristram, T. Trombetti, J. Valiviita, F. Van Tent, L. Vibert, P. Vielva, F. Villa, N. Vittorio, B. D. Wandelt, R. Watson, I. K. Wehus, M. White, A. Zacchei, and A. Zonca, "Planck intermediate results. XLVI. Reduction of large-scale systematic effects in HFI polarization maps and estimation of the reionization optical depth," *ArXiv e-prints*, May 2016.

[58] M. Levi *et al.*, "The DESI Experiment, a whitepaper for Snowmass 2013," *ArXiv e-prints*, 2013.

[59] L. M. Widrow, "Origin of galactic and extragalactic magnetic fields," *Rev. Mod. Phys.*, vol. 74, pp. 775–823, 2002.

[60] L. M. Widrow, D. Ryu, D. R. G. Schleicher, K. Subramanian, C. G. Tsagas, and R. A. Treumann, "The First Magnetic Fields," *Space Sci. Rev.*, vol. 166, pp. 37–70, 2012.

[61] R. M. Athreya, V. K. Kapahi, P. J. McCarthy, and W. van Breugel, "Large rotation measures in radio galaxies at Z > 2," *Astron. Astrophys.*, vol. 329, pp. 809–820, Jan. 1998.

[62] D. Grasso and H. R. Rubinstein, "Magnetic fields in the early universe," *Phys. Rept.*, vol. 348, pp. 163–266, 2001.

[63] T. Vachaspati, "Magnetic fields from cosmological phase transitions," *Phys. Lett.*, vol. B265, pp. 258–261, 1991.

[64] M. S. Turner and L. M. Widrow, "Inflation Produced, Large Scale Magnetic Fields," *Phys. Rev.*, vol. D37, p. 2743, 1988.

[65] B. Ratra, "Cosmological 'seed' magnetic field from inflation," *Astrophys. J.*, vol. 391, pp. L1–L4, 1992.

[66] A. Diaz-Gil, J. Garcia-Bellido, M. Garcia Perez, and A. Gonzalez-Arroyo, "Magnetic field production during preheating at the electroweak scale," *Phys. Rev. Lett.*, vol. 100, p. 241301, 2008.

[67] N. Barnaby, R. Namba, and M. Peloso, "Observable non-gaussianity from gauge field production in slow roll inflation, and a challenging connection with magnetogenesis," *Phys. Rev.*, vol. D85, p. 123523, 2012.

[68] A. J. Long, E. Sabancilar, and T. Vachaspati, "Leptogenesis and Primordial Magnetic Fields," *JCAP*, vol. 1402, p. 036, 2014.

DRAFT

[69] R. Durrer and A. Neronov, "Cosmological Magnetic Fields: Their Generation, Evolution and Observation," *Astron.Astrophys.Rev.*, vol. 21, p. 62, 2013.

[70] A. Zucca, Y. Li, and L. Pogosian, "Constraints on Primordial Magnetic Fields from Planck combined with the South Pole Telescope CMB B-mode polarization measurements," *Phys. Rev.*, vol. D95, no. 6, p. 063506, 2017.

[71] A. Kosowsky and A. Loeb, "Faraday rotation of microwave background polarization by a primordial magnetic field," *Astrophys.J.*, vol. 469, pp. 1–6, 1996.

[72] N. Oppermann *et al.*, "An improved map of the Galactic Faraday sky," *Astron. Astrophys.*, vol. 542, p. A93, 2012.

[73] S. De, L. Pogosian, and T. Vachaspati, "CMB Faraday rotation as seen through the Milky Way," *Phys.Rev.*, vol. D88, no. 6, p. 063527, 2013.

[74] L. Pogosian, "Searching for primordial magnetism with multifrequency cosmic microwave background experiments," *Mon. Not. Roy. Astron. Soc.*, vol. 438, no. 3, pp. 2508–2512, 2014.

[75] K. Freese, J. A. Frieman, and A. V. Olinto, "Natural inflation with pseudo - Nambu-Goldstone bosons," *Phys. Rev. Lett.*, vol. 65, pp. 3233–3236, 1990.

[76] J. A. Frieman, C. T. Hill, A. Stebbins, and I. Waga, "Cosmology with ultralight pseudo Nambu-Goldstone bosons," *Phys. Rev. Lett.*, vol. 75, pp. 2077–2080, 1995.

[77] S. M. Carroll, "Quintessence and the Rest of the World: Suppressing Long-Range Interactions," *Physical Review Letters*, vol. 81, pp. 3067–3070, Oct. 1998.

[78] N. Kaloper and L. Sorbo, "Of pNGB QuiNtessence," *JCAP*, vol. 0604, p. 007, 2006.

[79] C. R. Contaldi, J. Magueijo, and L. Smolin, "Anomalous Cosmic-Microwave-Background Polarization and Gravitational Chirality," *Phys. Rev. Lett.*, vol. 101, p. 141101, Oct. 2008.

[80] V. Gluscevic and M. Kamionkowski, "Testing Parity-Violating Mechanisms with Cosmic Microwave Background Experiments," *Phys. Rev.*, vol. D81, p. 123529, 2010.

[81] D. Harari and P. Sikivie, "Effects of a Nambu-Goldstone boson on the polarization of radio galaxies and the cosmic microwave background," *Phys. Lett.*, vol. B289, pp. 67–72, 1992.

[82] S. M. Carroll, G. B. Field, and R. Jackiw, "Limits on a Lorentz and Parity Violating Modification of Electrodynamics," *Phys. Rev.*, vol. D41, p. 1231, 1990.

[83] M. Kamionkowski, "How to De-Rotate the Cosmic Microwave Background Polarization," *Phys.Rev.Lett.*, vol. 102, p. 111302, 2009.

[84] V. Gluscevic, M. Kamionkowski, and A. Cooray, "De-Rotation of the Cosmic Microwave Background Polarization: Full-Sky Formalism," *Phys. Rev.*, vol. D80, p. 023510, 2009.

[85] V. Gluscevic, D. Hanson, M. Kamionkowski, and C. M. Hirata, "First CMB Constraints on Direction-Dependent Cosmological Birefringence from WMAP-7," *Phys. Rev.*, vol. D86, p. 103529, 2012.

[86] N. Aghanim *et al.*, "Planck intermediate results. XLIX. Parity-violation constraints from polarization data," *Astron. Astrophys.*, vol. 596, p. A110, 2016.

[87] P. A. R. Ade *et al.*, "BICEP2 / Keck Array IX: New bounds on anisotropies of CMB polarization rotation and implications for axionlike particles and primordial magnetic fields," *Phys. Rev.*, vol. D96, no. 10, p. 102003, 2017.

[88] P. Svrcek and E. Witten, "Axions In String Theory," *JHEP*, vol. 06, p. 051, 2006.

[89] M. Pospelov, A. Ritz, C. Skordis, A. Ritz, and C. Skordis, "Pseudoscalar perturbations and polarization of the cosmic microwave background," *Phys. Rev. Lett.*, vol. 103, p. 051302, 2009.

[90] V. Miranda, A. Lidz, C. H. Heinrich, and W. Hu, "CMB signatures of metal-free star formation and Planck 2015 polarization data," *MNRAS*, vol. 467, pp. 4050–4056, Jun. 2017.

[91] E. Calabrese, R. Hložek, N. Battaglia, J. R. Bond, F. de Bernardis, M. J. Devlin, A. Hajian, S. Henderson, J. C. Hil, A. Kosowsky, T. Louis, J. McMahon, K. Moodley, L. Newburgh, M. D. Niemack, L. A. Page, B. Partridge, N. Sehgal, J. L. Sievers, D. N. Spergel, S. T. Staggs, E. R. Switzer, H. Trac, and E. J. Wollack, "Precision epoch of reionization studies with next-generation CMB experiments," *JCAP*, vol. 8, p. 010, Aug. 2014.

[92] R. A. Monsalve, A. E. E. Rogers, J. D. Bowman, and T. J. Mozdzen, "Results from EDGES High-band. I. Constraints on Phenomenological Models for the Global 21 cm Signal," *Ap. J.*, vol. 847, p. 64, Sep. 2017.

[93] X. Fan, M. A. Strauss, R. H. Becker, R. L. White, J. E. Gunn, G. R. Knapp, G. T. Richards, D. P. Schneider, J. Brinkmann, and M. Fukugita, "Constraining the Evolution of the Ionizing Background and the Epoch of Reionization with z˜6 Quasars. II. A Sample of 19 Quasars," *Astronomical Journal*, vol. 132, pp. 117–136, Jul. 2006.

[94] Planck Collaboration, R. Adam, N. Aghanim, M. Ashdown, J. Aumont, C. Baccigalupi, M. Ballardini, A. J. Banday, R. B. Barreiro, N. Bartolo, S. Basak, R. Battye, K. Benabed, J.-P. Bernard, M. Bersanelli, P. Bielewicz, J. J. Bock, A. Bonaldi, L. Bonavera, J. R. Bond, J. Borrill, F. R. Bouchet, F. Boulanger, M. Bucher, C. Burigana, E. Calabrese, J.-F. Cardoso, J. Carron, H. C. Chiang, L. P. L. Colombo, C. Combet, B. Comis, F. Couchot, A. Coulais, B. P. Crill, A. Curto, F. Cuttaia, R. J. Davis, P. de Bernardis, A. de Rosa, G. de Zotti, J. Delabrouille, E. Di Valentino, C. Dickinson, J. M. Diego, O. Doré, M. Douspis, A. Ducout, X. Dupac, F. Elsner, T. A. Enßlin, H. K. Eriksen, E. Falgarone, Y. Fantaye, F. Finelli, F. Forastieri,

DRAFT

M. Frailis, A. A. Fraisse, E. Franceschi, A. Frolov, S. Galeotta, S. Galli, K. Ganga, R. T. Génova-Santos, M. Gerbino, T. Ghosh, J. González-Nuevo, K. M. Górski, A. Gruppuso, J. E. Gudmundsson, F. K. Hansen, G. Helou, S. Henrot-Versillé, D. Herranz, E. Hivon, Z. Huang, S. Ilić, A. H. Jaffe, W. C. Jones, E. Keihänen, R. Keskitalo, T. S. Kisner, L. Knox, N. Krachmalnicoff, M. Kunz, H. Kurki-Suonio, G. Lagache, A. Lähteenmäki, J.-M. Lamarre, M. Langer, A. Lasenby, M. Lattanzi, C. R. Lawrence, M. Le Jeune, F. Levrier, A. Lewis, M. Liguori, P. B. Lilje, M. López-Caniego, Y.-Z. Ma, J. F. Macías-Pérez, G. Maggio, A. Mangilli, M. Maris, P. G. Martin, E. Martínez-González, S. Matarrese, N. Mauri, J. D. McEwen, P. R. Meinhold, A. Melchiorri, A. Mennella, M. Migliaccio, M.-A. Miville-Deschênes, D. Molinari, A. Moneti, L. Montier, G. Morgante, A. Moss, P. Naselsky, P. Natoli, C. A. Oxborrow, L. Pagano, D. Paoletti, B. Partridge, G. Patanchon, L. Patrizii, O. Perdereau, L. Perotto, V. Pettorino, F. Piacentini, S. Plaszczynski, L. Polastri, G. Polenta, J.-L. Puget, J. P. Rachen, B. Racine, M. Reinecke, M. Remazeilles, A. Renzi, G. Rocha, M. Rossetti, G. Roudier, J. A. Rubiño-Martín, B. Ruiz-Granados, L. Salvati, M. Sandri, M. Savelainen, D. Scott, G. Sirri, R. Sunyaev, A.-S. Suur-Uski, J. A. Tauber, M. Tenti, L. Toffolatti, M. Tomasi, M. Tristram, T. Trombetti, J. Valiviita, F. Van Tent, P. Vielva, F. Villa, N. Vittorio, B. D. Wandelt, I. K. Wehus, M. White, A. Zacchei, and A. Zonca, "Planck intermediate results. XLVII. Planck constraints on reionization history," *Astron. Astrophys.*, vol. 596, p. A108, Dec. 2016.

[95] K. M. Smith and S. Ferraro, "Detecting Patchy Reionization in the Cosmic Microwave Background," *Physical Review Letters*, vol. 119, no. 2, p. 021301, Jul. 2017.

[96] C. Dvorkin and K. M. Smith, "Reconstructing patchy reionization from the cosmic microwave background," *Phys. Rev. D.*, vol. 79, no. 4, p. 043003, Feb. 2009.

[97] T. Essinger-Hileman, A. Ali, M. Amiri, J. W. Appel, D. Araujo, C. L. Bennett, F. Boone, M. Chan, H.-M. Cho, D. T. Chuss, F. Colazo, E. Crowe, K. Denis, R. Dünner, J. Eimer, D. Gothe, M. Halpern, K. Harrington, G. C. Hilton, G. F. Hinshaw, C. Huang, K. Irwin, G. Jones, J. Karakla, A. J. Kogut, D. Larson, M. Limon, L. Lowry, T. Marriage, N. Mehrle, A. D. Miller, N. Miller, S. H. Moseley, G. Novak, C. Reintsema, K. Rostem, T. Stevenson, D. Towner, K. U-Yen, E. Wagner, D. Watts, E. J. Wollack, Z. Xu, and L. Zeng, "CLASS: the cosmology large angular scale surveyor," in *Millimeter, Submillimeter, and Far-Infrared Detectors and Instrumentation for Astronomy VII*, ser. *Proceedings of SPIE*, vol. 9153, Jul. 2014, p. 91531I.

[98] Planck Collaboration, N. Aghanim, Y. Akrami, M. Ashdown, J. Aumont, C. Baccigalupi, M. Ballardini, A. J. Banday, R. B. Barreiro, N. Bartolo, S. Basak, K. Benabed, J.-P. Bernard, M. Bersanelli, P. Bielewicz, J. J. Bock, J. R. Bond, J. Borrill, F. R. Bouchet, F. Boulanger, M. Bucher, C. Burigana, E. Calabrese, J.-F. Cardoso, J. Carron, A. Challinor, H. C. Chiang, L. P. L. Colombo, C. Combet, B. P. Crill, F. Cuttaia, P. de Bernardis, G. de Zotti, J. Delabrouille, E. Di Valentino, J. M. Diego, O. Doré, M. Douspis, A. Ducout, X. Dupac, G. Efstathiou, F. Elsner, T. A. Enßlin, H. K. Eriksen, Y. Fantaye, R. Fernandez-Cobos, F. Forastieri, M. Frailis, A. A. Fraisse, E. Franceschi, A. Frolov, S. Galeotta, S. Galli, K. Ganga, R. T. Génova-Santos, M. Gerbino, T. Ghosh, J. González-Nuevo, K. M. Górski, S. Gratton, A. Gruppuso, J. E. Gudmundsson, J. Hamann, W. Handley, F. K. Hansen, D. Herranz, E. Hivon, Z. Huang, A. H. Jaffe, W. C. Jones, A. Karakci, E. Keihänen, R. Keskitalo, K. Kiiveri, J. Kim, L. Knox, N. Krachmalnicoff, M. Kunz, H. Kurki-Suonio, G. Lagache, J.-M. Lamarre, A. Lasenby, M. Lattanzi, C. R. Lawrence, M. Le Jeune, F. Levrier, A. Lewis, M. Liguori, P. B. Lilje, V. Lindholm, M. López-Caniego, P. M. Lubin, Y.-Z. Ma, J. F. Macías-Pérez, G. Maggio, D. Maino, N. Mandolesi, A. Mangilli, A. Marcos-Caballero, M. Maris, P. G. Martin, E. Martínez-González, S. Matarrese, N. Mauri, J. D. McEwen, A. Melchiorri, A. Mennella, M. Migliaccio, M.-A. Miville-Deschênes, D. Molinari, A. Moneti, L. Montier, G. Morgante, A. Moss, P. Natoli, L. Pagano, D. Paoletti, B. Partridge, G. Patanchon, F. Perrotta, V. Pettorino, F. Piacentini, L. Polastri, G. Polenta, J.-L. Puget, J. P. Rachen, M. Reinecke, M. Remazeilles, A. Renzi, G. Rocha, C. Rosset, G. Roudier, J. A. Rubiño-Martín, B. Ruiz-Granados, L. Salvati, M. Sandri, M. Savelainen, D. Scott, C. Sirignano, R. Sunyaev, A.-S. Suur-Uski, J. A. Tauber, D. Tavagnacco, M. Tenti, L. Toffolatti, M. Tomasi, T. Trombetti, J. Valiviita, B. Van Tent, P. Vielva, F. Villa, N. Vittorio, B. D. Wandelt, I. K. Wehus, M. White, S. D. M. White, A. Zacchei, and A. Zonca, "Planck 2018 results. VIII. Gravitational lensing," *ArXiv e-prints*, Jul. 2018.

[99] Y. B. Zeldovich and R. A. Sunyaev, "The Interaction of Matter and Radiation in a Hot-Model Universe," *ApSS*, vol. 4, pp. 301–316, Jul. 1969.

[100] R. A. Sunyaev and Y. B. Zeldovich, "The Observations of Relic Radiation as a Test of the Nature of X-Ray Radiation from the Clusters of Galaxies," *Comments on Astrophysics and Space Physics*, vol. 4, p. 173, Nov. 1972.

[101] E. J. Baxter, R. Keisler, S. Dodelson, K. A. Aird, S. W. Allen, M. L. N. Ashby, M. Bautz, M. Bayliss, B. A. Benson, L. E. Bleem, S. Bocquet, M. Brodwin, J. E. Carlstrom, C. L. Chang, I. Chiu, H.-M. Cho, A. Clocchiatti, T. M. Crawford, A. T. Crites, S. Desai, J. P. Dietrich, T. de Haan, M. A. Dobbs, R. J. Foley, W. R. Forman, E. M. George, M. D. Gladders, A. H. Gonzalez, N. W. Halverson, N. L. Harrington, C. Hennig, H. Hoekstra, G. P. Holder, W. L. Holzapfel, Z. Hou, J. D. Hrubes, C. Jones, L. Knox, A. T. Lee, E. M. Leitch, J. Liu, M. Lueker, D. Luong-Van, A. Mantz, D. P. Marrone, M. McDonald, J. J. McMahon, S. S. Meyer, M. Millea, L. M. Mocanu, S. S. Murray, S. Padin, C. Pryke, C. L. Reichardt, A. Rest, J. E. Ruhl, B. R. Saliwanchik, A. Saro, J. T. Sayre, K. K. Schaffer, E. Shirokoff, J. Song, H. G. Spieler, B. Stalder, S. A. Stanford, Z. Staniszewski, A. A. Stark, K. T. Story, A. van Engelen, K. Vanderlinde, J. D. Vieira, A. Vikhlinin, R. Williamson, O. Zahn, and A. Zenteno, "A Measurement of Gravitational Lensing of the Cosmic Microwave Background by Galaxy Clusters Using Data from the South Pole Telescope," *Ap. J.*, vol. 806, p. 247, Jun. 2015.

[102] M. Madhavacheril, N. Sehgal, R. Allison, N. Battaglia, J. R. Bond, E. Calabrese, J. Caligiuri, K. Coughlin, D. Crichton, R. Datta, M. J. Devlin, J. Dunkley, R. Dünner, K. Fogarty, E. Grace, A. Hajian, M. Hasselfield, J. C. Hill, M. Hilton,

DRAFT

A. D. Hincks, R. Hlozek, J. P. Hughes, A. Kosowsky, T. Louis, M. Lungu, J. McMahon, K. Moodley, C. Munson, S. Naess, F. Nati, L. Newburgh, M. D. Niemack, L. A. Page, B. Partridge, B. Schmitt, B. D. Sherwin, J. Sievers, D. N. Spergel, S. T. Staggs, R. Thornton, A. Van Engelen, J. T. Ward, and E. J. Wollack, "Evidence of lensing of the cosmic microwave background by dark matter halos," *Phys. Rev. Lett.*, vol. 114, p. 151302, Apr 2015. [Online]. Available: https://link.aps.org/doi/10.1103/PhysRevLett.114.151302

[103] Planck Collaboration, P. A. R. Ade, N. Aghanim, M. Arnaud, M. Ashdown, J. Aumont, C. Baccigalupi, A. J. Banday, R. B. Barreiro, J. G. Bartlett, and et al., "Planck 2015 results. XXIV. Cosmology from Sunyaev-Zeldovich cluster counts," *Astron. Astrophys.*, vol. 594, p. A24, Sep. 2016.

[104] J.-B. Melin and J. G. Bartlett, "Measuring cluster masses with CMB lensing: a statistical approach," *Astron. Astrophys.*, vol. 578, p. A21, Jun. 2015.

[105] J. Delabrouille, J.-F. Cardoso, M. Le Jeune, M. Betoule, G. Fay, and F. Guilloux, "A full sky, low foreground, high resolution CMB map from WMAP," *Astron. Astrophys.*, vol. 493, pp. 835–857, Jan. 2009.

[106] J. L. Sievers, R. A. Hlozek, M. R. Nolta, V. Acquaviva, G. E. Addison, P. A. R. Ade, P. Aguirre, M. Amiri, J. W. Appel, L. F. Barrientos, E. S. Battistelli, N. Battaglia, J. R. Bond, B. Brown, B. Burger, E. Calabrese, J. Chervenak, D. Crichton, S. Das, M. J. Devlin, S. R. Dicker, W. Bertrand Doriese, J. Dunkley, R. Dünner, T. Essinger-Hileman, D. Faber, R. P. Fisher, J. W. Fowler, P. Gallardo, M. S. Gordon, M. B. Gralla, A. Hajian, M. Halpern, M. Hasselfield, C. Hernández-Monteagudo, J. C. Hill, G. C. Hilton, M. Hilton, A. D. Hincks, D. Holtz, K. M. Huffenberger, D. H. Hughes, J. P. Hughes, L. Infante, K. D. Irwin, D. R. Jacobson, B. Johnstone, J. Baptiste Juin, M. Kaul, J. Klein, A. Kosowsky, J. M. Lau, M. Limon, Y.-T. Lin, T. Louis, R. H. Lupton, T. A. Marriage, D. Marsden, K. Martocci, P. Mauskopf, M. McLaren, F. Menanteau, K. Moodley, H. Moseley, C. B. Netterfield, M. D. Niemack, L. A. Page, W. A. Page, L. Parker, B. Partridge, R. Plimpton, H. Quintana, E. D. Reese, B. Reid, F. Rojas, N. Sehgal, B. D. Sherwin, B. L. Schmitt, D. N. Spergel, S. T. Staggs, O. Stryzak, D. S. Swetz, E. R. Switzer, R. Thornton, H. Trac, C. Tucker, M. Uehara, K. Visnjic, R. Warne, G. Wilson, E. Wollack, Y. Zhao, and C. Zunckel, "The Atacama Cosmology Telescope: cosmological parameters from three seasons of data," *JCAP*, vol. 10, p. 060, Oct. 2013.

[107] E. M. George, C. L. Reichardt, K. A. Aird, B. A. Benson, L. E. Bleem, J. E. Carlstrom, C. L. Chang, H.-M. Cho, T. M. Crawford, A. T. Crites, T. de Haan, M. A. Dobbs, J. Dudley, N. W. Halverson, N. L. Harrington, G. P. Holder, W. L. Holzapfel, Z. Hou, J. D. Hrubes, R. Keisler, L. Knox, A. T. Lee, E. M. Leitch, M. Lueker, D. Luong-Van, J. J. McMahon, J. Mehl, S. S. Meyer, M. Millea, L. M. Mocanu, J. J. Mohr, T. E. Montroy, S. Padin, T. Plagge, C. Pryke, J. E. Ruhl, K. K. Schaffer, L. Shaw, E. Shirokoff, H. G. Spieler, Z. Staniszewski, A. A. Stark, K. T. Story, A. van Engelen, K. Vanderlinde, J. D. Vieira, R. Williamson, and O. Zahn, "A Measurement of Secondary Cosmic Microwave Background Anisotropies from the 2500 Square-degree SPT-SZ Survey," *Ap. J.*, vol. 799, p. 177, Feb. 2015.

[108] Planck Collaboration, N. Aghanim, Y. Akrami, M. I. R. Alves, M. Ashdown, J. Aumont, C. Baccigalupi, M. Ballardini, A. J. Banday, R. B. Barreiro, N. Bartolo, S. Basak, K. Benabed, J. P. Bernard, M. Bersanelli, P. Bielewicz, J. J. Bock, J. R. Bond, J. Borrill, F. R. Bouchet, F. Boulanger, A. Bracco, M. Bucher, C. Burigana, E. Calabrese, J. F. Cardoso, J. Carron, R. R. Chary, H. C. Chiang, L. P. L. Colombo, C. Combet, B. P. Crill, F. Cuttaia, P. de Bernardis, G. de Zotti, J. Delabrouille, J. M. Delouis, E. Di Valentino, C. Dickinson, J. M. Diego, O. Doré, M. Douspis, A. Ducout, X. Dupac, G. Efstathiou, F. Elsner, T. A. Enßlin, H. K. Eriksen, Y. Fantaye, R. Fernandez-Cobos, K. Ferrière, F. Forastieri, M. Frailis, A. A. Fraisse, E. Franceschi, A. Frolov, S. Galeotta, S. Galli, K. Ganga, R. T. Génova-Santos, M. Gerbino, T. Ghosh, J. González-Nuevo, K. M. Górski, S. Gratton, G. Green, A. Gruppuso, J. E. Gudmundsson, V. Guillet, W. Handley, F. K. Hansen, G. Helou, D. Herranz, E. Hivon, Z. Huang, A. H. Jaffe, W. C. Jones, E. Keihänen, R. Keskitalo, K. Kiiveri, J. Kim, N. Krachmalnicoff, M. Kunz, H. Kurki-Suonio, G. Lagache, J. M. Lamarre, A. Lasenby, M. Lattanzi, C. R. Lawrence, M. Le Jeune, F. Levrier, M. Liguori, P. B. Lilje, V. Lindholm, M. López-Caniego, P. M. Lubin, Y. Z. Ma, J. F. Macías-Pérez, G. Maggio, D. Maino, N. Mandolesi, A. Mangilli, A. Marcos-Caballero, M. Maris, P. G. Martin, E. Martínez-González, S. Matarrese, N. Mauri, J. D. McEwen, A. Melchiorri, A. Mennella, M. Migliaccio, M. A. Miville-Deschênes, D. Molinari, A. Moneti, L. Montier, G. Morgante, A. Moss, P. Natoli, L. Pagano, D. Paoletti, G. Patanchon, F. Perrotta, V. Pettorino, F. Piacentini, L. Polastri, G. Polenta, J. L. Puget, J. P. Rachen, M. Reinecke, M. Remazeilles, A. Renzi, I. Ristorcelli, G. Rocha, C. Rosset, G. Roudier, J. A. Rubiño-Martín, B. Ruiz-Granados, L. Salvati, M. Sandri, M. Savelainen, D. Scott, C. Sirignano, R. Sunyaev, A. S. Suur-Uski, J. A. Tauber, D. Tavagnacco, M. Tenti, L. Toffolatti, M. Tomasi, T. Trombetti, J. Valiviita, B. Van Tent, P. Vielva, F. Villa, N. Vittorio, B. D. Wandelt, I. K. Wehus, A. Zacchei, and A. Zonca, "Planck 2018 results. XII. Galactic astrophysics using polarized dust emission," *ArXiv e-prints*, p. arXiv:1807.06212, Jul. 2018.

[109] D. T. Chuss, B.-G. Andersson, J. Bally, J. L. Dotson, C. D. Dowell, J. A. Guerra, D. A. Harper, M. Houde, T. J. Jones, A. Lazarian, E. Lopez Rodriguez, J. M. Michail, M. R. Morris, G. Novak, J. Siah, J. Staguhn, J. E. Vaillancourt, C. G. Volpert, M. Werner, E. J. Wollack, D. J. Benford, M. Berthoud, E. G. Cox, R. Crutcher, D. A. Dale, L. M. Fissel, P. F. Goldsmith, R. T. Hamilton, S. Hanany, T. K. Henning, L. W. Looney, S. H. Moseley, F. P. Santos, I. Stephens, K. Tassis, C. Q. Trinh, E. Van Camp, and D. Ward-Thompson, "HAWC+/SOFIA Multiwavelength Polarimetric Observations of OMC-1," *ArXiv e-prints*, p. arXiv:1810.08233, Oct. 2018.

[110] F. Bacciotti, J. M. Girart, M. Padovani, L. Podio, R. Paladino, L. Testi, E. Bianchi, D. Galli, C. Codella, D. Coffey, C. Favre, and D. Fedele, "ALMA Observations of Polarized Emission toward the CW Tau and DG Tau Protoplanetary Disks: Con-

DRAFT

straints on Dust Grain Growth and Settling," *Ap. J.*, vol. 865, p. L12, Oct. 2018.

[111] C. H. Smith, C. M. Wright, D. K. Aitken, P. F. Roche, and J. H. Hough, "Studies in mid-infrared spectropolarimetry - II. An atlas of spectra," *MNRAS*, vol. 312, pp. 327–361, Feb. 2000.

[112] J. E. Chiar, A. J. Adamson, D. C. B. Whittet, A. Chrysostomou, J. H. Hough, T. H. Kerr, R. E. Mason, P. F. Roche, and G. Wright, "Spectropolarimetry of the 3.4 μm Feature in the Diffuse ISM toward the Galactic Center Quintuplet Cluster," *Ap. J.*, vol. 651, pp. 268–271, Nov. 2006.

[113] R. E. Mason, G. S. Wright, A. Adamson, and Y. Pendleton, "Spectropolarimetry of the 3.4 μm Absorption Feature in NGC 1068," *Ap. J.*, vol. 656, pp. 798–804, Feb. 2007.

[114] Planck Collaboration Int. XXII, "Planck intermediate results. XXII. Frequency dependence of thermal emission from Galactic dust in intensity and polarization," *Astron. Astrophys.*, vol. 576, p. A107, Apr. 2015.

[115] P. C. Ashton, P. A. R. Ade, F. E. Angilè, S. J. Benton, M. J. Devlin, B. Dober, L. M. Fissel, Y. Fukui, N. Galitzki, N. N. Gandilo, J. Klein, A. L. Korotkov, Z.-Y. Li, P. G. Martin, T. G. Matthews, L. Moncelsi, F. Nakamura, C. B. Netterfield, G. Novak, E. Pascale, F. Poidevin, F. P. Santos, G. Savini, D. Scott, J. A. Shariff, J. D. Soler, N. E. Thomas, C. E. Tucker, G. S. Tucker, and D. Ward-Thompson, "First Observation of the Submillimeter Polarization Spectrum in a Translucent Molecular Cloud," *Ap. J.*, vol. 857, p. 10, Apr. 2018.

[116] A. M. Meisner and D. P. Finkbeiner, "Modeling Thermal Dust Emission with Two Components: Application to the Planck High Frequency Instrument Maps," *Ap. J.*, vol. 798, p. 88, Jan. 2015.

[117] V. Guillet, L. Fanciullo, L. Verstraete, F. Boulanger, A. P. Jones, M.-A. Miville-Deschênes, N. Ysard, F. Levrier, and M. Alves, "Dust models compatible with Planck intensity and polarization data in translucent lines of sight," *Astron. Astrophys.*, vol. 610, p. A16, Feb. 2018.

[118] B. T. Draine and B. Hensley, "Magnetic Nanoparticles in the Interstellar Medium: Emission Spectrum and Polarization," *Ap. J.*, vol. 765, p. 159, Mar. 2013.

[119] C. Dickinson, Y. Ali-Haïmoud, A. Barr, E. S. Battistelli, A. Bell, L. Bernstein, S. Casassus, K. Cleary, B. T. Draine, R. Génova-Santos, S. E. Harper, B. Hensley, J. Hill-Valler, T. Hoang, F. P. Israel, L. Jew, A. Lazarian, J. P. Leahy, J. Leech, C. H. López-Caraballo, I. McDonald, E. J. Murphy, T. Onaka, R. Paladini, M. W. Peel, Y. Perrott, F. Poidevin, A. C. S. Readhead, J.-A. Rubiño-Martín, A. C. Taylor, C. T. Tibbs, M. Todorović, and M. Vidal, "The State-of-Play of Anomalous Microwave Emission (AME) research," *New Ast. Rev.*, vol. 80, pp. 1–28, Feb. 2018.

[120] C. Dickinson, A. Barr, H. C. Chiang, C. Copley, R. D. P. Grumitt, S. E. Harper, H. M. Heilgendorff, L. R. P. Jew, J. L. Jonas, M. E. Jones, J. P. Leahy, J. Leech, E. M. Leitch, S. J. C. Muchovej, T. J. Pearson, M. W. Peel, A. C. S. Readhead, J. Sievers, M. A. Stevenson, and A. C. Taylor, "The C-Band All-Sky Survey (C-BASS): Constraining diffuse Galactic radio emission in the North Celestial Pole region," *ArXiv e-prints*, p. arXiv:1810.11681, Oct. 2018.

[121] S. E. Clark, J. E. G. Peek, and M. E. Putman, "Magnetically Aligned H I Fibers and the Rolling Hough Transform," *Ap. J.*, vol. 789, p. 82, Jul. 2014.

[122] S. E. Clark, J. C. Hill, J. E. G. Peek, M. E. Putman, and B. L. Babler, "Neutral Hydrogen Structures Trace Dust Polarization Angle: Implications for Cosmic Microwave Background Foregrounds," *Physical Review Letters*, vol. 115, no. 24, p. 241302, Dec. 2015.

[123] P. M. W. Kalberla, J. Kerp, U. Haud, B. Winkel, N. Ben Bekhti, L. Flöer, and D. Lenz, "Cold Milky Way HI Gas in Filaments," *Ap. J.*, vol. 821, p. 117, Apr. 2016.

[124] P. M. W. Kalberla and J. Kerp, "Anisotropies in the HI gas distribution toward 3C 196," *Astron. Astrophys.*, vol. 595, p. A37, Oct. 2016.

[125] R. M. Crutcher, B. Wandelt, C. Heiles, E. Falgarone, and T. H. Troland, "Magnetic Fields in Interstellar Clouds from Zeeman Observations: Inference of Total Field Strengths by Bayesian Analysis," *Ap. J.*, vol. 725, pp. 466–479, Dec. 2010.

[126] HI4PI Collaboration, "HI4PI: A full-sky H I survey based on EBHIS and GASS," *Astron. Astrophys.*, vol. 594, p. A116, Oct. 2016.

[127] J. E. G. Peek, B. L. Babler, Y. Zheng, S. E. Clark, K. A. Douglas, E. J. Korpela, M. E. Putman, S. Stanimirović, S. J. Gibson, and C. Heiles, "The GALFA-H I Survey Data Release 2," *Ap. J. Suppl.*, vol. 234, p. 2, Jan. 2018.

[128] N. M. McClure-Griffiths, S. Stanimirovic, C. Murray, D. Li, J. M. Dickey, E. Vazquez-Semadeni, J. E. G. Peek, M. Putman, S. E. Clark, M. A. Miville-Deschenes, J. Bland-Hawthorn, and L. Staveley-Smith, "Galactic and Magellanic Evolution with the SKA," in *Advancing Astrophysics with the Square Kilometre Array (AASKA14)*, Apr. 2015, p. 130.

[129] T. P. Ellsworth-Bowers, E. Rosolowsky, J. Glenn, A. Ginsburg, N. J. Evans, II, C. Battersby, Y. L. Shirley, and B. Svoboda, "The Bolocam Galactic Plane Survey. XII. Distance Catalog Expansion Using Kinematic Isolation of Dense Molecular Cloud Structures with ^{13}CO(1-0)," *Ap. J.*, vol. 799, p. 29, Jan. 2015.

[130] Planck Collaboration Int. XXXV, "*Planck* intermediate results. XXXV. Probing the role of the magnetic field in the formation of structure in molecular clouds," *Astron. Astrophys.*, vol. 586, p. A138, 2016.

[131] A. Allen, Z.-Y. Li, and F. H. Shu, "Collapse of Magnetized Singular Isothermal Toroids. II. Rotation and Magnetic Braking," *Ap. J.*, vol. 599, pp. 363–379, Dec. 2003.

[132] Z.-Y. Li, R. Krasnopolsky, H. Shang, and B. Zhao, "On the Role of Pseudodisk Warping and Reconnection in Protostellar

DRAFT

Disk Formation in Turbulent Magnetized Cores," *Ap. J.*, vol. 793, p. 130, Oct. 2014.

[133] D. A. Harper, M. C. Runyan, C. D. Dowell, C. J. Wirth, M. Amato, T. Ames, M. Amiri, S. Banks, A. Bartels, D. J. Benford, M. Berthoud, E. Buchanan, S. Casey, N. L. Chapman, D. T. Chuss, R. Derro, J. L. Dotson, R. Evans, D. Fixsen, I. Gatley, J. A. Guerra, M. Halpern, R. T. Hamilton, L. A. Hamlin, C. J. Hansen, S. Heimsath, A. Hermida, G. C. Hilton, R. Hirsch, M. I. Hollister, C. F. Hostetter, K. Irwin, C. A. Jhabvala, M. Jhabvala, J. Kastner, A. Kovács, R. F. Loewenstein, L. W. Looney, E. Lopez-Rodriguez, S. F. Maher, J. M. Michail, T. M. Miller, S. H. Moseley, G. Novak, R. J. Pernic, T. Rennick, H. Rhody, E. Sandberg, D. Sandford, F. P. Santos, R. Shafer, E. H. Sharp, P. Shirron, J. Siah, R. Silverberg, L. M. Sparr, R. Spotz, J. G. Staguhn, A. S. Toorian, S. Towey, J. Tuttle, J. Vaillancourt, G. Voellmer, C. G. Volpert, S. i Wang, and E. J. Wollack, "1 the hawc+ far infrared camera and polarimeter for sofia," *JAI*, vol. 7, no. 2, p. 1840008, 2018.

[134] A. Lazarian, "Enhancement and Suppression of Heat Transfer by MHD Turbulence," *Ap. J. Lett.*, vol. 645, pp. L25–L28, Jul. 2006.

[135] ——, "Damping of Alfvén Waves by Turbulence and Its Consequences: From Cosmic-ray Streaming to Launching Winds," *Ap. J.*, vol. 833, p. 131, Dec. 2016.

[136] A. Lazarian and E. T. Vishniac, "Reconnection in a Weakly Stochastic Field," *Ap. J.*, vol. 517, pp. 700–718, Jun. 1999.

[137] S. Xu and A. Lazarian, "Magnetohydrodynamic turbulence and turbulent dynamo in a partially ionized plasma," *New Journal of Physics*, Oct. 2018.

[138] J. Silk and G. A. Mamon, "The current status of galaxy formation," *Research in Astronomy and Astrophysics*, vol. 12, pp. 917–946, Aug. 2012.

[139] R. S. Somerville and R. Davé, "Physical Models of Galaxy Formation in a Cosmological Framework," *ARAA*, vol. 53, pp. 51–113, Aug. 2015.

[140] S. Fujimoto, M. Ouchi, K. Kohno, Y. Yamaguchi, B. Hatsukade, Y. Ueda, T. Shibuya, S. Inoue, T. Oogi, S. Toft, C. Gómez-Guijarro, T. Wang, D. Espada, T. Nagao, I. Tanaka, Y. Ao, H. Umehata, Y. Taniguchi, K. Nakanishi, W. Rujopakarn, R. J. Ivison, W.-h. Wang, M. M. Lee, K.-i. Tadaki, Y. Tamura, and J. S. Dunlop, "ALMA 26 Arcmin^2 Survey of GOODS-S at One Millimeter (ASAGAO): Average Morphology of High-z Dusty Star-forming Galaxies in an Exponential Disk ($n \simeq 1$)," *Ap. J.*, vol. 861, p. 7, Jul. 2018.

[141] A. M. Swinbank, I. Smail, S. Longmore, A. I. Harris, A. J. Baker, C. De Breuck, J. Richard, A. C. Edge, R. J. Ivison, R. Blundell, K. E. K. Coppin, P. Cox, M. Gurwell, L. J. Hainline, M. Krips, A. Lundgren, R. Neri, B. Siana, G. Siringo, D. P. Stark, D. Wilner, and J. D. Younger, "Intense star formation within resolved compact regions in a galaxy at z = 2.3," *Nature*, vol. 464, pp. 733–736, Apr. 2010.

[142] F. Combes, M. Rex, T. D. Rawle, E. Egami, F. Boone, I. Smail, J. Richard, R. J. Ivison, M. Gurwell, C. M. Casey, A. Omont, A. Berciano Alba, M. Dessauges-Zavadsky, A. C. Edge, G. G. Fazio, J.-P. Kneib, N. Okabe, R. Pelló, P. G. Pérez-González, D. Schaerer, G. P. Smith, A. M. Swinbank, and P. van der Werf, "A bright z = 5.2 lensed submillimeter galaxy in the field of Abell 773. HLSJ091828.6+514223," *Astron. Astrophys.*, vol. 538, p. L4, Feb. 2012.

[143] Planck Collaboration XXVI, "Planck 2015 results. XXVI. The Second Planck Catalogue of Compact Sources," *Astron. Astrophys.*, vol. 594, p. A26, Sep. 2016.

[144] M. Negrello, S. Amber, A. Amvrosiadis, Z.-Y. Cai, A. Lapi, J. Gonzalez-Nuevo, G. De Zotti, C. Furlanetto, S. J. Maddox, M. Allen, T. Bakx, R. S. Bussmann, A. Cooray, G. Covone, L. Danese, H. Dannerbauer, H. Fu, J. Greenslade, M. Gurwell, R. Hopwood, L. V. E. Koopmans, N. Napolitano, H. Nayyeri, A. Omont, C. E. Petrillo, D. A. Riechers, S. Serjeant, C. Tortora, E. Valiante, G. Verdoes Kleijn, G. Vernardos, J. L. Wardlow, M. Baes, A. J. Baker, N. Bourne, D. Clements, S. M. Crawford, S. Dye, L. Dunne, S. Eales, R. J. Ivison, L. Marchetti, M. J. Michałowski, M. W. L. Smith, M. Vaccari, and P. van der Werf, "The Herschel-ATLAS: a sample of 500 μm-selected lensed galaxies over 600 deg^2," *MNRAS*, vol. 465, pp. 3558–3580, Mar. 2017.

[145] M. Negrello, J. Gonzalez-Nuevo, G. De Zotti, M. Bonato, Z.-Y. Cai, D. Clements, L. Danese, H. Dole, J. Greenslade, A. Lapi, and L. Montier, "On the statistics of proto-cluster candidates detected in the Planck all-sky survey," *ArXiv e-prints*, May 2017.

[146] R. Cañameras, N. Nesvadba, R. Kneissl, B. Frye, R. Gavazzi, S. Koenig, E. Le Floc'h, M. Limousin, I. Oteo, and D. Scott, "Planck's dusty GEMS. IV. Star formation and feedback in a maximum starburst at z = 3 seen at 60-pc resolution," *Astron. Astrophys.*, vol. 604, p. A117, Aug. 2017.

[147] A. King and K. Pounds, "Powerful Outflows and Feedback from Active Galactic Nuclei," *ARAA*, vol. 53, pp. 115–154, Aug. 2015.

[148] S. Dye, C. Furlanetto, L. Dunne, S. A. Eales, M. Negrello, H. Nayyeri, P. P. van der Werf, S. Serjeant, D. Farrah, M. J. Michałowski, M. Baes, L. Marchetti, A. Cooray, D. A. Riechers, and A. Amvrosiadis, "Modelling high-resolution ALMA observations of strongly lensed highly star-forming galaxies detected by Herschel," *MNRAS*, vol. 476, pp. 4383–4394, Jun. 2018.

[149] C. Lamarche, A. Verma, A. Vishwas, G. J. Stacey, D. Brisbin, C. Ferkinhoff, T. Nikola, S. J. U. Higdon, J. Higdon, and M. Tecza, "Resolving Star Formation on Sub-Kiloparsec Scales in the High-Redshift Galaxy SDP.11 Using Gravitational Lensing," *ArXiv e-prints*, Sep. 2018.

DRAFT

[150] P. Sharda, C. Federrath, E. da Cunha, A. M. Swinbank, and S. Dye, "Testing star formation laws in a starburst galaxy at redshift 3 resolved with ALMA," *MNRAS*, vol. 477, pp. 4380–4390, Jul. 2018.

[151] T. Treu, "Strong Lensing by Galaxies," *Ann. Rev. Astr. Ap.*, vol. 48, pp. 87–125, Sep. 2010.

[152] M. Negrello, R. Hopwood, G. De Zotti, A. Cooray, A. Verma, J. Bock, D. T. Frayer, M. A. Gurwell, A. Omont, R. Neri, H. Dannerbauer, L. L. Leeuw, E. Barton, J. Cooke, S. Kim, E. da Cunha, G. Rodighiero, P. Cox, D. G. Bonfield, M. J. Jarvis, S. Serjeant, R. J. Ivison, S. Dye, I. Aretxaga, D. H. Hughes, E. Ibar, F. Bertoldi, I. Valtchanov, S. Eales, L. Dunne, S. P. Driver, R. Auld, S. Buttiglione, A. Cava, C. A. Grady, D. L. Clements, A. Dariush, J. Fritz, D. Hill, J. B. Hornbeck, L. Kelvin, G. Lagache, M. Lopez-Caniego, J. Gonzalez-Nuevo, S. Maddox, E. Pascale, M. Pohlen, E. E. Rigby, A. Robotham, C. Simpson, D. J. B. Smith, P. Temi, M. A. Thompson, B. E. Woodgate, D. G. York, J. E. Aguirre, A. Beelen, A. Blain, A. J. Baker, M. Birkinshaw, R. Blundell, C. M. Bradford, D. Burgarella, L. Danese, J. S. Dunlop, S. Fleuren, J. Glenn, A. I. Harris, J. Kamenetzky, R. E. Lupu, R. J. Maddalena, B. F. Madore, P. R. Maloney, H. Matsuhara, M. J. Michałowski, E. J. Murphy, B. J. Naylor, H. Nguyen, C. Popescu, S. Rawlings, D. Rigopoulou, D. Scott, K. S. Scott, M. Seibert, I. Smail, R. J. Tuffs, J. D. Vieira, P. P. van der Werf, and J. Zmuidzinas, "The Detection of a Population of Submillimeter-Bright, Strongly Lensed Galaxies," *Science*, vol. 330, p. 800, Nov. 2010.

[153] R. A. Overzier, "The realm of the galaxy protoclusters. A review," *Astron. Astrophys. Rev.*, vol. 24, p. 14, Nov. 2016.

[154] Planck Collaboration XXXIX, "Planck intermediate results. XXXIX. The Planck list of high-redshift source candidates," *Astron. Astrophys.*, vol. 596, p. A100, Dec. 2016.

[155] C.-Y. Chen, P. K. King, and Z.-Y. Li, "Change of Magnetic Field-gas Alignment at the Gravity-driven Alfvénic Transition in Molecular Clouds: Implications for Dust Polarization Observations," *Ap. J.*, vol. 829, p. 84, Oct. 2016.

[156] R. J. Ivison, A. M. Swinbank, I. Smail, A. I. Harris, R. S. Bussmann, A. Cooray, P. Cox, H. Fu, A. Kovács, M. Krips, D. Narayanan, M. Negrello, R. Neri, J. Peñarrubia, J. Richard, D. A. Riechers, K. Rowlands, J. G. Staguhn, T. A. Targett, S. Amber, A. J. Baker, N. Bourne, F. Bertoldi, M. Bremer, J. A. Calanog, D. L. Clements, H. Dannerbauer, A. Dariush, G. De Zotti, L. Dunne, S. A. Eales, D. Farrah, S. Fleuren, A. Franceschini, J. E. Geach, R. D. George, J. C. Helly, R. Hopwood, E. Ibar, M. J. Jarvis, J.-P. Kneib, S. Maddox, A. Omont, D. Scott, S. Serjeant, M. W. L. Smith, M. A. Thompson, E. Valiante, I. Valtchanov, J. Vieira, and P. van der Werf, "Herschel-ATLAS: A Binary HyLIRG Pinpointing a Cluster of Starbursting Protoellipticals," *Ap. J.*, vol. 772, p. 137, Aug. 2013.

[157] T. Wang, D. Elbaz, E. Daddi, A. Finoguenov, D. Liu, C. Schreiber, S. Martín, V. Strazzullo, F. Valentino, R. van der Burg, A. Zanella, L. Ciesla, R. Gobat, A. Le Brun, M. Pannella, M. Sargent, X. Shu, Q. Tan, N. Cappelluti, and Y. Li, "Discovery of a Galaxy Cluster with a Violently Starbursting Core at z = 2.506," *Ap. J.*, vol. 828, p. 56, Sep. 2016.

[158] I. Oteo, R. J. Ivison, L. Dunne, A. Manilla-Robles, S. Maddox, A. J. R. Lewis, G. de Zotti, M. Bremer, D. L. Clements, A. Cooray, H. Dannerbauer, S. Eales, J. Greenslade, A. Omont, I. Perez-Fournón, D. Riechers, D. Scott, P. van der Werf, A. Weiss, and Z.-Y. Zhang, "An Extreme Protocluster of Luminous Dusty Starbursts in the Early Universe," *Ap. J.*, vol. 856, p. 72, Mar. 2018.

[159] B. D. Metzger, P. K. G. Williams, and E. Berger, "Extragalactic Synchrotron Transients in the Era of Wide-field Radio Surveys. I. Detection Rates and Light Curve Characteristics," *Ap. J.*, vol. 806, p. 224, Jun. 2015.

[160] Planck Collaboration, P. A. R. Ade, N. Aghanim, C. Armitage-Caplan, M. Arnaud, M. Ashdown, F. Atrio-Barandela, J. Aumont, C. Baccigalupi, A. J. Banday, R. B. Barreiro, J. G. Bartlett, E. Battaner, K. Benabed, A. Benoît, A. Benoit-Lévy, J. P. Bernard, M. Bersanelli, M. Bethermin, P. Bielewicz, K. Blagrave, J. Bobin, J. J. Bock, A. Bonaldi, J. R. Bond, J. D. Borrill, F. R. Bouchet, F. Boulanger, M. Bridges, M. Bucher, C. Burigana, R. C. Butler, J. F. Cardoso, A. Catalano, A. Challinor, A. Chamballu, X. Chen, H. C. Chiang, L. Y. Chiang, P. R. Christensen, S. Church, D. L. Clements, S. Colombi, Colombo, L. P. L., F. Couchot, A. Coulais, B. P. Crill, A. Curto, F. Cuttaia, L. Danese, R. D. Davies, R. J. Davis, P. de Bernardis, A. de Rosa, G. de Zotti, J. Delabrouille, J. M. Delouis, F. X. Désert, C. Dickinson, J. M. Diego, H. Dole, S. Donzelli, O. Doré, M. Douspis, X. Dupac, G. Efstathiou, T. A. Enßlin, H. K. Eriksen, F. Finelli, O. Forni, M. Frailis, E. Franceschi, S. Galeotta, K. Ganga, T. Ghosh, M. Giard, Y. Giraud-Héraud, J. González-Nuevo, K. M. Górski, S. Gratton, A. Gregorio, A. Gruppuso, F. K. Hansen, D. Hanson, D. Harrison, G. Helou, S. Henrot-Versillé, C. Hernández-Monteagudo, D. Herranz, S. R. Hildebrandt, E. Hivon, M. Hobson, W. A. Holmes, A. Hornstrup, W. Hovest, K. M. Huffenberger, A. H. Jaffe, T. R. Jaffe, W. C. Jones, M. Juvela, P. Kalberla, E. Keihänen, J. Kerp, R. Keskitalo, T. S. Kisner, R. Kneissl, J. Knoche, L. Knox, M. Kunz, H. Kurki-Suonio, F. Lacasa, G. Lagache, A. Lähteenmäki, J. M. Lamarre, M. Langer, A. Lasenby, R. J. Laureijs, C. R. Lawrence, R. Leonardi, J. León-Tavares, J. Lesgourgues, M. Liguori, P. B. Lilje, M. Linden-Vørnle, M. López-Caniego, P. M. Lubin, J. F. Macías-Pérez, B. Maffei, D. Maino, N. Mandolesi, M. Maris, D. J. Marshall, P. G. Martin, E. Martínez-González, S. Masi, M. Massardi, S. Matarrese, F. Matthai, P. Mazzotta, A. Melchiorri, L. Mendes, A. Mennella, M. Migliaccio, S. Mitra, M. A. Miville-Deschênes, A. Moneti, L. Montier, G. Morgante, D. Mortlock, D. Munshi, J. A. Murphy, P. Naselsky, F. Nati, P. Natoli, C. B. Netterfield, H. U. Nørgaard-Nielsen, F. Noviello, D. Novikov, I. Novikov, S. Osborne, C. A. Oxborrow, F. Paci, L. Pagano, F. Pajot, R. Paladini, D. Paoletti, B. Partridge, F. Pasian, G. Patanchon, O. Perdereau, L. Perotto, F. Perrotta, F. Piacentini, M. Piat, E. Pierpaoli, D. Pietrobon, S. Plaszczynski, E. Pointecouteau, G. Polenta, N. Ponthieu, L. Popa, T. Poutanen, G. W. Pratt, G. Prézeau, S. Prunet, J.-L. Puget, J. P. Rachen, W. T. Reach, R. Rebolo, M. Reinecke, M. Remazeilles, C. Renault, S. Ricciardi, T. Riller, I. Ristorcelli, G. Rocha, C. Rosset, G. Roudier, M. Rowan-Robinson, J. A. Rubiño-Martín, B. Rusholme, M. Sandri, D. Santos, G. Savini, D. Scott, M. D. Seiffert, P. Serra,

DRAFT

E. P. S. Shellard, L. D. Spencer, J. L. Starck, V. Stolyarov, R. Stompor, R. Sudiwala, R. Sunyaev, F. Sureau, D. Sutton, A. S. Suur-Uski, J. F. Sygnet, J. A. Tauber, D. Tavagnacco, L. Terenzi, L. Toffolatti, M. Tomasi, M. Tristram, M. Tucci, J. Tuovinen, M. Türler, L. Valenziano, J. Valiviita, B. Van Tent, P. Vielva, F. Villa, N. Vittorio, L. A. Wade, B. D. Wandelt, N. Welikala, M. White, S. D. M. White, B. Winkel, D. Yvon, A. Zacchei, and A. Zonca, "Planck 2013 results. XXX. Cosmic infrared background measurements and implications for star formation," *Astronomy and Astrophysics*, vol. 571, p. A30, Nov. 2014.

[161] Planck Collaboration, P. A. R. Ade, N. Aghanim, C. Armitage-Caplan, M. Arnaud, M. Ashdown, F. Atrio-Barandela, J. Aumont, C. Baccigalupi, A. J. Banday, R. B. Barreiro, J. G. Bartlett, S. Basak, E. Battaner, K. Benabed, A. Benoît, A. Benoit-Lévy, J. P. Bernard, M. Bersanelli, M. Bethermin, P. Bielewicz, J. Bobin, J. J. Bock, A. Bonaldi, J. R. Bond, J. D. Borrill, F. R. Bouchet, F. Boulanger, M. Bridges, M. Bucher, C. Burigana, R. C. Butler, J. F. Cardoso, A. Catalano, A. Challinor, A. Chamballu, H. C. Chiang, L. Y. Chiang, P. R. Christensen, S. Church, D. L. Clements, S. Colombi, Colombo, L. P. L., F. Couchot, A. Coulais, B. P. Crill, A. Curto, F. Cuttaia, L. Danese, R. D. Davies, P. de Bernardis, A. de Rosa, G. de Zotti, J. Delabrouille, J. M. Delouis, F. X. Désert, J. M. Diego, H. Dole, S. Donzelli, O. Doré, M. Douspis, X. Dupac, G. Efstathiou, T. A. Enßlin, H. K. Eriksen, F. Finelli, O. Forni, M. Frailis, E. Franceschi, S. Galeotta, K. Ganga, M. Giard, G. Giardino, Y. Giraud-Héraud, J. González-Nuevo, K. M. Górski, S. Gratton, A. Gregorio, A. Gruppuso, J. E. Gudmundsson, F. K. Hansen, D. Hanson, D. Harrison, S. Henrot-Versillé, C. Hernández-Monteagudo, D. Herranz, S. R. Hildebrandt, E. Hivon, M. Hobson, W. A. Holmes, A. Hornstrup, W. Hovest, K. M. Huffenberger, A. H. Jaffe, T. R. Jaffe, W. C. Jones, M. Juvela, E. Keihänen, R. Keskitalo, T. S. Kisner, R. Kneissl, J. Knoche, L. Knox, M. Kunz, H. Kurki-Suonio, F. Lacasa, G. Lagache, A. Lähteenmäki, J. M. Lamarre, A. Lasenby, R. J. Laureijs, C. R. Lawrence, R. Leonardi, J. León-Tavares, J. Lesgourgues, M. Liguori, P. B. Lilje, M. Linden-Vørnle, M. López-Caniego, P. M. Lubin, J. F. Macías-Pérez, B. Maffei, D. Maino, N. Mandolesi, M. Maris, D. J. Marshall, P. G. Martin, E. Martínez-González, S. Masi, M. Massardi, S. Matarrese, F. Matthai, P. Mazzotta, A. Melchiorri, L. Mendes, A. Mennella, M. Migliaccio, S. Mitra, M. A. Miville-Deschênes, A. Moneti, L. Montier, G. Morgante, D. Mortlock, D. Munshi, P. Naselsky, F. Nati, P. Natoli, C. B. Netterfield, H. U. Nørgaard-Nielsen, F. Noviello, D. Novikov, I. Novikov, S. Osborne, C. A. Oxborrow, F. Paci, L. Pagano, F. Pajot, D. Paoletti, F. Pasian, G. Patanchon, O. Perdereau, L. Perotto, F. Perrotta, F. Piacentini, M. Piat, E. Pierpaoli, D. Pietrobon, S. Plaszczynski, E. Pointecouteau, G. Polenta, N. Ponthieu, L. Popa, T. Poutanen, G. W. Pratt, G. Prézeau, S. Prunet, J.-L. Puget, J. P. Rachen, R. Rebolo, M. Reinecke, M. Remazeilles, C. Renault, S. Ricciardi, T. Riller, I. Ristorcelli, G. Rocha, C. Rosset, G. Roudier, M. Rowan-Robinson, B. Rusholme, M. Sandri, D. Santos, G. Savini, D. Scott, M. D. Seiffert, P. Serra, E. P. S. Shellard, L. D. Spencer, J. L. Starck, V. Stolyarov, R. Stompor, R. Sudiwala, R. Sunyaev, F. Sureau, D. Sutton, A. S. Suur-Uski, J. F. Sygnet, J. A. Tauber, D. Tavagnacco, L. Terenzi, L. Toffolatti, M. Tomasi, M. Tristram, M. Tucci, J. Tuovinen, L. Valenziano, J. Valiviita, B. Van Tent, P. Vielva, F. Villa, N. Vittorio, L. A. Wade, B. D. Wandelt, S. D. M. White, D. Yvon, A. Zacchei, and A. Zonca, "Planck 2013 results. XVIII. The gravitational lensing-infrared background correlation," *Astronomy and Astrophysics*, vol. 571, p. A18, Nov. 2014.

[162] P. Madau and M. Dickinson, "Cosmic Star-Formation History," *ARA&A*, vol. 52, pp. 415–486, Aug. 2014.

[163] H.-Y. Wu and O. DorÃ©, "Optimizing future experiments of cosmic far-infrared background: a principal component approach," *Mon. Not. Roy. Astron. Soc.*, vol. 467, no. 4, pp. 4150–4160, 2017.

[164] B. D. Sherwin and M. Schmittfull, "Delensing the CMB with the cosmic infrared background," *Phys. Rev. D.*, vol. 92, no. 4, p. 043005, Aug. 2015.

[165] M. Tucci, V. Desjacques, and M. Kunz, "Cosmic infrared background anisotropies as a window into primordial non-Gaussianity," *MNRAS*, vol. 463, pp. 2046–2063, Dec. 2016.

[166] M. Schmittfull and U. Seljak, "Parameter constraints from cross-correlation of CMB lensing with galaxy clustering," *Phys. Rev. D.*, vol. 97, no. 12, p. 123540, Jun. 2018.

[167] J. H. Kang, P. Ade, Z. Ahmed, R. Aikin, K. Alexander, D. Barkats, S. Benton, C. Bischoff, J. Bock, H. Boenish *et al.*, "2017 upgrade and performance of bicep3: a 95ghz refracting telescope for degree-scale cmb polarization," in *Millimeter, Submillimeter, and Far-Infrared Detectors and Instrumentation for Astronomy IX*, vol. 10708. International Society for Optics and Photonics, 2018, p. 107082N.

[168] A. S. Rahlin, P. A. R. Ade, M. Amiri, S. J. Benton, J. J. Bock, J. R. Bond, S. A. Bryan, H. C. Chiang, C. R. Contaldi, B. P. Crill, O. Doré, M. Farhang, J. P. Filippini, L. M. Fissel, A. A. Fraisse, A. E. Gambrel, N. N. Gandilo, S. Golwala, J. E. Gudmundsson, M. Halpern, M. F. Hasselfield, G. Hilton, W. A. Holmes, V. V. Hristov, K. D. Irwin, W. C. Jones, Z. D. Kermish, C. L. Kuo, C. J. MacTavish, P. V. Mason, K. Megerian, L. Moncelsi, T. A. Morford, J. M. Nagy, C. B. Netterfield, R. O'Brient, C. Reintsema, J. E. Ruhl, M. C. Runyan, J. A. Shariff, J. D. Soler, A. Trangsrud, C. Tucker, R. S. Tucker, A. D. Turner, A. C. Weber, D. V. Wiebe, and E. Y. Young, "Pre-flight integration and characterization of the SPIDER balloon-borne telescope," in *Millimeter, Submillimeter, and Far-Infrared Detectors and Instrumentation for Astronomy VII*, ser. SPIE Proceedings, vol. 9153, Jul. 2014, p. 915313.

[169] N. Krachmalnicoff, E. Carretti, C. Baccigalupi, G. Bernardi, S. Brown, B. M. Gaensler, M. Haverkorn, M. Kesteven, F. Perrotta, S. Poppi, and L. Staveley-Smith, "The S-PASS view of polarized Galactic Synchrotron at 2.3 GHz as a contaminant to CMB observations," *ArXiv e-prints*, p. arXiv:1802.01145, Feb. 2018.

[170] U. Fuskeland, I. K. Wehus, H. K. Eriksen, and S. K. Næss, "Spatial Variations in the Spectral Index of Polarized Synchrotron

DRAFT

Emission in the 9 yr WMAP Sky Maps," *Ap. J.*, vol. 790, p. 104, Aug. 2014.

[171] Planck Collaboration, A. Abergel, P. A. R. Ade, N. Aghanim, M. I. R. Alves, G. Aniano, C. Armitage-Caplan, M. Arnaud, M. Ashdown, F. Atrio-Barandela, J. Aumont, C. Baccigalupi, A. J. Banday, R. B. Barreiro, J. G. Bartlett, E. Battaner, K. Benabed, A. Benoît, A. Benoit-Lévy, J. P. Bernard, M. Bersanelli, P. Bielewicz, J. Bobin, J. J. Bock, A. Bonaldi, J. R. Bond, J. Borrill, F. R. Bouchet, F. Boulanger, M. Bridges, M. Bucher, C. Burigana, R. C. Butler, J. F. Cardoso, A. Catalano, A. Chamballu, R. R. Chary, H. C. Chiang, L. Y. Chiang, P. R. Christensen, S. Church, M. Clemens, D. L. Clements, S. Colombi, L. P. L. Colombo, C. Combet, F. Couchot, A. Coulais, B. P. Crill, A. Curto, F. Cuttaia, L. Danese, R. D. Davies, R. J. Davis, P. de Bernardis, A. de Rosa, G. de Zotti, J. Delabrouille, J. M. Delouis, F. X. Désert, C. Dickinson, J. M. Diego, H. Dole, S. Donzelli, O. Doré, M. Douspis, B. T. Draine, X. Dupac, G. Efstathiou, T. A. Enßlin, H. K. Eriksen, E. Falgarone, F. Finelli, O. Forni, M. Frailis, A. A. Fraisse, E. Franceschi, S. Galeotta, K. Ganga, T. Ghosh, M. Giard, G. Giardino, Y. Giraud-Héraud, J. González-Nuevo, K. M. Górski, S. Gratton, A. Gregorio, I. A. Grenier, A. Gruppuso, V. Guillet, F. K. Hansen, D. Hanson, D. L. Harrison, G. Helou, S. Henrot-Versillé, C. Hernández- Monteagudo, D. Herranz, S. R. Hildebrandt, E. Hivon, M. Hobson, W. A. Holmes, A. Hornstrup, W. Hovest, K. M. Huffenberger, A. H. Jaffe, T. R. Jaffe, J. Jewell, G. Joncas, W. C. Jones, M. Juvela, E. Keihänen, R. Keskitalo, T. S. Kisner, J. Knoche, L. Knox, M. Kunz, H. Kurki-Suonio, G. Lagache, A. Lähteenmäki, J. M. Lamarre, A. Lasenby, R. J. Laureijs, C. R. Lawrence, R. Leonardi, J. León-Tavares, J. Lesgourgues, F. Levrier, M. Liguori, P. B. Lilje, M. Linden-Vørnle, M. López-Caniego, P. M. Lubin, J. F. Macías-Pérez, B. Maffei, D. Maino, N. Mandolesi, M. Maris, D. J. Marshall, P. G. Martin, E. Martínez-González, S. Masi, M. Massardi, S. Matarrese, F. Matthai, P. Mazzotta, P. McGehee, A. Melchiorri, L. Mendes, A. Mennella, M. Migliaccio, S. Mitra, M. A. Miville-Deschênes, A. Moneti, L. Montier, G. Morgante, D. Mortlock, D. Munshi, J. A. Murphy, P. Naselsky, F. Nati, P. Natoli, C. B. Netterfield, H. U. Nørgaard-Nielsen, F. Noviello, D. Novikov, I. Novikov, S. Osborne, C. A. Oxborrow, F. Paci, L. Pagano, F. Pajot, R. Paladini, D. Paoletti, F. Pasian, G. Patanchon, O. Perdereau, L. Perotto, F. Perrotta, F. Piacentini, M. Piat, E. Pierpaoli, D. Pietrobon, S. Plaszczynski, E. Pointecouteau, G. Polenta, N. Ponthieu, L. Popa, T. Poutanen, G. W. Pratt, G. Prézeau, S. Prunet, J. L. Puget, J. P. Rachen, W. T. Reach, R. Rebolo, M. Reinecke, M. Remazeilles, C. Renault, S. Ricciardi, T. Riller, I. Ristorcelli, G. Rocha, C. Rosset, G. Roudier, M. Rowan- Robinson, J. A. Rubiño-Martín, B. Rusholme, M. Sandri, D. Santos, G. Savini, D. Scott, M. D. Seiffert, E. P. S. Shellard, L. D. Spencer, J. L. Starck, V. Stolyarov, R. Stompor, R. Sudiwala, R. Sunyaev, F. Sureau, D. Sutton, A. S. Suur-Uski, J. F. Sygnet, J. A. Tauber, D. Tavagnacco, L. Terenzi, L. Toffolatti, M. Tomasi, M. Tristram, M. Tucci, J. Tuovinen, M. Türler, G. Umana, L. Valenziano, J. Valiviita, B. Van Tent, L. Verstraete, P. Vielva, F. Villa, N. Vittorio, L. A. Wade, B. D. Wandelt, N. Welikala, N. Ysard, D. Yvon, A. Zacchei, and A. Zonca, "Planck 2013 results. XI. All-sky model of thermal dust emission," *Astron. Astrophys.*, vol. 571, p. A11, Nov. 2014.

[172] T. Trombetti, C. Burigana, G. De Zotti, V. Galluzzi, and M. Massardi, "Average fractional polarization of extragalactic sources at Planck frequencies," *Astron. Astrophys.*, vol. 618, p. A29, Oct. 2018.

[173] G. Puglisi, V. Galluzzi, L. Bonavera, J. Gonzalez-Nuevo, A. Lapi, M. Massardi, F. Perrotta, C. Baccigalupi, A. Celotti, and L. Danese, "Forecasting the Contribution of Polarized Extragalactic Radio Sources in CMB Observations," *Ap. J.*, vol. 858, p. 85, May 2018.

[174] Y. Fantaye, F. Stivoli, J. Grain, S. M. Leach, M. Tristram, C. Baccigalupi, and R. Stompor, "Estimating the tensor-to-scalar ratio and the effect of residual foreground contamination," *JCAP*, vol. 8, p. 1, Aug. 2011.

[175] C. Armitage-Caplan, J. Dunkley, H. K. Eriksen, and C. Dickinson, "Impact on the tensor-to-scalar ratio of incorrect Galactic foreground modelling," *MNRAS*, vol. 424, pp. 1914–1924, Aug. 2012.

[176] A. Kogut and D. J. Fixsen, "Foreground Bias from Parametric Models of Far-IR Dust Emission," *Ap. J.*, vol. 826, p. 101, Aug. 2016.

[177] M. Remazeilles, C. Dickinson, H. K. K. Eriksen, and I. K. Wehus, "Sensitivity and foreground modelling for large-scale cosmic microwave background B-mode polarization satellite missions," *MNRAS*, vol. 458, pp. 2032–2050, May 2016.

[178] R. Stompor, J. Errard, and D. Poletti, "Forecasting performance of CMB experiments in the presence of complex foreground contaminations," *Phys. Rev. D.*, vol. 94, no. 8, p. 083526, Oct. 2016.

[179] B. Thorne, J. Dunkley, D. Alonso, and S. Næss, "The Python Sky Model: software for simulating the Galactic microwave sky," *MNRAS*, vol. 469, pp. 2821–2833, Aug. 2017.

[180] K. M. Górski, E. Hivon, A. J. Banday, B. D. Wandelt, F. K. Hansen, M. Reinecke, and M. Bartelmann, "HEALPix: A Framework for High-Resolution Discretization and Fast Analysis of Data Distributed on the Sphere," *Ap. J.*, vol. 622, pp. 759–771, Apr. 2005.

[181] J. Delabrouille, M. Betoule, J. B. Melin, M. A. Miville- Deschênes, J. Gonzalez-Nuevo, M. Le Jeune, G. Castex, G. de Zotti, S. Basak, M. Ashdown, J. Aumont, C. Baccigalupi, A. J. Banday, J. P. Bernard, F. R. Bouchet, D. L. Clements, A. da Silva, C. Dickinson, F. Dodu, K. Dolag, F. Elsner, L. Fauvet, G. Faÿ, G. Giardino, S. Leach, J. Lesgourgues, M. Liguori, J. F. Macías-Pérez, M. Massardi, S. Matarrese, P. Mazzotta, L. Montier, S. Mottet, R. Paladini, B. Partridge, R. Piffaretti, G. Prezeau, S. Prunet, S. Ricciardi, M. Roman, B. Schaefer, and L. Toffolatti, "The pre-launch Planck Sky Model: a model of sky emission at submillimetre to centimetre wavelengths," *Astron. Astrophys.*, vol. 553, p. A96, May 2013.

[182] J. Errard, S. M. Feeney, H. V. Peiris, and A. H. Jaffe, "Robust forecasts on fundamental physics from the foreground-obscured, gravitationally-lensed CMB polarization," *JCAP*, vol. 3, p. 052, Mar. 2016.

DRAFT

[183] W. Hu, M. M. Hedman, and M. Zaldarriaga, "Benchmark parameters for CMB polarization experiments," *Phys. Rev. D.*, vol. 67, pp. 043 004–+, Feb. 2003, astro-ph/0210096.

[184] M. Shimon, B. Keating, N. Ponthieu, and E. Hivon, "CMB polarization systematics due to beam asymmetry: Impact on inflationary science," *Phys. Rev. D.*, vol. 77, no. 8, pp. 083 003–+, Apr. 2008.

[185] A. P. S. Yadav, M. Su, and M. Zaldarriaga, "Primordial B-mode diagnostics and self-calibrating the CMB polarization," *Phys. Rev. D.*, vol. 81, no. 6, pp. 063 512–+, Mar. 2010.

[186] Y. D. Takahashi, P. A. R. Ade, D. Barkats, J. O. Battle, E. M. Bierman, J. J. Bock, H. C. Chiang, C. D. Dowell, L. Duband, E. F. Hivon, W. L. Holzapfel, V. V. Hristov, W. C. Jones, B. G. Keating, J. M. Kovac, C. L. Kuo, A. E. Lange, E. M. Leitch, P. V. Mason, T. Matsumura, H. T. Nguyen, N. Ponthieu, C. Pryke, S. Richter, G. Rocha, and K. W. Yoon, "Characterization of the BICEP Telescope for High-precision Cosmic Microwave Background Polarimetry," *Ap. J.*, vol. 711, pp. 1141–1156, Mar. 2010.

[187] Bicep2 Collaboration, P. A. R. Ade, R. W. Aikin, D. Barkats, S. J. Benton, C. A. Bischoff, J. J. Bock, J. A. Brevik, I. Buder, E. Bullock, C. D. Dowell, L. Duband, J. P. Filippini, S. Fliescher, S. R. Golwala, M. Halpern, M. Hasselfield, S. R. Hildebrandt, G. C. Hilton, K. D. Irwin, K. S. Karkare, J. P. Kaufman, B. G. Keating, S. A. Kernasovskiy, J. M. Kovac, C. L. Kuo, E. M. Leitch, M. Lueker, C. B. Netterfield, H. T. Nguyen, R. O'Brient, R. W. Ogburn, IV, A. Orlando, C. Pryke, S. Richter, R. Schwarz, C. D. Sheehy, Z. K. Staniszewski, R. V. Sudiwala, G. P. Teply, J. E. Tolan, A. D. Turner, A. G. Vieregg, C. L. Wong, and K. W. Yoon, "Bicep2 III: Instrumental Systematics," *Ap. J.*, vol. 814, p. 110, Dec. 2015.

[188] C. L. Bennett, D. Larson, J. L. Weiland, N. Jarosik, G. Hinshaw, N. Odegard, K. M. Smith, R. S. Hill, B. Gold, M. Halpern, E. Komatsu, M. R. Nolta, L. Page, D. N. Spergel, E. Wollack, J. Dunkley, A. Kogut, M. Limon, S. S. Meyer, G. S. Tucker, and E. L. Wright, "Nine-year Wilkinson Microwave Anisotropy Probe (WMAP) Observations: Final Maps and Results," *The Astrophysical Journal Supplement Series*, vol. 208, p. 20, Oct. 2013.

[189] M. Hazumi, J. Borrill, Y. Chinone, M. A. Dobbs, H. Fuke, A. Ghribi, M. Hasegawa, K. Hattori, M. Hattori, W. L. Holzapfel, Y. Inoue, K. Ishidoshiro, H. Ishino, K. Karatsu, N. Katayama, I. Kawano, A. Kibayashi, Y. Kibe, N. Kimura, K. Koga, E. Komatsu, A. T. Lee, H. Matsuhara, T. Matsumura, S. Mima, K. Mitsuda, H. Morii, S. Murayama, M. Nagai, R. Nagata, S. Nakamura, K. Natsume, H. Nishino, A. Noda, T. Noguchi, I. Ohta, C. Otani, P. L. Richards, S. Sakai, N. Sato, Y. Sato, Y. Sekimoto, A. Shimizu, K. Shinozaki, H. Sugita, A. Suzuki, T. Suzuki, O. Tajima, S. Takada, Y. Takagi, Y. Takei, T. Tomaru, Y. Uzawa, H. Watanabe, N. Yamasaki, M. Yoshida, T. Yoshida, and K. Yotsumoto, "LiteBIRD: a small satellite for the study of B-mode polarization and inflation from cosmic background radiation detection," in *Space Telescopes and Instrumentation 2012: Optical, Infrared, and Millimeter Wave*, vol. 8442, Sep. 2012, p. 844219.

[190] C. G. R. Wallis, M. L. Brown, R. A. Battye, and J. Delabrouille, "Optimal scan strategies for future CMB satellite experiments," *MNRAS*, vol. 466, pp. 425–442, Apr. 2017.

[191] P. Natoli, M. Ashdown, R. Banerji, J. Borrill, A. Buzzelli, G. de Gasperis, J. Delabrouille, E. Hivon, D. Molinari, G. Patanchon, L. Polastri, M. Tomasi, F. R. Bouchet, S. Henrot-Versillé, D. T. Hoang, R. Keskitalo, K. Kiiveri, T. Kisner, V. Lindholm, D. McCarthy, F. Piacentini, O. Perdereau, G. Polenta, M. Tristram, A. Achucarro, P. Ade, R. Allison, C. Baccigalupi, M. Ballardini, A. J. Banday, J. Bartlett, N. Bartolo, S. Basak, D. Baumann, M. Bersanelli, A. Bonaldi, M. Bonato, F. Boulanger, T. Brinckmann, M. Bucher, C. Burigana, Z. Y. Cai, M. Calvo, C. S. Carvalho, M. G. Castellano, A. Challinor, J. Chluba, S. Clesse, I. Colantoni, A. Coppolecchia, M. Crook, G. D'Alessandro, P. de Bernardis, G. De Zotti, E. Di Valentino, J. M. Diego, J. Errard, S. Feeney, R. Fernandez-Cobos, F. Finelli, F. Forastieri, S. Galli, R. Genova-Santos, M. Gerbino, J. González-Nuevo, S. Grandis, J. Greenslade, A. Gruppuso, S. Hagstotz, S. Hanany, W. Handley, C. Hernandez-Monteagudo, C. Hervías-Caimapo, M. Hills, E. Keihänen, T. Kitching, M. Kunz, H. Kurki- Suonio, L. Lamagna, A. Lasenby, M. Lattanzi, J. Lesgourgues, A. Lewis, M. Liguori, M. López-Caniego, G. Luzzi, B. Maffei, N. Mandolesi, E. Martinez-González, C. J. A. P. Martins, S. Masi, S. Matarrese, A. Melchiorri, J. B. Melin, M. Migliaccio, A. Monfardini, M. Negrello, A. Notari, L. Pagano, A. Paiella, D. Paoletti, M. Piat, G. Pisano, A. Pollo, V. Poulin, M. Quartin, M. Remazeilles, M. Roman, G. Rossi, J. A. Rubino- Martin, L. Salvati, G. Signorelli, A. Tartari, D. Tramonte, N. Trappe, T. Trombetti, C. Tucker, J. Valiviita, R. Van de Weijgaert, B. van Tent, V. Vennin, P. Vielva, N. Vittorio, C. Wallis, K. Young, and M. Zannoni, "Exploring cosmic origins with CORE: Mitigation of systematic effects," *Journal of Cosmology and Astro-Particle Physics*, vol. 2018, p. 022, Apr. 2018.

[192] Planck Collaboration, P. A. R. Ade, N. Aghanim, M. Arnaud, M. Ashdown, J. Aumont, C. Baccigalupi, A. J. Banday, R. B. Barreiro, J. G. Bartlett, and et al., "Planck 2015 results. XII. Full focal plane simulations," *Astron. Astrophys.*, vol. 594, p. A12, Sep. 2016.

[193] L. Pogosian and A. Zucca, "Searching for primordial magnetic fields with CMB B-modes," *Classical and Quantum Gravity*, vol. 35, no. 12, p. 124004, May 2018.

[194] Planck collaboration, "Planck intermediate results. XLIX. Parity-violation constraints from polarization data," *Astronomy and Astrophysics*, vol. 596, p. A110, Dec. 2016.

[195] C. Rosset, M. Tristram, N. Ponthieu, P. Ade, J. Aumont, A. Catalano, L. Conversi, F. Couchot, B. P. Crill, F. Désert, K. Ganga, M. Giard, Y. Giraud-Héraud, J. Haïssinski, S. Henrot-Versillé, W. Holmes, W. C. Jones, J. Lamarre, A. Lange, C. Leroy, J. Macías-Pérez, B. Maffei, P. de Marcillac, M. Miville-Deschênes, L. Montier, F. Noviello, F. Pajot, O. Perdereau, F. Piacentini, M. Piat, S. Plaszczynski, E. Pointecouteau, J. Puget, I. Ristorcelli, G. Savini, R. Sudiwala, M. Veneziani, and

DRAFT

D. Yvon, "Planck pre-launch status: High Frequency Instrument polarization calibration," *A&A*, vol. 520, pp. A13+, Sep. 2010.

[196] J. Aumont, J. F. Macías-Pérez, A. Ritacco, N. Ponthieu, and A. Mangilli, "Absolute calibration of the polarisation angle for future CMB *B*-mode experiments from current and future measurements of the Crab nebula," *ArXiv e-prints*, May 2018.

[197] Planck Collaboration, Y. Akrami, F. Argüeso, M. Ashdown, J. Aumont, C. Baccigalupi, M. Ballardini, A. J. Banday, R. B. Barreiro, N. Bartolo, S. Basak, K. Benabed, J.-P. Bernard, M. Bersanelli, P. Bielewicz, L. Bonavera, J. R. Bond, J. Borrill, F. R. Bouchet, F. Boulanger, M. Bucher, C. Burigana, R. C. Butler, E. Calabrese, J.-F. Cardoso, L. P. L. Colombo, B. P. Crill, F. Cuttaia, P. de Bernardis, A. de Rosa, G. de Zotti, J. Delabrouille, E. Di Valentino, C. Dickinson, J. M. Diego, S. Donzelli, A. Ducout, X. Dupac, G. Efstathiou, F. Elsner, T. A. Enßlin, H. K. Eriksen, Y. Fantaye, F. Finelli, M. Frailis, E. Franceschi, A. Frolov, S. Galeotta, S. Galli, K. Ganga, R. T. Génova-Santos, M. Gerbino, T. Ghosh, J. González-Nuevo, K. M. Górski, S. Gratton, A. Gruppuso, J. E. Gudmundsson, W. Handley, F. K. Hansen, D. Herranz, E. Hivon, Z. Huang, A. H. Jaffe, W. C. Jones, A. Karakci, E. Keihänen, R. Keskitalo, K. Kiiveri, J. Kim, T. S. Kisner, N. Krachmalnicoff, M. Kunz, H. Kurki-Suonio, J.-M. Lamarre, A. Lasenby, M. Lattanzi, C. R. Lawrence, J. P. Leahy, F. Levrier, M. Liguori, P. B. Lilje, V. Lindholm, M. López-Caniego, Y.-Z. Ma, J. F. Macías-Pérez, G. Maggio, D. Maino, N. Mandolesi, A. Mangilli, M. Maris, P. G. Martin, E. Martínez-González, S. Matarrese, N. Mauri, J. D. McEwen, P. R. Meinhold, A. Melchiorri, A. Mennella, M. Migliaccio, D. Molinari, L. Montier, G. Morgante, A. Moss, P. Natoli, L. Pagano, D. Paoletti, B. Partridge, G. Patanchon, L. Patrizii, M. Peel, F. Perrotta, V. Pettorino, F. Piacentini, G. Polenta, J.-L. Puget, J. P. Rachen, B. Racine, M. Reinecke, M. Remazeilles, A. Renzi, G. Rocha, G. Roudier, J. A. Rubiño-Martín, L. Salvati, M. Sandri, M. Savelainen, D. Scott, D. S. Seljebotn, C. Sirignano, G. Sirri, L. D. Spencer, A.-S. Suur-Uski, J. A. Tauber, D. Tavagnacco, M. Tenti, L. Terenzi, L. Toffolatti, M. Tomasi, T. Trombetti, J. Valiviita, F. Vansyngel, B. Van Tent, P. Vielva, F. Villa, N. Vittorio, B. D. Wandelt, R. Watson, I. K. Wehus, A. Zacchei, and A. Zonca, "Planck 2018 results. II. Low Frequency Instrument data processing," *ArXiv e-prints*, Jul. 2018.

[198] C. Dragone, "Offset multireflector antennas with perfect pattern symmetry and polarization discrimination," *AT&T Technical Journal*, vol. 57, pp. 2663–2684, Sep. 1978.

[199] ——, "A first-order treatment of aberrations in Cassegrainian and Gregorian antennas," *IEEE Transactions on Antennas and Propagation*, vol. 30, pp. 331–339, May 1982.

[200] ——, "Unique reflector arrangement within very wide field of view for multibeam antennas," *Electronics Letters*, vol. 19, p. 1061, Dec. 1983.

[201] G. Fargant, D. Dubruel, M. Cornut, J.-B. Riti, T. Passvogel, P. J. De Maagt, M. Anderegg, and J. Tauber, "Very wide band telescope for Planck using optical and radio frequency techniques," in *UV, Optical, and IR Space Telescopes and Instruments*, ser. Society of Photo-Optical Instrumentation Engineers (SPIE) Conference Series, J. B. Breckinridge and P. Jakobsen, Eds., vol. 4013, Jul. 2000, pp. 69–79.

[202] D. S. Swetz, P. A. R. Ade, M. Amiri, J. W. Appel, E. S. Battistelli, B. Burger, J. Chervenak, M. J. Devlin, S. R. Dicker, W. B. Doriese, R. Dünner, T. Essinger-Hileman, R. P. Fisher, J. W. Fowler, M. Halpern, M. Hasselfield, G. C. Hilton, A. D. Hincks, K. D. Irwin, N. Jarosik, M. Kaul, J. Klein, J. M. Lau, M. Limon, T. A. Marriage, D. Marsden, K. Martocci, P. Mauskopf, H. Moseley, C. B. Netterfield, M. D. Niemack, M. R. Nolta, L. A. Page, L. Parker, S. T. Staggs, O. Stryzak, E. R. Switzer, R. Thornton, C. Tucker, E. Wollack, and Y. Zhao, "Overview of the Atacama Cosmology Telescope: Receiver, Instrumentation, and Telescope Systems," *The Astrophysical Journal Supplement Series*, vol. 194, p. 41, Jun. 2011.

[203] S. Padin, Z. Staniszewski, R. Keisler, M. Joy, A. A. Stark, P. A. R. Ade, K. A. Aird, B. A. Benson, L. E. Bleem, J. E. Carlstrom, C. L. Chang, T. M. Crawford, A. T. Crites, M. A. Dobbs, N. W. Halverson, S. Heimsath, R. E. Hills, W. L. Holzapfel, C. Lawrie, A. T. Lee, E. M. Leitch, J. Leong, W. Lu, M. Lueker, J. J. McMahon, S. S. Meyer, J. J. Mohr, T. E. Montroy, T. Plagge, C. Pryke, J. E. Ruhl, K. K. Schaffer, E. Shirokoff, H. G. Spieler, and J. D. Vieira, "South Pole Telescope optics," *Appl. Optics*, vol. 47, pp. 4418–4428, Aug. 2008.

[204] K. Young, M. Alvarez, N. Battaglia, J. Bock, J. Borrill, D. Chuss, B. Crill, J. Delabrouille, M. Devlin, L. Fissel, R. Flauger, D. Green, K. Gorski, S. Hanany, R. Hills, J. Hubmayr, B. Johnson, W. Jones, L. Knox, A. Kogut, C. Lawrence, T. Matsumura, J. McGuire, J. McMahon, R. O'Brient, C. Pryke, B. M. Sutin, X. Z. Tan, A. Trangsrud, Q. Wen, and G. De Zotti, "Optical design of PICO: a concept for a space mission to probe inflation and cosmic origins," in *Society of Photo-Optical Instrumentation Engineers (SPIE) Conference Series*, vol. 10698, Aug. 2018, p. 1069846.

[205] P. de Bernardis, P. A. R. Ade, J. J. A. Baselmans, E. S. Battistelli, A. Benoit, M. Bersanelli, A. Bideaud, M. Calvo, F. J. Casas, M. G. Castellano, A. Catalano, I. Charles, I. Colantoni, F. Columbro, A. Coppolecchia, M. Crook, G. D'Alessandro, M. De Petris, J. Delabrouille, S. Doyle, C. Franceschet, A. Gomez, J. Goupy, S. Hanany, M. Hills, L. Lamagna, J. Macias-Perez, B. Maffei, S. Martin, E. Martinez-Gonzalez, S. Masi, D. McCarthy, A. Mennella, A. Monfardini, F. Noviello, A. Paiella, F. Piacentini, M. Piat, G. Pisano, G. Signorelli, C. Y. Tan, A. Tartari, N. Trappe, S. Triqueneaux, C. Tucker, G. Vermeulen, K. Young, M. Zannoni, A. Achúcarro, R. Allison, E. Artall, M. Ashdown, M. Ballardini, A. J. Banday, R. Banerji, J. Bartlett, N. Bartolo, S. Basak, A. Bonaldi, M. Bonato, J. Borrill, F. Bouchet, F. Boulanger, T. Brinckmann, M. Bucher, C. Burigana, A. Buzzelli, Z. Y. Cai, C. S. Carvalho, A. Challinor, J. Chluba, S. Clesse, G. De Gasperis, G. De Zotti, E. Di Valentino, J. M. Diego, J. Errard, S. Feeney, R. Fernandez- Cobos, F. Finelli, F. Forastieri, S. Galli, R. Génova-Santos, M. Gerbino, J. Gonzá lez-Nuevo, S. Hagstotz, J. Greenslade, W. Handley, C. Hernández-Monteagudo, C. Hervias- Caimapo, E. Hivon, K. Ki-

DRAFT

iveri, T. Kisner, T. Kitching, M. Kunz, H. Kurki-Suonio, A. Lasenby, M. Lattanzi, J. Lesgourgues, A. Lewis, M. Liguori, V. Lindholm, G. Luzzi, C. J. A. P. Martins, S. Matarrese, A. Melchiorri, J. B. Melin, D. Molinari, P. Natoli, M. Negrello, A. Notari, D. Paoletti, G. Patanchon, L. Polastri, G. Polenta, A. Pollo, V. Poulin, M. Quartin, M. Remazeilles, M. Roman, J. A. Rubiño-Martín, L. Salvati, M. Tomasi, D. Tramonte, T. Trombetti, J. Väliviita, R. Van de Weyjgaert, B. van Tent, V. Vennin, P. Vielva, and N. Vittorio, "Exploring cosmic origins with CORE: The instrument," *Journal of Cosmology and Astro-Particle Physics*, vol. 2018, p. 015, Apr. 2018.

[206] C. Granet, "Designing classical Dragonian offset dual-reflector antennas from combinations of prescribed geometric parameters," *IEEE Antennas and Propagation Magazine*, vol. 43, pp. 100–107, Dec. 2001.

[207] A. Suzuki, K. Arnold, J. Edwards, G. Engargiola, W. Holzapfel, B. Keating, A. T. Lee, X. F. Meng, M. J. Myers, R. O'Brient, E. Quealy, G. Rebeiz, P. L. Richards, D. Rosen, and P. Siritanasak, "Multi-Chroic Dual-Polarization Bolometric Detectors for Studies of the Cosmic Microwave Background," *Journal of Low Temperature Physics*, vol. 176, pp. 650–656, Sep. 2014.

[208] R. Datta, J. Hubmayr, C. Munson, J. Austermann, J. Beall, D. Becker, H. M. Cho, N. Halverson, G. Hilton, K. Irwin, D. Li, J. McMahon, L. Newburgh, J. Nibarger, M. Niemack, B. Schmitt, H. Smith, S. Staggs, J. Van Lanen, and E. Wollack, "Horn Coupled Multichroic Polarimeters for the Atacama Cosmology Telescope Polarization Experiment," *Journal of Low Temperature Physics*, vol. 176, pp. 670–676, Sep. 2014.

[209] S. M. Duff, J. Austermann, J. A. Beall, D. Becker, R. Datta, P. A. Gallardo, S. W. Henderson, G. C. Hilton, S. P. Ho, J. Hubmayr, B. J. Koopman, D. Li, J. McMahon, F. Nati, M. D. Niemack, C. G. Pappas, M. Salatino, B. L. Schmitt, S. M. Simon, S. T. Staggs, J. R. Stevens, J. Van Lanen, E. M. Vavagiakis, J. T. Ward, and E. J. Wollack, "Advanced ACTPol Multichroic Polarimeter Array Fabrication Process for 150 mm Wafers," *Journal of Low Temperature Physics*, vol. 184, pp. 634–641, Aug. 2016.

[210] BICEP2 Collaboration, Keck Array Collaboration, SPIDER Collaboration, P. A. R. Ade, R. W. Aikin, M. Amiri, D. Barkats, S. J. Benton, C. A. Bischoff, J. J. Bock, J. A. Bonetti, J. A. Brevik, I. Buder, E. Bullock, G. Chattopadhyay, G. Davis, P. K. Day, C. D. Dowell, L. Duband, J. P. Filippini, S. Fliescher, S. R. Golwala, M. Halpern, M. Hasselfield, S. R. Hildebrandt, G. C. Hilton, V. Hristov, H. Hui, K. D. Irwin, W. C. Jones, K. S. Karkare, J. P. Kaufman, B. G. Keating, S. Kefeli, S. A. Kernasovskiy, J. M. Kovac, C. L. Kuo, H. G. LeDuc, E. M. Leitch, N. Llombart, M. Lueker, P. Mason, K. Megerian, L. Moncelsi, C. B. Netterfield, H. T. Nguyen, R. O'Brient, I. Ogburn, R. W., A. Orlando, C. Pryke, A. S. Rahlin, C. D. Reintsema, S. Richter, M. C. Runyan, R. Schwarz, C. D. Sheehy, Z. K. Staniszewski, R. V. Sudiwala, G. P. Teply, J. E. Tolan, A. Trangsrud, R. S. Tucker, A. D. Turner, A. G. Vieregg, A. Weber, D. V. Wiebe, P. Wilson, C. L. Wong, K. W. Yoon, and J. Zmuidzinas, "Antenna-coupled TES Bolometers Used in BICEP2, Keck Array, and Spider," *Ap. J.*, vol. 812, p. 176, Oct. 2015.

[211] J. M. Edwards, R. O'Brient, A. T. Lee, and G. M. Rebeiz, "Dual-Polarized Sinuous Antennas on Extended Hemispherical Silicon Lenses," *IEEE Transactions on Antennas and Propagation*, vol. 60, pp. 4082–4091, Sep. 2012.

[212] R. O'Brient, P. Ade, K. Arnold, J. Edwards, G. Engargiola, W. L. Holzapfel, A. T. Lee, M. J. Myers, E. Quealy, G. Rebeiz, P. Richards, and A. Suzuki, "A dual-polarized broadband planar antenna and channelizing filter bank for millimeter wavelengths," *Applied Physics Letters*, vol. 102, p. 063506, Feb. 2013.

[213] E. D. Shirokoff, "The South Pole Telescope bolometer array and the measurement of secondary Cosmic Microwave Background anisotropy at small angular scales," Ph.D. dissertation, University of California, Berkeley, Jan. 2011.

[214] L. Bleem, P. Ade, K. Aird, J. Austermann, J. Beall, D. Becker, B. Benson, J. Britton, J. Carlstrom, C. L. Chang, H. Cho, T. de Haan, T. Crawford, A. Crites, A. Datesman, M. Dobbs, W. Everett, A. Ewall-Wice, E. George, N. Halverson, N. Harrington, J. Henning, G. Hilton, W. Holzapfel, S. Hoover, J. Hubmayr, K. Irwin, R. Keisler, J. Kennedy, A. Lee, E. Leitch, D. Li, M. Lueker, D. P. Marrone, J. McMahon, J. Mehl, S. Meyer, J. Montgomery, T. Montroy, T. Natoli, J. Nibarger, M. Niemack, V. Novosad, S. Padin, C. Pryke, C. Reichardt, J. Ruhl, B. Saliwanchik, J. Sayre, K. Schafer, E. Shirokoff, K. Story, K. Vanderlinde, J. Vieira, G. Wang, R. Williamson, V. Yefremenko, K. W. Yoon, and E. Young, "An Overview of the SPTpol Experiment," *Journal of Low Temperature Physics*, vol. 167, pp. 859–864, Jun. 2012.

[215] A. D. Turner, J. J. Bock, J. W. Beeman, J. Glenn, P. C. Hargrave, V. V. Hristov, H. T. Nguyen, F. Rahman, S. Sethuraman, and A. L. Woodcraft, "Silicon nitride Micromesh Bolometer Array for Submillimeter Astrophysics," *Appl. Optics*, vol. 40, pp. 4921–4932, Oct. 2001.

[216] A. S. Rahlin, P. A. R. Ade, M. Amiri, S. J. Benton, J. J. Bock, J. R. Bond, S. A. Bryan, H. C. Chiang, C. R. Contaldi, B. P. Crill, O. Doré, M. Farhang, J. P. Filippini, L. M. Fissel, A. A. Fraisse, A. E. Gambrel, N. N. Gandilo, S. Golwala, J. E. Gudmundsson, M. Halpern, M. F. Hasselfield, G. Hilton, W. A. Holmes, V. V. Hristov, K. D. Irwin, W. C. Jones, Z. D. Kermish, C. L. Kuo, C. J. MacTavish, P. V. Mason, K. Megerian, L. Moncelsi, T. A. Morford, J. M. Nagy, C. B. Netterfield, R. O'Brient, C. Reintsema, J. E. Ruhl, M. C. Runyan, J. A. Shariff, J. D. Soler, A. Trangsrud, C. Tucker, R. S. Tucker, A. D. Turner, A. C. Weber, D. V. Wiebe, and E. Y. Young, "Pre-flight integration and characterization of the SPIDER balloon-borne telescope," in *Millimeter, Submillimeter, and Far-Infrared Detectors and Instrumentation for Astronomy VII*, vol. 9153, Jul. 2014, p. 915313.

[217] S. W. Henderson, R. Allison, J. Austermann, T. Baildon, N. Battaglia, J. A. Beall, D. Becker, F. De Bernardis, J. R. Bond, E. Calabrese, S. K. Choi, K. P. Coughlin, K. T. Crowley, R. Datta, M. J. Devlin, S. M. Duff, J. Dunkley, R. Dünner, A. van Engelen, P. A. Gallardo, E. Grace, M. Hasselfield, F. Hills, G. C. Hilton, A. D. Hincks, R. Hloẑek, S. P. Ho, J. Hubmayr,

DRAFT

K. Huffenberger, J. P. Hughes, K. D. Irwin, B. J. Koopman, A. B. Kosowsky, D. Li, J. McMahon, C. Munson, F. Nati, L. Newburgh, M. D. Niemack, P. Niraula, L. A. Page, C. G. Pappas, M. Salatino, A. Schillaci, B. L. Schmitt, N. Sehgal, B. D. Sherwin, J. L. Sievers, S. M. Simon, D. N. Spergel, S. T. Staggs, J. R. Stevens, R. Thornton, J. Van Lanen, E. M. Vavagiakis, J. T. Ward, and E. J. Wollack, "Advanced ACTPol Cryogenic Detector Arrays and Readout," *Journal of Low Temperature Physics*, vol. 184, pp. 772–779, Aug. 2016.

[218] The EBEX Collaboration, A. Aboobaker, P. Ade, D. Araujo, F. Aubin, C. Baccigalupi, C. Bao, D. Chapman, J. Didier, M. Dobbs, W. Grainger, S. Hanany, K. Helson, S. Hillbrand, J. Hubmayr, A. Jaffe, B. Johnson, T. Jones, J. Klein, A. Korotkov, A. Lee, L. Levinson, M. Limon, K. MacDermid, A. D. Miller, M. Milligan, L. Moncelsi, E. Pascale, K. Raach, B. Reichborn- Kjennerud, I. Sagiv, C. Tucker, G. S. Tucker, B. Westbrook, K. Young, and K. Zilic, "The EBEX Balloon-borne Experiment—Gondola, Attitude Control, and Control Software," *The Astrophysical Journal Supplement Series*, vol. 239, p. 9, Nov. 2018.

[219] F. Pajot, "Planck compression," Private communication.

[220] Planck HFI Core Team, P. A. R. Ade, N. Aghanim, R. Ansari, M. Arnaud, M. Ashdown, J. Aumont, A. J. Banday, M. Bartelmann, J. G. Bartlett, E. Battaner, K. Benabed, A. Benoît, J. P. Bernard, M. Bersanelli, R. Bhatia, J. J. Bock, J. R. Bond, J. Borrill, F. R. Bouchet, F. Boulanger, T. Bradshaw, E. Bréelle, M. Bucher, P. Camus, J. F. Cardoso, A. Catalano, A. Challinor, A. Chamballu, J. Charra, M. Charra, R. R. Chary, C. Chiang, S. Church, D. L. Clements, S. Colombi, F. Couchot, A. Coulais, C. Cressiot, B. P. Crill, M. Crook, P. de Bernardis, J. Delabrouille, J. M. Delouis, F. X. Désert, K. Dolag, H. Dole, O. Doré, M. Douspis, G. Efstathiou, P. Eng, C. Filliard, O. Forni, P. Fosalba, J. J. Fourmond, K. Ganga, M. Giard, D. Girard, Y. Giraud-Héraud, R. Gispert, K. M. Górski, S. Gratton, M. Griffin, G. Guyot, J. Haissinski, D. Harrison, G. Helou, S. Henrot-Versillé, C. Hernández-Monteagudo, S. R. Hildebrandt, R. Hills, E. Hivon, M. Hobson, W. A. Holmes, K. M. Huffenberger, A. H. Jaffe, W. C. Jones, J. Kaplan, R. Kneissl, L. Knox, G. Lagache, J. M. Lamarre, P. Lami, A. E. Lange, A. Lasenby, A. Lavabre, C. R. Lawrence, B. Leriche, C. Leroy, Y. Longval, J. F. Macías-Pérez, T. Maciaszek, C. J. MacTavish, B. Maffei, N. Mandolesi, R. Mann, B. Mansoux, S. Masi, T. Matsumura, P. McGehee, J. B. Melin, C. Mercier, M. A. Miville-Deschênes, A. Moneti, L. Montier, D. Mortlock, A. Murphy, F. Nati, C. B. Netterfield, H. U. Nørgaard-Nielsen, C. North, F. Noviello, D. Novikov, S. Osborne, C. Paine, F. Pajot, G. Patanchon, T. Peacocke, T. J. Pearson, O. Perdereau, L. Perotto, F. Piacentini, M. Piat, S. Plaszczynski, E. Pointecouteau, R. Pons, N. Ponthieu, G. Prézeau, S. Prunet, J. L. Puget, W. T. Reach, C. Renault, I. Ristorcelli, G. Rocha, C. Rosset, G. Roudier, M. Rowan-Robinson, B. Rusholme, D. Santos, G. Savini, B. M. Schaefer, P. Shellard, L. Spencer, J. L. Starck, P. Stassi, V. Stolyarov, R. Stompor, R. Sudiwala, R. Sunyaev, J. F. Sygnet, J. A. Tauber, C. Thum, J. P. Torre, F. Touze, M. Tristram, F. van Leeuwen, L. Vibert, D. Vibert, L. A. Wade, B. D. Wandelt, S. D. M. White, H. Wiesemeyer, A. Woodcraft, V. Yurchenko, D. Yvon, and A. Zacchei, "Planck early results. IV. First assessment of the High Frequency Instrument in-flight performance," *Astron. Astrophys.*, vol. 536, p. A4, Dec. 2011.

[221] M. Donabedian, A. I. of Aeronautics, and Astronautics, *Spacecraft Thermal Control Handbook, Vol. 2: Cryogenics*, ser. EngineeringPro collection. Aerospace Press, 2003. [Online]. Available: https://books.google.com/books?id=nsLqjwEACAAJ

[222] R. G. Ross, "Estimation of thermal conduction loads for structural supports of cryogenic spacecraft assemblies," *Cryogenics*, vol. 44, pp. 421–424, Jun. 2004.

[223] P. J. Shirron, M. O. Kimball, D. J. Fixsen, A. J. Kogut, X. Li, and M. J. DiPirro, "Design of the PIXIE adiabatic demagnetization refrigerators," *Cryogenics*, vol. 52, pp. 140–144, Apr. 2012.

[224] P. J. Shirron, M. O. Kimball, B. L. James, T. Muench, M. J. DiPirro, T. G. Bialas, G. A. Sneiderman, F. S. Porter, and R. L. Kelley, "Thermodynamic performance of the 3-stage ADR for the Astro-H Soft-X-ray Spectrometer instrument," *Cryogenics*, vol. 74, pp. 24–30, Mar. 2016.

[225] D. Durand, R. Colbert, C. Jaco, M. Michaelian, T. Nguyen, M. Petach, and J. Raab, "Mid Infrared Instrument (miri) Cooler Subsystem Prototype Demonstration," in *Advances in Cryogenic Engineering*, ser. American Institute of Physics Conference Series, J. G. Weisend, J. Barclay, S. Breon, J. Demko, M. Dipirro, J. P. Kelley, P. Kittel, A. Klebaner, A. Zeller, M. Zagarola, S. van Sciver, A. Rowe, J. Pfotenhauer, T. Peterson, and J. Lock, Eds., vol. 52, Mar. 2008, pp. 807–814.

[226] J. Rabb, "Ngas scw-4k," Presentation at the 2013 Space Cryogenics Workshop, 2013.

[227] D. S. Glaister, W. Gully, R. Ross, P. Hendershott, E. Marquardt, and V. Kotsubo, "Ball Aerospace 4-6 K Space Cryocooler," in *Advances in Cryogenic Engineering: Transactions of the Cryogenic Engineering Conference*, ser. American Institute of Physics Conference Series, I. Weisend, J. G., J. Barclay, S. Breon, J. Demko, M. Dipirro, J. P. Kelley, P. Kittel, A. Klebaner, J. Lock, J. Maddocks, T. Peterson, J. Pfotenhauer, A. Rowe, S. van Sciver, and A. Zeller, Eds., vol. 823, Apr. 2006, pp. 632–639.

[228] F. Pajot, P. A. R. Ade, J. L. Beney, E. Bréelle, D. Broszkiewicz, P. Camus, C. Carabétian, A. Catalano, A. Chardin, M. Charra, J. Charra, R. Cizeron, F. Couchot, A. Coulais, B. P. Crill, K. Dassas, J. Daubin, P. de Bernardis, P. de Marcillac, J. M. Delouis, F. X. Désert, P. Duret, P. Eng, C. Evesque, J. J. Fourmond, S. François, M. Giard, Y. Giraud-Héraud, L. Guglielmi, G. Guyot, J. Haissinski, S. Henrot-Versillé, V. Hervier, W. Holmes, W. C. Jones, J. M. Lamarre, P. Lami, A. E. Lange, M. Lefebvre, B. Leriche, C. Leroy, J. Macias- Perez, T. Maciaszek, B. Maffei, A. Mahendran, B. Mansoux, C. Marty, S. Masi, C. Mercier, M. A. Miville-Deschenes, L. Montier, C. Nicolas, F. Noviello, O. Perdereau, F. Piacentini, M. Piat,

DRAFT

S. Plaszczynski, E. Pointecouteau, R. Pons, N. Ponthieu, J. L. Puget, D. Rambaud, C. Renault, J. C. Renault, C. Rioux, I. Ristorcelli, C. Rosset, G. Savini, R. Sudiwala, J. P. Torre, M. Tristram, D. Vallée, M. Veneziani, and D. Yvon, "Planck pre-launch status: HFI ground calibration," *Astron. Astrophys.*, vol. 520, p. A10, Sep. 2010.

[229] C. L. Bennett, M. Bay, M. Halpern, G. Hinshaw, C. Jackson, N. Jarosik, A. Kogut, M. Limon, S. S. Meyer, L. Page, D. N. Spergel, G. S. Tucker, D. T. Wilkinson, E. Wollack, and E. L. Wright, "The Microwave Anisotropy Probe Mission," *Ap. J.*, vol. 583, pp. 1–23, Jan. 2003.

[230] J. A. Tauber, N. Mandolesi, J. L. Puget, T. Banos, M. Bersanelli, F. R. Bouchet, R. C. Butler, J. Charra, G. Crone, J. Dodsworth, G. Efstathiou, R. Gispert, G. Guyot, A. Gregorio, J. J. Juillet, J. M. Lamarre, R. J. Laureijs, C. R. Lawrence, H. U. Nørgaard- Nielsen, T. Passvogel, J. M. Reix, D. Texier, L. Vibert, A. Zacchei, P. A. R. Ade, N. Aghanim, B. Aja, E. Alippi, L. Aloy, P. Armand, M. Arnaud, A. Arondel, A. Arreola-Villanueva, E. Artal, E. Artina, A. Arts, M. Ashdown, J. Aumont, M. Azzaro, A. Bacchetta, C. Baccigalupi, M. Baker, M. Balasini, A. Balbi, A. J. Banday, G. Barbier, R. B. Barreiro, M. Bartelmann, P. Battaglia, E. Battaner, K. Benabed, J. L. Beney, R. Beneyton, K. Bennett, A. Benoit, J. P. Bernard, P. Bhandari, R. Bhatia, M. Biggi, R. Biggins, G. Billig, Y. Blanc, H. Blavot, J. J. Bock, A. Bonaldi, R. Bond, J. Bonis, J. Borders, J. Borrill, L. Boschini, F. Boulanger, J. Bouvier, M. Bouzit, R. Bowman, E. Bréelle, T. Bradshaw, M. Braghin, M. Bremer, D. Brienza, D. Broszkiewicz, C. Burigana, M. Burkhalter, P. Cabella, T. Cafferty, M. Cairola, S. Caminade, P. Camus, C. M. Cantalupo, B. Cappellini, J. F. Cardoso, R. Carr, A. Catalano, L. Cayón, M. Cesa, M. Chaigneau, A. Challinor, A. Chamballu, J. P. Chambelland, M. Charra, L. Y. Chiang, G. Chlewicki, P. R. Christensen, S. Church, E. Cianciettа, M. Cibrario, R. Cizeron, D. Clements, B. Collaudin, J. M. Colley, S. Colombi, A. Colombo, F. Colombo, O. Corre, F. Couchot, B. Cougrand, A. Coulais, P. Couzin, B. Crane, B. Crill, M. Crook, D. Crumb, F. Cuttaia, U. Dörl, P. da Silva, R. Daddato, C. Damasio, L. Danese, G. D'Aquino, O. D'Arcangelo, K. Dassas, R. D. Davies, W. Davies, R. J. Davis, P. de Bernardis, D. de Chambure, G. de Gasperis, M. L. de La Fuente, P. de Paco, A. de Rosa, G. de Troia, G. de Zotti, M. Dehamme, J. Delabrouille, J. M. Delouis, F. X. Désert, G. di Girolamo, C. Dickinson, E. Doelling, K. Dolag, I. Domken, M. Douspis, D. Doyle, S. Du, D. Dubruel, C. Dufour, C. Dumesnil, X. Dupac, P. Duret, C. Eder, A. Elfving, T. A. Enßlin, P. Eng, K. English, H. K. Eriksen, P. Estaria, M. C. Falvella, F. Ferrari, F. Finelli, A. Fishman, S. Fogliani, S. Foley, A. Fonseca, G. Forma, O. Forni, P. Fosalba, J. J. Fourmond, M. Frailis, C. Franceschet, E. Franceschi, S. François, M. Frerking, M. F. Gómez- Reñasco, K. M. Górski, T. C. Gaier, S. Galeotta, K. Ganga, J. García Lázaro, A. Garnica, M. Gaspard, E. Gavila, M. Giard, G. Giardino, G. Gienger, Y. Giraud- Heraud, J. M. Glorian, M. Griffin, A. Gruppuso, L. Guglielmi, D. Guichon, B. Guillaume, P. Guillouet, J. Haissinski, F. K. Hansen, J. Hardy, D. Harrison, A. Hazell, M. Hechler, V. Heckenauer, D. Heinzer, R. Hell, S. Henrot-Versillé, C. Hernández- Monteagudo, D. Herranz, J. M. Herreros, V. Hervier, A. Heske, A. Heurtel, S. R. Hildebrandt, R. Hills, E. Hivon, M. Hobson, D. Hollert, W. Holmes, A. Hornstrup, W. Hovest, R. J. Hoyland, G. Huey, K. M. Huffenberger, N. Hughes, U. Israelsson, B. Jackson, A. Jaffe, T. R. Jaffe, T. Jagemann, N. C. Jessen, J. Jewell, W. Jones, M. Juvela, J. Kaplan, P. Karlman, F. Keck, E. Keihänen, M. King, T. S. Kisner, P. Kletzkine, R. Kneissl, J. Knoche, L. Knox, T. Koch, M. Krassenburg, H. Kurki-Suonio, A. Lähteenmäki, G. Lagache, E. Lagorio, P. Lami, J. Lande, A. Lange, F. Langlet, R. Lapini, M. Lapolla, A. Lasenby, M. Le Jeune, J. P. Leahy, M. Lefebvre, F. Legrand, G. Le Meur, R. Leonardi, B. Leriche, C. Leroy, P. Leutenegger, S. M. Levin, P. B. Lilje, C. Lindensmith, M. Linden-Vørnle, A. Loc, Y. Longval, P. M. Lubin, T. Luchik, I. Luthold, J. F. Macias-Perez, T. Maciaszek, C. MacTavish, S. Madden, B. Maffei, C. Magneville, D. Maino, A. Mambretti, B. Mansoux, D. Marchioro, M. Maris, F. Marliani, J. C. Marrucho, J. Martí-Canales, E. Martínez-González, A. Martín-Polegre, P. Martin, C. Marty, W. Marty, S. Masi, M. Massardi, S. Matarrese, F. Matthai, P. Mazzotta, A. McDonald, P. McGrath, A. Mediavilla, P. R. Meinhold, J. B. Mélin, F. Melot, L. Mendes, A. Mennella, C. Mervier, L. Meslier, M. Miccolis, M. A. Miville-Deschenes, A. Moneti, D. Montet, L. Montier, J. Mora, G. Morgante, G. Morigi, G. Morinaud, N. Morisset, D. Mortlock, S. Mottet, J. Mulder, D. Munshi, A. Murphy, P. Murphy, P. Musi, J. Narbonne, P. Naselsky, A. Nash, F. Nati, P. Natoli, B. Netterfield, J. Newell, M. Nexon, C. Nicolas, P. H. Nielsen, N. Ninane, F. Noviello, D. Novikov, I. Novikov, I. J. O'Dwyer, P. Oldeman, P. Olivier, L. Ouchet, C. A. Oxborrow, L. Pé rez-Cuevas, L. Pagan, C. Paine, F. Pajot, R. Paladini, F. Pancher, J. Panh, G. Parks, P. Parnaudeau, B. Partridge, B. Parvin, J. P. Pascual, F. Pasian, D. P. Pearson, T. Pearson, M. Pecora, O. Perdereau, L. Perotto, F. Perrotta, F. Piacentini, M. Piat, E. Pierpaoli, O. Piersanti, E. Plaige, S. Plaszczynski, P. Platania, E. Pointecouteau, G. Polenta, N. Ponthieu, L. Popa, G. Poulleau, T. Poutanen, G. Prézeau, L. Pradell, M. Prina, S. Prunet, J. P. Rachen, D. Rambaud, F. Rame, I. Rasmussen, J. Rautakoski, W. T. Reach, R. Rebolo, M. Reinecke, J. Reiter, C. Renault, S. Ricciardi, P. Rideau, T. Riller, I. Ristorcelli, J. B. Riti, G. Rocha, Y. Roche, R. Pons, R. Rohlfs, D. Romero, S. Roose, C. Rosset, S. Rouberol, M. Rowan- Robinson, J. A. Rubiño-Martín, P. Rusconi, B. Rusholme, M. Salama, E. Salerno, M. Sandri, D. Santos, J. L. Sanz, L. Sauter, F. Sauvage, G. Savini, M. Schmelzel, A. Schnorhk, W. Schwarz, D. Scott, M. D. Seiffert, P. Shellard, C. Shih, M. Sias, J. I. Silk, R. Silvestri, R. Sippel, G. F. Smoot, J. L. Starck, P. Stassi, J. Sternberg, F. Stivoli, V. Stolyarov, R. Stompor, L. Stringhetti, D. Strommen, T. Stute, R. Sudiwala, R. Sugimura, R. Sunyaev, J. F. Sygnet, M. Türler, E. Taddei, J. Tallon, C. Tamiatto, M. Taurigna, D. Taylor, L. Terenzi, S. Thuerey, J. Tillis, G. Tofani, L. Toffolatti, E. Tommasi, M. Tomasi, E. Tonazzini, J. P. Torre, S. Tosti, F. Touze, M. Tristram, J. Tuovinen, M. Tuttlebee, G. Umana, L. Valenziano, D. Vallée, M. van der Vlis, F. van Leeuwen, J. C. Vanel, B. van-Tent, J. Varis, E. Vassallo, C. Vescovi, F. Vezzu, D. Vibert, P. Vielva, J. Vierra, F. Villa, N. Vittorio, C. Vuerli, L. A. Wade, A. R. Walker, B. D. Wandelt, C. Watson, D. Werner, M. White, S. D. M. White, A. Wilkinson, P. Wilson, A. Woodcraft, B. Yoffo, M. Yun, V. Yurchenko, D. Yvon, B. Zhang, O. Zimmermann, A. Zonca,

DRAFT

and D. Zorita, "Planck pre-launch status: The Planck mission," *Astron. Astrophys.*, vol. 520, p. A1, Sep. 2010.

[231] Space Exploration Technologies Corp., *Falcon 9 Launch Vehicle: Payload User's Guide, Rev 2*. Space Exploration Technologies Corp., October 2015. [Online]. Available: https://www.spacex.com/sites/spacex/files/falcon_9_users_guide_rev_2.0.pdf

[232] W. Hu, M. M. Hedman, and M. Zaldarriaga, "Benchmark parameters for CMB polarization experiments," *Phys. Rev. D.*, vol. 67, p. 043004, Feb. 2003.

[233] H. Kurki-Suonio, E. Keihänen, R. Keskitalo, T. Poutanen, A. S. Sirviö, D. Maino, and C. Burigana, "Destriping CMB temperature and polarization maps," *Astron. Astrophys.*, vol. 506, pp. 1511–1539, Nov. 2009.

[234] T. S. Brown, *A GNC Perspective of the Launch and Commissioning of NASA's New SMAP (Soil Moisture Active Passive) Spacecraft*. American Institute of Aeronautics and Astronautics, 2018/11/19 2016. [Online]. Available: https://doi.org/10.2514/6.2016-0479

[235] Planck Collaboration, P. A. R. Ade, N. Aghanim, C. Armitage-Caplan, M. Arnaud, M. Ashdown, F. Atrio-Barandela, J. Aumont, C. Baccigalupi, A. J. Banday, R. B. Barreiro, E. Battaner, K. Benabed, A. Benoît, A. Benoit-Lévy, J. P. Bernard, M. Bersanelli, P. Bielewicz, J. Bobin, J. J. Bock, J. R. Bond, J. Borrill, F. R. Bouchet, F. Boulanger, J. W. Bowyer, M. Bridges, M. Bucher, C. Burigana, J. F. Cardoso, A. Catalano, A. Chamballu, R. R. Chary, X. Chen, H. C. Chiang, L. Y. Chiang, P. R. Christensen, S. Church, D. L. Clements, S. Colombi, L. P. L. Colombo, C. Combet, F. Couchot, A. Coulais, B. P. Crill, A. Curto, F. Cuttaia, L. Danese, R. D. Davies, R. J. Davis, P. de Bernardis, A. de Rosa, G. de Zotti, J. Delabrouille, J. M. Delouis, F. X. Désert, C. Dickinson, J. M. Diego, H. Dole, S. Donzelli, O. Doré, M. Douspis, J. Dunkley, X. Dupac, G. Efstathiou, T. A. Enßlin, H. K. Eriksen, F. Finelli, O. Forni, M. Frailis, A. A. Fraisse, E. Franceschi, S. Galeotta, K. Ganga, M. Giard, G. Giardino, D. Girard, Y. Giraud-Héraud, J. González-Nuevo, K. M. Górski, S. Gratton, A. Gregorio, A. Gruppuso, J. E. Gudmundsson, F. K. Hansen, D. Hanson, D. Harrison, G. Helou, S. Henrot-Versillé, O. Herent, C. Hernández-Monteagudo, D. Herranz, S. R. Hildebrandt, E. Hivon, M. Hobson, W. A. Holmes, A. Hornstrup, Z. Hou, W. Hovest, K. M. Huffenberger, G. Hurier, A. H. Jaffe, T. R. Jaffe, W. C. Jones, M. Juvela, E. Keihänen, R. Keskitalo, T. S. Kisner, R. Kneissl, J. Knoche, L. Knox, M. Kunz, H. Kurki-Suonio, G. Lagache, J. M. Lamarre, A. Lasenby, R. J. Laureijs, C. R. Lawrence, M. Le Jeune, R. Leonardi, C. Leroy, J. Lesgourgues, M. Liguori, P. B. Lilje, M. Linden-Vørnle, M. López-Caniego, P. M. Lubin, J. F. Macías-Pérez, C. J. MacTavish, B. Maffei, N. Mandolesi, M. Maris, F. Marleau, D. J. Marshall, P. G. Martin, E. Martínez-González, S. Masi, M. Massardi, S. Matarrese, F. Matthai, P. Mazzotta, P. McGehee, P. R. Meinhold, A. Melchiorri, F. Melot, L. Mendes, A. Mennella, M. Migliaccio, S. Mitra, M. A. Miville-Deschênes, A. Moneti, L. Montier, G. Morgante, D. Mortlock, S. Mottet, D. Munshi, J. A. Murphy, P. Naselsky, F. Nati, P. Natoli, C. B. Netterfield, H. U. Nørgaard-Nielsen, C. North, F. Noviello, D. Novikov, I. Novikov, F. Orieux, S. Osborne, C. A. Oxborrow, F. Paci, L. Pagano, F. Pajot, R. Paladini, D. Paoletti, F. Pasian, G. Patanchon, O. Perdereau, L. Perotto, F. Perrotta, F. Piacentini, M. Piat, E. Pierpaoli, D. Pietrobon, S. Plaszczynski, E. Pointecouteau, G. Polenta, N. Ponthieu, L. Popa, T. Poutanen, G. W. Pratt, G. Prézeau, S. Prunet, J. L. Puget, J. P. Rachen, B. Racine, W. T. Reach, R. Rebolo, M. Reinecke, M. Remazeilles, C. Renault, S. Ricciardi, T. Riller, I. Ristorcelli, G. Rocha, C. Rosset, G. Roudier, M. Rowan-Robinson, B. Rusholme, L. Sanselme, D. Santos, A. Sauvé, G. Savini, D. Scott, E. P. S. Shellard, L. D. Spencer, J. L. Starck, V. Stolyarov, R. Stompor, R. Sudiwala, F. Sureau, D. Sutton, A. S. Suur-Uski, J. F. Sygnet, J. A. Tauber, D. Tavagnacco, S. Techene, L. Terenzi, M. Tomasi, M. Tristram, M. Tucci, G. Umana, L. Valenziano, J. Valiviita, B. Van Tent, L. Vibert, P. Vielva, F. Villa, N. Vittorio, L. A. Wade, B. D. Wandelt, S. D. M. White, D. Yvon, A. Zacchei, and A. Zonca, "Planck 2013 results. VI. High Frequency Instrument data processing," *Astron. Astrophys.*, vol. 571, p. A6, Nov. 2014.

[236] Planck Collaboration, N. Aghanim, Y. Akrami, M. Ashdown, J. Aumont, C. Baccigalupi, M. Ballardini, A. J. Banday, R. B. Barreiro, N. Bartolo, S. Basak, K. Benabed, J.-P. Bernard, M. Bersanelli, P. Bielewicz, J. R. Bond, J. Borrill, F. R. Bouchet, F. Boulanger, M. Bucher, C. Burigana, E. Calabrese, J.-F. Cardoso, J. Carron, A. Challinor, H. C. Chiang, L. P. L. Colombo, C. Combet, F. Couchot, B. P. Crill, F. Cuttaia, P. de Bernardis, A. de Rosa, G. de Zotti, J. Delabrouille, J.-M. Delouis, E. Di Valentino, J. M. Diego, O. Doré, M. Douspis, A. Ducout, X. Dupac, G. Efstathiou, F. Elsner, T. A. Enßlin, H. K. Eriksen, E. Falgarone, Y. Fantaye, F. Finelli, M. Frailis, A. A. Fraisse, E. Franceschi, A. Frolov, S. Galeotta, S. Galli, K. Ganga, R. T. Génova-Santos, M. Gerbino, T. Ghosh, J. González-Nuevo, K. M. Górski, S. Gratton, A. Gruppuso, J. E. Gudmundsson, W. Handley, F. K. Hansen, S. Henrot-Versillé, D. Herranz, E. Hivon, Z. Huang, A. H. Jaffe, W. C. Jones, A. Karakci, E. Keihänen, R. Keskitalo, K. Kiiveri, J. Kim, T. S. Kisner, N. Krachmalnicoff, M. Kunz, H. Kurki-Suonio, G. Lagache, J.-M. Lamarre, A. Lasenby, M. Lattanzi, C. R. Lawrence, F. Levrier, M. Liguori, P. B. Lilje, V. Lindholm, M. López-Caniego, Y.-Z. Ma, J. F. Macías-Pérez, G. Maggio, D. Maino, N. Mandolesi, A. Mangilli, P. G. Martin, E. Martínez-González, S. Matarrese, N. Mauri, J. D. McEwen, A. Melchiorri, A. Mennella, M. Migliaccio, M.-A. Miville-Deschênes, D. Molinari, A. Moneti, L. Montier, G. Morgante, A. Moss, S. Mottet, P. Natoli, L. Pagano, D. Paoletti, B. Partridge, G. Patanchon, L. Patrizii, O. Perdereau, F. Perrotta, V. Pettorino, F. Piacentini, J.-L. Puget, J. P. Rachen, M. Reinecke, M. Remazeilles, A. Renzi, G. Rocha, G. Roudier, L. Salvati, M. Sandri, M. Savelainen, D. Scott, C. Sirignano, G. Sirri, L. D. Spencer, R. Sunyaev, A.-S. Suur-Uski, J. A. Tauber, D. Tavagnacco, M. Tenti, L. Toffolatti, M. Tomasi, M. Tristram, T. Trombetti, J. Valiviita, F. Vansyngel, B. Van Tent, L. Vibert, P. Vielva, F. Villa, N. Vittorio, B. D. Wandelt, I. K. Wehus, and A. Zonca, "Planck 2018 results. III. High Frequency Instrument data processing and frequency maps," *ArXiv e-prints*, Jul. 2018.

[237] R. Gualtieri, J. P. Filippini, P. A. R. Ade, M. Amiri, S. J. Benton, A. S. Bergman, R. Bihary, J. J. Bock, J. R. Bond, S. A.

DRAFT

Bryan, H. C. Chiang, C. R. Contaldi, O. Doré, A. J. Duivenvoorden, H. K. Eriksen, M. Farhang, L. M. Fissel, A. A. Fraisse, K. Freese, M. Galloway, A. E. Gambrel, N. N. Gandilo, K. Ganga, R. V. Gramillano, J. E. Gudmundsson, M. Halpern, J. Hartley, M. Hasselfield, G. Hilton, W. Holmes, V. V. Hristov, Z. Huang, K. D. Irwin, W. C. Jones, C. L. Kuo, Z. D. Kermish, S. Li, P. V. Mason, K. Megerian, L. Moncelsi, T. A. Morford, J. M. Nagy, C. B. Netterfield, M. Nolta, B. Osherson, I. L. Padilla, B. Racine, A. S. Rahlin, C. Reintsema, J. E. Ruhl, M. C. Runyan, T. M. Ruud, J. A. Shariff, J. D. Soler, X. Song, A. Trangsrud, C. Tucker, R. S. Tucker, A. D. Turner, J. F. v. d. List, A. C. Weber, I. K. Wehus, D. V. Wiebe, and E. Y. Young, "SPIDER: CMB Polarimetry from the Edge of Space," *Journal of Low Temperature Physics*, Oct. 2018.

[238] M. H. Abitbol, Z. Ahmed, D. Barron, R. Basu Thakur, A. N. Bender, B. A. Benson, C. A. Bischoff, S. A. Bryan, J. E. Carlstrom, C. L. Chang, D. T. Chuss, K. T. Crowley, A. Cukierman, T. de Haan, M. Dobbs, T. Essinger-Hileman, J. P. Filippini, K. Ganga, J. E. Gudmundsson, N. W. Halverson, S. Hanany, S. W. Henderson, C. A. Hill, S.-P. P. Ho, J. Hubmayr, K. Irwin, O. Jeong, B. R. Johnson, S. A. Kernasovskiy, J. M. Kovac, A. Kusaka, A. T. Lee, S. Maria, P. Mauskopf, J. J. McMahon, L. Moncelsi, A. W. Nadolski, J. M. Nagy, M. D. Niemack, R. C. O'Brient, S. Padin, S. C. Parshley, C. Pryke, N. A. Roe, K. Rostem, J. Ruhl, S. M. Simon, S. T. Staggs, A. Suzuki, E. R. Switzer, O. Tajima, K. L. Thompson, P. Timbie, G. S. Tucker, J. D. Vieira, A. G. Vieregg, B. Westbrook, E. J. Wollack, K. W. Yoon, K. S. Young, and E. Y. Young, "CMB-S4 Technology Book, First Edition," *ArXiv e-prints*, Jun. 2017.

[239] W. S. Holland, D. Bintley, E. L. Chapin, A. Chrysostomou, G. R. Davis, J. T. Dempsey, W. D. Duncan, M. Fich, P. Friberg, M. Halpern, K. D. Irwin, T. Jenness, B. D. Kelly, M. J. MacIntosh, E. I. Robson, D. Scott, P. A. R. Ade, E. Atad-Ettedgui, D. S. Berry, S. C. Craig, X. Gao, A. G. Gibb, G. C. Hilton, M. I. Hollister, J. B. Kycia, D. W. Lunney, H. McGregor, D. Montgomery, W. Parkes, R. P. J. Tilanus, J. N. Ullom, C. A. Walther, A. J. Walton, A. L. Woodcraft, M. Amiri, D. Atkinson, B. Burger, T. Chuter, I. M. Coulson, W. B. Doriese, C. Dunare, F. Economou, M. D. Niemack, H. A. L. Parsons, C. D. Reintsema, B. Sibthorpe, I. Smail, R. Sudiwala, and H. S. Thomas, "SCUBA-2: the 10 000 pixel bolometer camera on the James Clerk Maxwell Telescope," *MNRAS*, vol. 430, pp. 2513–2533, Apr. 2013.

[240] B. Dober, D. T. Becker, D. A. Bennett, S. A. Bryan, S. M. Duff, J. D. Gard, J. P. Hays-Wehle, G. C. Hilton, J. Hubmayr, J. A. B. Mates, C. D. Reintsema, L. R. Vale, and J. N. Ullom, "Microwave SQUID multiplexer demonstration for cosmic microwave background imagers," *Applied Physics Letters*, vol. 111, p. 243510, Dec. 2017.

[241] K. D. Irwin and K. W. Lehnert, "Microwave SQUID multiplexer," *Applied Physics Letters*, vol. 85, p. 2107, Sep. 2004.

[242] H. McCarrick, M. H. Abitbol, P. A. R. Ade, P. Barry, S. Bryan, G. Che, P. Day, S. Doyle, D. Flanigan, B. R. Johnson, G. Jones, H. G. LeDuc, M. Limon, P. Mauskopf, A. Miller, C. Tucker, and J. Zmuidzinas, "Development of dual-polarization LEKIDs for CMB observations," in *Millimeter, Submillimeter, and Far-Infrared Detectors and Instrumentation for Astronomy VIII*, vol. 9914, Jul. 2016, p. 99140O.

[243] B. A. Steinbach, J. J. Bock, H. T. Nguyen, R. C. O'Brient, and A. D. Turner, "Thermal Kinetic Inductance Detectors for Ground-Based Millimeter-Wave Cosmology," *Journal of Low Temperature Physics*, vol. 193, pp. 88–95, Nov. 2018.

[244] P. Gloesener, "Large Aluminium Convex Mirror for the Cryo-Optical Test of the Planck Primary Reflector," in *ESA Special Publication*, vol. 621, Jun. 2006, p. 43.

[245] Y. Toulemont, T. Passvogel, G. Pillbrat, D. de Chambure, D. Pierot, and D. Castel, "The 3.5m all SiC telescope for Herschel," in *5th International Conference on Space Optics*, B. Warmbein, Ed., vol. 554, Jun. 2004, pp. 341–348.

[246] Planck Collaboration, P. A. R. Ade, N. Aghanim, M. Arnaud, M. Ashdown, J. Aumont, C. Baccigalupi, M. Baker, A. Balbi, A. J. Banday, R. B. Barreiro, E. Battaner, K. Benabed, A. Benoît, J. P. Bernard, M. Bersanelli, P. Bhandari, R. Bhatia, J. J. Bock, A. Bonaldi, J. R. Bond, J. Borders, J. Borrill, F. R. Bouchet, B. Bowman, T. Bradshaw, E. Bréelle, M. Bucher, C. Burigana, R. C. Butler, P. Cabella, P. Camus, C. M. Cantalupo, B. Cappellini, J. F. Cardoso, A. Catalano, L. Cayón, A. Challinor, A. Chamballu, J. P. Chambelland, J. Charra, M. Charra, L. Y. Chiang, C. Chiang, P. R. Christensen, D. L. Clements, B. Collaudin, S. Colombi, F. Couchot, A. Coulais, B. P. Crill, M. Crook, F. Cuttaia, C. Damasio, L. Danese, R. D. Davies, R. J. Davis, P. de Bernardis, G. de Gasperis, A. de Rosa, J. Delabrouille, J. M. Delouis, F. X. Désert, K. Dolag, S. Donzelli, O. Doré, U. Dörl, M. Douspis, X. Dupac, G. Efstathiou, T. A. Enßlin, H. K. Eriksen, C. Filliard, F. Finelli, S. Foley, O. Forni, P. Fosalba, J. J. Fourmond, M. Frailis, E. Franceschi, S. Galeotta, K. Ganga, E. Gavila, M. Giard, G. Giardino, Y. Giraud-Héraud, J. González-Nuevo, K. M. Górski, S. Gratton, A. Gregorio, A. Gruppuso, G. Guyot, D. Harrison, G. Helou, S. Henrot-Versillé, C. Hernández-Monteagudo, D. Herranz, S. R. Hildebrandt, E. Hivon, M. Hobson, W. A. Holmes, A. Hornstrup, W. Hovest, R. J. Hoyland, K. M. Huffenberger, U. Israelsson, A. H. Jaffe, W. C. Jones, M. Juvela, E. Keihänen, R. Keskitalo, T. S. Kisner, R. Kneissl, L. Knox, H. Kurki- Suonio, G. Lagache, J. M. Lamarre, P. Lami, A. Lasenby, R. J. Laureijs, A. Lavabre, C. R. Lawrence, S. Leach, R. Lee, R. Leonardi, C. Leroy, P. B. Lilje, M. López-Caniego, P. M. Lubin, J. F. Macías-Pérez, T. Maciaszek, C. J. MacTavish, B. Maffei, D. Maino, N. Mandolesi, R. Mann, M. Maris, E. Martínez-González, S. Masi, S. Matarrese, F. Matthai, P. Mazzotta, P. McGehee, P. R. Meinhold, A. Melchiorri, F. Melot, L. Mendes, A. Mennella, M. A. Miville- Deschênes, A. Moneti, L. Montier, J. Mora, G. Morgante, N. Morisset, D. Mortlock, D. Munshi, A. Murphy, P. Naselsky, A. Nash, P. Natoli, C. B. Netterfield, D. Novikov, I. Novikov, I. J. O'Dwyer, S. Osborne, F. Pajot, F. Pasian, G. Patanchon, D. Pearson, O. Perdereau, L. Perotto, F. Perrotta, F. Piacentini, M. Piat, S. Plaszczynski, P. Platania, E. Pointecouteau, G. Polenta, N. Ponthieu, T. Poutanen, G. Prézeau, M. Prina, S. Prunet, J. L. Puget, J. P. Rachen, R. Rebolo, M. Reinecke, C. Renault, S. Ricciardi, T. Riller, I. Ristorcelli, G. Rocha, C. Rosset, J. A. Rubiño-Martín, B. Rusholme, M. Sandri, D. Santos, G. Savini, B. M. Schaefer, D. Scott, M. D. Seiffert, P. Shellard,

DRAFT

G. F. Smoot, J. L. Starck, P. Stassi, F. Stivoli, V. Stolyarov, R. Stompor, R. Sudiwala, J. F. Sygnet, J. A. Tauber, L. Terenzi, L. Toffolatti, M. Tomasi, J. P. Torre, M. Tristram, J. Tuovinen, L. Valenziano, L. Vibert, P. Vielva, F. Villa, N. Vittorio, L. A. Wade, B. D. Wandelt, C. Watson, S. D. M. White, A. Wilkinson, P. Wilson, D. Yvon, A. Zacchei, B. Zhang, and A. Zonca, "Planck early results. II. The thermal performance of Planck," *Astron. Astrophys.*, vol. 536, p. A2, Dec. 2011.

[247] S. Bard, "Development of a High-Performance Cryogenic Radiator with V-Groove Radiation Shields," *Journal of Spacecraft and Rockets*, vol. 24, pp. 193–197, May 1987.

[248] European Space Agency, "Planck cooling system," September 2009. [Online]. Available: http://sci.esa.int/planck/45498-cooling-system/?fbodylongid=2123

[249] ——, "Cmb polarisation mission study – cdf summary presentation," May 2016. [Online]. Available: http://sci.esa.int/trs/57805-cmb-polarisation-study---cdf-summary-presentation/

[250] L. E. Z. Jasper and P. Xaypraseuth, "Data production on past and future nasa missions," in *2017 IEEE Aerospace Conference*, March 2017, pp. 1–11.

DRAFT